

THE AGES OF 55 GLOBULAR CLUSTERS AS DETERMINED USING AN IMPROVED $\Delta V_{\text{TO}}^{\text{HB}}$ METHOD ALONG WITH COLOR-MAGNITUDE DIAGRAM CONSTRAINTS, AND THEIR IMPLICATIONS FOR BROADER ISSUES

Don A. VandenBerg, K. Brogaard¹, R. Leaman^{2,3,4}

*Department of Physics & Astronomy, University of Victoria, P.O. Box 3055, Victoria,
B.C., V8W 3P6, Canada*

vandenbe@uvic.ca, kfb@phys.au.dk, rleaman@uvic.ca

L. Casagrande

*Research School of Astronomy & Astrophysics, Mt. Stromlo Observatory, The Australian
National University, ACT 2611, Australia*

luca@mso.anu.edu.au

ABSTRACT

Ages have been derived for 55 globular clusters (GCs) for which *Hubble Space Telescope* ACS photometry is publicly available. For most of them, the assumed distances are based on fits of theoretical zero-age horizontal branch (ZAHB) loci to the lower bound of the observed distributions of HB stars, assuming reddenings from empirical dust maps and metallicities from the latest spectroscopic analyses. The age of the isochrone that provides the best fit to the stars in the vicinity of the turnoff (TO) is taken to be the best estimate of the cluster age. The morphology of isochrones between the TO and the beginning part of the subgiant branch (SGB) is shown to be nearly independent of age and chemical abundances. For well-defined CMDs, the error bar arising just from the “fitting” of ZAHBs and isochrones is $\approx \pm 0.25$ Gyr, while that associated with distance

¹Current Address: Stellar Astrophysics Centre, Department of Physics & Astronomy, Aarhus University, 120 Ny Munkegade, Building 1520, 8000 Aarhus C, Denmark

²Instituto de Astrofísica de Canarias, Spain

³Dept. Astrofísica, Universidad de La Laguna, Spain

⁴Current Address: Instituto de Astrofísica de Canarias, Vía Láctea s/n, E-38200 La Laguna, Spain

and chemical abundance uncertainties is $\sim \pm 1.5$ –2 Gyr. The oldest GCs in our sample are predicted to have ages of ≈ 13.0 Gyr (subject to the aforementioned uncertainties). However, the main focus of this investigation is on relative GC ages. In conflict with recent findings based on the *relative main-sequence fitting* (rMSF) method, which have been studied in some detail and reconciled with our results, ages are found to vary from mean values of ≈ 12.5 Gyr at $[\text{Fe}/\text{H}] \lesssim -1.7$ to ≈ 11 Gyr at $[\text{Fe}/\text{H}] \gtrsim -1$. At intermediate metallicities, the age-metallicity relation (AMR) appears to be bifurcated: one branch apparently contains clusters with disk-like kinematics, whereas the other branch, which is displaced to lower $[\text{Fe}/\text{H}]$ values by ≈ 0.6 dex at a fixed age, is populated by clusters with halo-type orbits. The dispersion in age about each component of the AMR is $\sim \pm 0.5$ Gyr. There is no apparent dependence of age on Galactocentric distance (R_G) nor is there a clear correlation of HB type with age. As previously discovered in the case of M 3 and M 13, subtle variations have been found in the slope of the SGB in the color-magnitude diagrams (CMDs) of other metal-poor ($[\text{Fe}/\text{H}] \lesssim -1.5$) GCs. They have been tentatively attributed to cluster-to-cluster differences in the abundance of helium. Curiously, GCs that have relatively steep “M 13-like” SGBs tend to be massive systems, located at small R_G , that show the strongest evidence of *in situ* formation of multiple stellar populations. The clusters in the other group are typically low-mass systems (with 2–3 exceptions, including M 3) that, at the present time, should not be able to retain the matter lost by mass-losing stars due either to the development of GC winds or to ram-pressure stripping by the halo interstellar medium. The apparent separation of the two groups in terms of their *present-day* gas retention properties is difficult to understand if all GCs were initially ~ 20 times their current masses. The lowest mass systems, in particular, may have never been massive enough to retain enough gas to produce a significant population of second-generation stars. In this case, the observed light element abundance variations, which are characteristic of all GCs, were presumably present in the gas out of which the observed cluster stars formed.

Subject headings: globular clusters: general — stars: abundances — stars: evolution — stars: interiors — stars: Population II

1. Introduction

Until about a decade ago, the age of the oldest globular cluster (GC) was of widespread interest because it provided one of the best available constraints on the age of the universe and thereby on the cosmological model used to describe it (see, e.g., VandenBerg et al. 2002). As it has turned out, observations of the cosmic microwave background (CMB), taken with the WMAP and Planck satellites have since yielded what appears to be a robust, and very precise, estimate of the age of the universe (13.8 Gyr, with an uncertainty of $\lesssim \pm 0.1$ Gyr, see Komatsu et al. 2011, Ade et al. 2013). (This is the age predicted by the flat Λ CDM model that accurately reproduces the observed temperature power spectrum of the CMB.) However, absolute (and relative) GC ages are no less important today than they were prior to the CMB results. In particular, they are needed to test and constrain models for the origin of GCs over the entire metallicity range spanned by them and to provide some insights into the formation and early evolution of galaxies.

For instance, in their extensive review, Brodie & Strader (2006) argued that the most metal-poor GCs formed in low-mass dark matter halos in the early universe (at redshifts $z > 10$), whereas metal-rich systems were created during the subsequent mergers of gas-rich structures that built up the parent galaxies. In a later study, Bekki et al. (2008) used n -body simulations combined with semi-analytic treatments of the main processes that govern galaxy and GC formation (e.g., merging, star formation, supernova feedback, radiative gas cooling) to predict that $\sim 90\%$ of GCs formed in low-mass galaxies at $z > 3$ and that the mean ages of clusters that have $[\text{Fe}/\text{H}] \lesssim -1$ are ~ 0.5 Gyr older than more metal-rich systems. More recently, Elmegreen, Malhotra, & Rhoads (2012) pointed out that dwarf star-forming (Lyman- α emitting) galaxies at intermediate to high redshift have the right size, metallicity, luminosity, and star formation rate to be a natural site for the formation of metal-poor GCs. They suggest that “low metallicities are not the exclusive result of an earlier birth time compared to metal-rich disk and bulge GCs, but rather the result of a lower mass host, considering the (observed) mass-metallicity relation in galaxies”. In other words, metal-poor globular clusters could simply be those systems that happened to form in dwarf galaxies of low metallicity at whatever time the birth event occurred.

Even from these few examples, it is clear that the proposed formation scenarios make different predictions for the age of the oldest GC, the dispersion in age at a fixed iron abundance (perhaps especially at the lowest metallicities), and the variation in age with $[\text{Fe}/\text{H}]$ and galactocentric distance. Unfortunately, despite the efforts made by many researchers over the past ~ 35 years, it has not yet been possible to firmly establish the absolute, or the relative, ages of the Galactic GCs (see, e.g., VandenBerg, Bolte, & Stetson 1990; Chaboyer, Demarque, & Sarajedini 1996; Buonanno et al. 1998; Rosenberg et al. 1999; Carretta et al.

2000; VandenBerg 2000; Salaris & Weiss 2002; and De Angeli et al. 2005). This is apparent even if one considers only those papers that were published after 2008. For example, ages as young as 11 Gyr (di Cecco et al. 2010) or as old as 13.5 Gyr (VandenBerg, Casagrande, & Stetson 2010) have been derived for M 92, which has $[\text{Fe}/\text{H}] \approx -2.35$ (Carretta et al. 2009a, hereafter CBG09). (These seemingly discrepant results are, in fact, due mostly to differences in the adopted distance.) In addition, from an analysis of homogeneous *HST* photometry for 64 GCs, Marín-Franch et al. (2009, hereafter MF09) found that the majority of the clusters with $[m/\text{H}] \lesssim -0.6$ are coeval (to within the uncertainties) with the most metal-deficient systems. However, there are reasons to be concerned with this finding, especially after considering recent estimates of the age of 47 Tucanae.

On the one hand, MF09 obtained a normalized age (= absolute cluster age divided by the mean age of GCs that have $[\text{Fe}/\text{H}] < -1.4$) of 0.96 ± 0.07 for 47 Tuc (which has $[\text{Fe}/\text{H}] = -0.71$ on the metallicity scale by Zinn & West 1984), as compared with values of 1.00 ± 0.04 for M 15 (-2.15) and 1.02 ± 0.04 for M 92 (-2.24), when Dotter et al. (2007, hereafter DSEP) isochrones are used in the analysis. In a follow-up study of the same photometry, Dotter et al. (2010) derived ages of 12.75 ± 0.50 , 13.25 ± 1.00 , and 13.25 ± 1.00 Gyr for 47 Tuc, M 15, and M 92, respectively, using an isochrone-fitting procedure that permitted small adjustments to the distances, reddenings, and metallicities from initial estimates of these quantities given in the 2003 revision of the Harris (1996) catalog. In fact, the cluster parameters adopted by MF09 and Dotter et al. are sometimes quite different; e.g., the latter assumed $[\text{Fe}/\text{H}] = -2.40$ for both M 15 and M 92, as well as lower values of $[\alpha/\text{Fe}]$. Moreover, the observed color-magnitude diagrams (CMDs) are not reproduced very well by DSEP isochrones at low metallicities; see Figs. 4 and 5 in the Dotter et al. paper, which show, in turn, that the fiducial sequences of NGC 3201 and NGC 7099 (M 30), from just below the turnoff (TO) to the lower red-giant branch (RGB), cross over isochrones spanning about a 3 Gyr range in age. Of particular concern is the fact that the observed TOs are significantly redder than those of the isochrones in the adopted fits, as this has the effect of making the inferred age somewhat too large (see the discussion in § 3.2 below).

If the same difficulties were found for M 15 and M 92, which is expected to be the case since their CMDs in the vicinity of the turnoff are morphologically indistinguishable from that of M 30 (see VandenBerg 2000, his Fig. 2), then the ages derived by Dotter et al. for all three clusters should be reduced to ≈ 12.75 Gyr, which is identical to their estimate of the age of 47 Tuc. [Although Dotter et al. (2010) do not actually show how well their computations match the CMD of 47 Tuc, their Fig. 3 demonstrates that DSEP isochrones for $[\text{Fe}/\text{H}] = -1.1$ faithfully reproduce the CMD of NGC 6362, which suggests that these models are not problematic in the metal-rich regime. It is regrettable that Dotter et al. provided such plots for only three GCs, as it would have been helpful to see how well their models fare

for more of the most metal-deficient systems as well as those at the highest metallicities.]

On the other hand, using the same DSEP isochrones, Thompson et al. (2010) derived an age of 11.25 ± 0.21 (random) ± 0.85 (systematic) Gyr for 47 Tuc on the assumption of $[\text{Fe}/\text{H}] = -0.70$, $[\alpha/\text{Fe}] = 0.4$, $Y = 0.255$, and an apparent distance modulus, $(m - M)_V = 13.35 \pm 0.08$, which is based on the properties of the eclipsing binary member known as V69. This compares quite favorably with the determination of 11.0 Gyr by Vandenberg et al. (2010), if $(m - M)_V = 13.40$ and similar chemical abundances are assumed, in an investigation that also reported an age of 13.5 Gyr for M 92. Because the distance moduli adopted by Vandenberg et al. are within 0.05 mag of those implied by fits of computed zero-age horizontal-branch (ZAHB) loci to the lower bound of the distributions of cluster HB stars performed by Vandenberg (2000), it is not a surprise that both studies found 47 Tuc to be about 2.5 Gyr younger than M 92. In fact, notwithstanding small differences in the adopted cluster properties, the binary- and ZAHB-based distance moduli for 47 Tuc agree very well with the value of $(m - M)_V = 13.375$ that was obtained by Bergbusch & Stetson (2009) from fits of the cluster main-sequence (MS) to nearby subdwarfs having similar metal abundances and well-determined trigonometric parallaxes from *Hipparcos* (van Leeuwen 2007). Indeed, these results, coupled with the fact that high ages ($\gtrsim 13$ Gyr) are obtained for M 92 when its distance is similarly derived either from fits to local subdwarfs (An et al. 2009, see their Table 2) or from the luminosity of its HB stars (Vandenberg 2000, also see Benedict et al. 2011), appear to rule out a common age for 47 Tuc and the most metal-deficient GCs. At the very least, they call into question the findings of MF09 and Dotter et al. (2010).

The present investigation has been undertaken mainly to study and to try to resolve the discrepancies discussed above concerning relative GC ages. However, we have also taken this opportunity to derive the absolute ages of most of the clusters considered by MF09 on the assumption of ZAHB-based distances. § 2 briefly discusses the photometric data and the stellar evolutionary models that have been used, while § 3 describes what we consider to be the most robust and least model-dependent way of deriving the ages of globular clusters from their CMDs. The reliability of the adopted distance scale is examined in § 4. Ages are determined in § 5: the results are supported by plots for the majority of the GCs that we have analyzed to show how well the isochrones match the observations. Particular attention is paid to the so-called “second-parameter” clusters M 3 and M 13, as well as M 5, M 12 (NGC 6218), NGC 288, and NGC 362, and to those clusters in the metallicity range $-2.0 \lesssim [\text{Fe}/\text{H}] \lesssim -1.6$ with extended blue HBs. Some evidence is provided to support the possibility that enhanced helium abundances are responsible for most (but not all) of these phenomena. The main results of this study are reported in § 6, which also explains (see § 6.1.1) why MF09 obtained ages for metal-rich GCs that are too high and, therefore, why they failed to find a significant variation of age with $[\text{Fe}/\text{H}]$, as obtained here. Concluding remarks are given in

§ 7.

2. The Input Observational and Theoretical Data Bases

The same photometric data that were analyzed by MF09 are studied here; namely, the $F606W$, $F814W$ observations that were obtained by Sarajedini et al. (2007) for > 60 globular clusters using the Advanced Camera for Surveys (ACS) on the *Hubble Space Telescope*.¹ The adopted zero points in the publicly available catalog are those given by Sirianni et al. (2005), with the small adjustments to them subsequently determined by Bohlin (2007): the latter have the effect of making the $F606W$ and $F814W$ magnitudes fainter by 22 and 25 mmag, respectively.² In order to minimize the photometric scatter and to ensure that the principal cluster sequences are well-defined, the CMDs have been limited to only those stars for which the tabulated uncertainties in the magnitudes are < 0.030 mag. (The “readme” file associated with the catalog explains how these errors were calculated.) If the total number of stars that satisfies this criterion exceeded $\sim 25,000$, this cutoff was reduced to 0.015 mag. With relatively few exceptions, each of the resultant GC data sets contained at least 10,000 stars. To determine the intrinsic colors of the stars, we have assumed the $E(B - V)$ values given by the Schlegel, Finkbeiner, & Davis (1998) dust maps, except in a few cases (which are flagged) where they were obviously problematic, together with $E(m_{F606W} - m_{F814W}) = 0.984 E(B - V)$ (Sirianni et al. 2005). (It will become evident in the next section that, because the models are forced to match the turnoff color in order to derive the correct estimate of the cluster age for the assumed distance and metallicity, uncertainties associated with the adopted value of $E(B - V)$ or with the relation between $E(m_{F606W} - m_{F814W})$ and $E(B - V)$ are of no consequence for the age that is obtained.)

As far as the stellar models are concerned, we opted to use the grids of evolutionary tracks computed by VandenBerg et al. (2012, hereafter VBD12) for the so-called “GSCX” metals mixture. This assumes the Grevesse & Sauval (1998) solar abundances, with the enhancements in the abundances of the individual α -elements (at low metallicities) given by Cayrel et al. (2004), appropriately scaled to $[\text{Fe}/\text{H}]$ values from -3.0 to 0.0 , in 0.2 dex intervals. (Because $[\text{O}/\text{Fe}] = 0.5$, while most of the other α -elements have $[m/\text{Fe}] = 0.25$ – 0.4 dex enhancements, the overall value of $[\alpha/\text{Fe}]$ is $+0.46$ in the very metal-deficient stars observed by Cayrel et al.) As shown by VandenBerg et al. (2010), these models appear to provide good fits to optical CMDs for both metal-poor and metal-rich GCs and they

¹See <http://archive.stsci.edu/prepds/acsggct>

²See http://www.stsci.edu/hst/acs/analysis/zeropoints/old_page/localZeropoints.

reproduce quite satisfactorily the properties of local subdwarfs that have $-2.0 \lesssim [\text{Fe}/\text{H}] \lesssim -0.6$ and well-determined M_V values, as derived from *Hipparcos* parallaxes (van Leeuwen 2007). Since, in this investigation, the adopted GC distances are based on the predicted luminosities of ZAHB models, we have generated fully consistent ZAHB loci in the canonical way (see VandenBerg et al. 2000) using exactly the same stellar evolutionary code that is described in detail by VBD12.

To transpose the models from the theoretical to the observed plane, bolometric corrections (BCs) for several ACS bandpasses, including *F606W* and *F814W*, have been derived from synthetic spectra based on the latest MARCS model atmospheres (Gustafsson et al. 2008).³ As in the case of the Sarajedini et al. (2007) *HST* photometry, the Bohlin (2007) spectrum of Vega was used to set the zero points of the predicted BCs. Because MARCS model atmospheres were not computed for T_{eff} values > 8000 K, the aforementioned transformations were supplemented by the BCs for hotter stars that were kindly provided to us by S. Cassisi (private communication, also see Bedin et al. 2005). The latter, which apply to Castelli-Kurucz model atmospheres, were corrected by amounts ranging from -0.018 to $+0.012$ mag, depending on the metallicity, in order to ensure that there is good continuity of the BC values over the entire temperature range that encompasses the stellar models. (These numbers are the average differences between the bolometric corrections in the two data sets at 8000 K, as calculated from the BC entries at $\log g$ values from 2.0 to 5.0.) The only models in this study that have $T_{\text{eff}} > 8000$ K are ZAHB models and, as shown in § 3.2 and § 5, they generally provide rather good fits to the HB populations of GCs that are nearly unreddened, when the Schlegel et al. (1998) $E(B - V)$ values are assumed; i.e., there is no compelling evidence that the predicted colors should be further corrected in any way.

When comparing isochrones and ZAHB loci with observed CMDs, we have assumed the $[\text{Fe}/\text{H}]$ values given by CBG09 for the GCs in our sample, along with $[\alpha/\text{Fe}] = 0.46$ at $[\text{Fe}/\text{H}] \leq -0.76$ (approximately the metallicity where the $[\text{O}/\text{Fe}]$ and $[\alpha/\text{Fe}]$ versus $[\text{Fe}/\text{H}]$ relations for field halo stars change slope; e.g., Ramírez, Meléndez, & Chanamé 2012). At higher iron abundances, $[\alpha/\text{Fe}]$ has been assumed to decline linearly with $[\text{Fe}/\text{H}]$ in order to reach a value of 0.0 at $[\text{Fe}/\text{H}] = 0.0$. We have also adopted $Y = 0.2500$ at $[\text{Fe}/\text{H}] \leq -1.0$, in good agreement with the primordial helium abundance (0.2485 ± 0.0016 , Komatsu et al. 2011, see their §4.8), and slightly larger values at $[\text{Fe}/\text{H}] > -1.0$, to be consistent with $\Delta Y/\Delta Z = 1.4$. Approximately this value of the helium enrichment parameter is obtained if Y varies from

³These transformations, along with those which are applicable to many other widely used photometric systems, will be the subject of a forthcoming paper by L. Casagrande et al. (in preparation). These have been computed following the formalism described by Casagrande, Portinari, & Flynn (2006, also see VandenBerg et al. 2010, their §2).

0.2485 at $Z = 0.0$ to the initial Y , Z values which are typically assumed in Standard Solar Models (SSMs) that take diffusive processes into account (see, e.g., Bahcall & Pinsonneault 1995, Turcotte et al. 1998).⁴ In this way, the values of $[\text{Fe}/\text{H}]$, $[\alpha/\text{Fe}]$, and Y specific to each GC have been set. Isochrones for the same values of these chemical abundance parameters were then obtained by interpolating within the many grids of evolutionary tracks provided by VBD12, using the code described by them.

3. Ages Determined from $\Delta V_{\text{TO}}^{\text{HB}}$ Observations

3.1. General Considerations

The parameter $\Delta V_{\text{TO}}^{\text{HB}}$ was originally (Sandage 1982, Iben & Renzini 1984) used to represent the difference in magnitude between the MS turnoff and the HB, measured at the color of the TO. However, it was appreciated early on that, since a cluster fiducial is vertical at the TO (by definition) as well as a slowly varying function of color over a fairly large range in magnitude above and below this point, the turnoff luminosity and its variation with age cannot be determined to very high precision. To circumvent this difficulty, Chaboyer et al. (1996) suggested that $\Delta V_{\text{TO}}^{\text{HB}}$ be measured at a point that is brighter and slightly redder than the turnoff (by 0.05 mag) as this would involve a much smaller uncertainty. The other well-known difficulty with the $\Delta V_{\text{TO}}^{\text{HB}}$ technique for measuring cluster ages is that, in many GCs, the horizontal part of the HB is not populated; i.e., the core He-burning stars are located either well to the blue of the instability strip or close to the RGB in a “red clump”. However, in such cases, theoretical ZAHB loci may be used to extrapolate from the observed distributions of HB stars to the color where $\Delta V_{\text{TO}}^{\text{HB}}$ is evaluated, especially if the same models perform well when applied to clusters of similar metallicity in which their HB populations have colors that overlap those of their TO and subgiant (SGB) stars. Alternatively, a different method should be used to determine the relative ages of GCs, such as a calibration of the difference in color between the MSTO and the RGB in terms of age according to the prescription described in the pioneering study by VandenBerg et al. (1990).

Our implementation of the $\Delta V_{\text{TO}}^{\text{HB}}$ method is more implicit than those versions described

⁴We decided to use a slightly larger helium enrichment factor than that implied by our SSM for the Grevesse & Sauval (1998) metals mixture because the Victoria models do not take the diffusion of the metals into account — just the gravitational settling of helium (which is primarily responsible for the reduction in age at a given turnoff luminosity due to diffusive processes). To satisfy the solar constraint, our SSM requires $Y_i = 0.2661$ and $Z_i = 0.0162$ for the initial helium and metals mass-fraction abundances, as well as $\alpha_{\text{MLT}} = 2.007$ for the usual mixing-length parameter. This model implies $\Delta Y/\Delta Z \approx 1.1$.

above. No attempt is made to determine the luminosity of the HB at a particular color. Rather, a theoretical ZAHB for the appropriate chemical abundances is fitted to the lower bound of the observed distribution of HB stars (since core He-burning stars are predicted to evolve to higher luminosities as they age), after the observed colors have been dereddened, to determine the apparent distance modulus. Once the absolute magnitude scale has been set in this way, there is only one isochrone for the assumed metallicity that will provide a simultaneous match to the observed turnoff color and the beginning of the cluster SGB. To identify it, isochrones for different ages must each be shifted horizontally in color by whatever amount, if any, is required to reproduce the observed turnoff color when they are overlaid onto the photometric data. If a given isochrone is too young or too old, its SGB segment will be too bright or too faint, respectively, relative to the observed stars. By iterating on the age, the best-fit isochrone can be readily determined.

The same thing can be accomplished by first shifting all of the isochrones for an appropriate range in age to a common TO color (specifically, to the observed turnoff color), and then overlaying the resultant grid onto the cluster CMD. As before, the age of the cluster is equated to the age of the isochrone that provides the best superposition of the subgiant stars just past the TO. It should be appreciated that the color adjustments which are applied to the models do not affect the predicted age-luminosity relations for any point along the isochrones (e.g., at the turnoff or at the location on the SGB that is 0.05 mag redder than the TO). These offsets are needed because, in general, the predicted and observed color scales will not be in perfect agreement due to, for instance, errors in the color- T_{eff} relations, uncertainties in the treatment of some of the stellar physics ingredients (e.g., superadiabatic convection, surface boundary conditions), or incorrect assumptions regarding the cluster properties (reddening, distance, metallicity). Only by matching the predicted and observed TOs are we able to reliably ascertain which isochrone provides the best fit to an observed CMD in the vicinity of the TO, including the turnoff luminosity.

The main difference between our approach and that advocated by Chaboyer et al. (1996) is that we fit isochrones directly to the observed distributions of stars that have colors within approximately 0.05 mag of the turnoff — especially brighter than the TO, but also below it — instead of relying on just two points (i.e., the TO color and the selected SGB fiducial point) to infer an age. In the case of the Chaboyer et al. technique, one has no idea how well the isochrones are able to match the morphology of the observed CMD, though it is implicitly assumed that they do. In fact, as shown below, modern stellar models that take diffusive processes into account do reproduce the shapes of GC CMDs in the vicinity of the turnoff very well. As a consequence, essentially identical ages would be obtained using either the method that we have employed or that described by Chaboyer et al.

To better appreciate the reasons for, and the advantages of, comparing isochrones with observations in the particular way that we have described, it is helpful to consider several plots, beginning with Figure 1. This illustrates the appearance on the $[(M_{F606W} - M_{F814W}), M_{F606W}]$ -plane of a representative set of isochrones; in this case, for $[\text{Fe}/\text{H}] = -1.4$ (roughly the mean metallicity of the Galactic GCs), $[\alpha/\text{Fe}] = 0.46$, $Y = 0.250$, and ages of 10 to 13 Gyr, in 0.5 Gyr increments. Due to the use of the state-of-the-art interpolation code developed by P. Bergbusch (see Bergbusch & Vandenberg 2001, and references therein, as well as the latest updates reported by VBD12), and to the well-behaved derivatives of $\log L$ and $\log T_{\text{eff}}$ with respect to time along the computed evolutionary tracks, the isochrones have especially smooth morphologies.

In the upper left-hand panel of Figure 2, the 10 Gyr isochrone from the previous figure has been replotted so that the abscissa gives the color relative to the turnoff color and the ordinate specifies the magnitude with respect to a point on the upper MS that is 0.05 mag redder than the TO. Isochrones for all of the other ages were then superimposed in such a way that, after registering them to the same abscissa and ordinate zero points, additional (small) vertical shifts were applied, if needed, in order to minimize the differences in their magnitudes at the aforementioned color offset both above *and* below the TO. It is clear that, as the result of this centering procedure, which yielded the δM_{F606W} information provided in the legend, all of the isochrones have essentially identical turnoff luminosities. Thus, we have determined, for instance, that the turnoff luminosities of 10.5 and 13.0 Gyr isochrones are, respectively, 0.051 mag and 0.263 mag fainter than that of the 10.0 Gyr isochrone. These numbers are very precise, with uncertainties at the level of $\lesssim \pm 0.005$ mag. However, we do not need, or use, these numerical results in our age-dating technique. What is important is that we have demonstrated that the shapes of isochrones within 0.05 mag of the TO are essentially independent of age; consequently, there is no basis for preferring one isochrone over another (in a given grid) from a morphological perspective when they are restricted to comparisons with observed CMDs in the vicinity of the turnoff. The bottom left-hand panel shows that this conclusion holds for other metallicities.

We realized, after creating the upper left-hand panel of Fig. 2, that we could easily evaluate the errors associated with the MF09 “relative main-sequence fitting” (rMSF) method, at a fixed metallicity, through further manipulations of the isochrones. Beginning with the grid as plotted in that panel, all of the older isochrones were shifted horizontally to the red until their RGB segments overlaid that of the 10 Gyr isochrone — resulting in the middle panel (top row). From this starting point, it is easy to achieve a simultaneous coincidence of the RGB and lower MS segments of all of the isochrones, which is the essence of the MF09 approach, by simply shifting them along a line that is parallel to the giant branch. This can be easily accomplished if a horizontal line is drawn in the middle panel at, say, an ordinate

value of 1.0 and the difference in color between any two isochrones is evaluated from their intersection with that line. A triangle can then be defined in which this color difference is the length of one of its sides and the angles at each vertex may be determined from fact that the other two sides have slopes equal to those of the MS and the RGB. This is sufficient information that, with the aid of simple trigonometry, the small horizontal and vertical shifts that are needed to obtain the results shown in the upper right-hand panel are easily calculated. (The plots in the bottom row present similar results for isochrones computed on the assumption of $[\text{Fe}/\text{H}] = -2.40$.)

The legends in the right-hand panels for both metallicities list the adjustments in M_{F606W} so derived. These are the differences in the turnoff luminosities, relative to that of the youngest isochrone in each grid, that are obtained when isochrones are aligned according to the MF09 formalism. (Note that these results would be more uncertain if we had attempted to determine the TO luminosities explicitly, instead of employing our indirect, but more accurate and precise method.) Interestingly, they agree quite well with the results reported in the legends of the left-hand panels (particularly at the lowest $[\text{Fe}/\text{H}]$ value); and, as expected, the former are somewhat less than the latter. Some compression of the range of TO luminosities for the same age range can be expected because, as readily appreciated by considering Fig. 1, it is necessary to move the older isochrones upwards and to the left, in a direction parallel to the lower MS, in order to force their giant branches to match the RGB of the youngest isochrone without causing any separation of their respective lower main sequences. The errors, which are small compared with other sources of uncertainty, arise simply because the location of the RGB is not independent of age, though the dependence is quite weak (as noted by MF09). Indeed, Fig. 2 provides encouraging support for the rMSF method, at least when applied to GCs having similar metal abundances, which implies that any problems with the MF09 study must arise in the connection of their results for the different metallicity groups. This is fully discussed in § 6.1.1.

Figure 3 is similar to the left-hand panels of Fig. 2 except that isochrones for the same age (12 Gyr), helium content, and α -element abundances, but different $[\text{Fe}/\text{H}]$ values ($-2.4 \leq [\text{Fe}/\text{H}] \leq -1.4$, in 0.2 dex increments) are considered. The thinness of the line at the turnoff, as well as slightly above and below it, indicate that all of the isochrones have exactly the same TO luminosities as a result of the color and magnitude adjustments that have been applied. (The table contained within the plot lists the differences in the TO magnitudes between the more metal-rich isochrones and that for $[\text{Fe}/\text{H}] = -2.4$. We see from a comparison of these results with those given in the left-hand panels of Fig. 2 that the effect on the turnoff luminosity of varying the metallicity by 0.2 dex is slightly larger than the impact of varying the age by 0.5 Gyr.) Although the remaining parts of the isochrones that lay within the region enclosed by the dashed rectangle are not quite as “perfectly” coincident as they are

at the TO, the models span a much larger range in metallicity than one would normally consider when comparing isochrones with the CMD of a given cluster. Most would agree that the $[\text{Fe}/\text{H}]$ values of the majority of GCs are known to within ± 0.1 – 0.2 dex (compare, e.g., the $[\text{Fe}/\text{H}]$ determinations for clusters in common to the studies by Zinn & West 1984, Kraft & Ivans 2003, and CBG09), and had we restricted Fig. 3 to a plot of isochrones that span a range in $[\text{Fe}/\text{H}]$ of only 0.2–0.3 dex, a noticeable reduction in the morphological variations near the TO would have been apparent. Be that as it may, the main conclusion to be drawn from Fig. 3 is that the shapes of isochrones (for a given heavy-element mixture) within ~ 0.05 mag of the turnoff are predicted to be *nearly* independent of $[\text{Fe}/\text{H}]$, at least at values of -1.4 and less.

At higher metallicities, the opacities in stellar interiors become larger at an increasingly rapid rate, which impacts the predicted mass-luminosity relations (i.e., the turnoff mass at a fixed age) to an ever greater extent. As a result of the latter, the subgiant branch of, say, a 12 Gyr isochrone becomes noticeably flatter as the $[\text{Fe}/\text{H}]$ value increases above ≈ -1.2 . This is illustrated in Figure 4. (The drop in SGB luminosities occurs because it takes more energy to expand the envelope of a more massive star as it evolves towards the RGB.) Interestingly, when measured at the same luminosity offset from the turnoff, the MSTO-to-RGB color difference at a fixed age is predicted to have no more than a slight dependence on metal abundance at $[\text{Fe}/\text{H}] \gtrsim -1.4$.

As shown in Figure 5, the near invariance of the morphology of the turnoff portions of isochrones for high ages is also found when Y , $[\alpha/\text{Fe}]$, and even the value of the mixing-length parameter, α_{MLT} , are varied. Except for the beginning of the SGB (the part inside the dashed rectangle), the shapes of isochrones for post-TO phases, as well as the location of the RGB relative to the turnoff, clearly depend quite sensitively on these parameters (as well as on age and $[\text{Fe}/\text{H}]$). As a result, one should not be concerned if the isochrone that is fitted to the turnoff observations fails to reproduce the location of the giant branch: there are too many uncertainties that affect the predicted T_{eff} and color scales to expect perfect consistency. The only models that we have found which are appreciably offset from the others within the region enclosed by the dashed rectangle are those that neglect diffusive processes (as represented by the *long-dashed curve*), though the differences are still quite small. However, helioseismic studies established the importance of this physics many years ago (see, e.g., Christensen-Dalsgaard, Proffitt, & Thompson 1993; Bahcall et al. 1997; Turcotte et al. 1998). The main point of Figs. 2, 3, and 5 is that parameter variations appear to have little or no impact on the shapes of isochrones near the turnoff (at least for ages $\gtrsim 10$ – 11 Gyr), and hence that our isochrone-fitting procedure has a solid footing. Small differences are, in any case, neither observationally detectable nor of significant importance for the inferred ages.

It is worth pointing out that the same conclusions would have been reached had the isochrones been plotted on the $V - I$, V or $B - V$, V diagrams. For instance, the superpositions of the various loci in Figure 6 look no different from those shown in the left-hand panels of Fig. 2. The same thing will likely be found when other photometric systems and filter bandpasses are used because the total range in T_{eff} spanned by ~ 10 –13 Gyr between the TO and the beginning of the SGB is quite small. However, this is something that will need to be checked on a case-by-case basis: it is beyond the scope of this study to do so here. Similarly, our results should not be extrapolated to ages outside the ranges that we have considered. Had we included isochrones for younger ages in the aforementioned plots, some deviations between them and the older isochrones in the vicinity of the turnoff would have been evident. Our results have been restricted to the age ranges that are relevant to the GCs in our sample.

3.2. Application to M 5

In the case of a well-defined CMD, our implementation of the $\Delta V_{\text{TO}}^{\text{HB}}$ method will provide a highly precise age, whose accuracy depends almost entirely on the adopted distance and chemical abundances. So-called “fitting errors” are not of significant importance. Consider, for example, the CMD of M 5 (NGC 5904) from the Sarajedini et al. (2007) database that is shown in Figure 7 for the region within $\sim \pm 1.5$ mag of the turnoff. From least-squares fits to the median points that are derived after the photometry has been sorted into 0.10 mag bins, the observed turnoff color is found to be 0.4738. (As long as this number has been determined to better than ~ 0.005 mag, which is appreciably larger than its uncertainty, the age that is found from an overlay of isochrones onto the turnoff photometry is not significantly affected; see below.) To place the data on the $[(m_{F606W} - m_{F814W})_0, M_{F606W}]$ -plane, we have assumed the indicated reddening and an apparent distance modulus of 14.38, which is based on the fit of a ZAHB to the cluster counterpart (to be discussed shortly).

To determine the age of M 5, isochrones for $Y = 0.250$, $[\text{Fe}/\text{H}] = -1.33$ (CBG09), and enhanced α -element abundances (see § 2) were generated for ages from 10.5 to 12.5 Gyr, in steps of 0.25 Gyr, once preliminary fits had narrowed the age range. Each isochrone was then shifted horizontally, in turn, by whatever amount was needed in order for the predicted and observed turnoff colors to match, until the one was found that provided the best fit to the beginning part of the SGB (the stars within the dotted rectangle brighter than $M_{F606W} \sim 4$). Just by inspection, it is obvious that an isochrone for 11.5 Gyr (the solid curve) reproduces the mean stellar distribution in the vicinity of the TO very well and that isochrones for ages which differ by ± 0.5 Gyr or ± 1.0 Gyr (the dashed curves) do not. The

“fitting” error, which appears to be at the level of $\lesssim \pm 0.2$ Gyr, is a small fraction of the total uncertainty associated with the derived age given that, in particular, a change of ± 0.10 mag in the assumed distance modulus would result in an age that differs by about ± 1.0 Gyr (see the tabular results in the right-hand panels of Fig. 2). Moreover, varying the adopted abundances of helium or oxygen would affect the age at a given turnoff luminosity by a small or a large amount, depending on the size of the variation; see VBD12. For instance, a change in the oxygen abundance by a factor of two would alter the inferred age by ~ 1.0 Gyr.

Fortunately, the other heavy elements are much less important for predicted TO luminosity versus age relations (see VBD12), though they do have some impact on ZAHB-based distance determinations. In the left-hand panel of Figure 8, a ZAHB for the same chemical abundances that were assumed in the previous figure has been fitted to the lower bound of the distribution of HB stars in M 5, yielding $(m - M)_{APP} = 14.38$. As shown in the right-hand panel, an equally good fit to the cluster HB is obtained on the assumption of an apparent modulus of 14.34 and $[\text{Fe}/\text{H}] = -1.18$ (instead of -1.33), with the values of Y and $[\alpha/\text{Fe}]$ left unchanged. The ages that are obtained by matching the corresponding isochrones onto the TO observations differ by only 0.25 Gyr. Thus, a 0.15 dex change in the adopted $[\text{Fe}/\text{H}]$ value does not have major consequences for the derived age, though (of course) the *actual* distance and reddening of M 5 must be known in order to determine the true age of this system. However, this is not a concern for *relative* GC ages. In fact, it is a further advantage of using the $\Delta V_{\text{TO}}^{\text{HB}}$ method to determine cluster-to-cluster variations in age that the inferred ages have a reduced dependence on the adopted metal abundance — because both the HB and the TO, at a fixed age, become fainter as the $[\text{Fe}/\text{H}]$ value increases, albeit not at exactly the same rate. On the other hand, as shown in our analysis of the M 13 CMD in § 5.3.1, $\Delta V_{\text{TO}}^{\text{HB}}$ ages are highly sensitive to the assumed helium content given that the luminosity of the HB is predicted to be a strong function of Y .

As in the case of M 5, we have found that the best-fit isochrones generally need to be offset to the blue by 0.01–0.025 mag (see § 5) in order to reproduce the observed turnoff colors, even though our ZAHBs appear to be able to match the cluster HBs without such color adjustments. Indeed, throughout this investigation, the $\delta(\text{color})$ values that are specified in plots similar to Fig. 8 have been applied only to the isochrones, not to the ZAHB loci. (This practice will have little, or no, impact on our results because our distance determinations are based primarily on the nearly horizontal part of a ZAHB. If small color offsets were applied to our ZAHB models, they would have noticeable consequences only at the blue end.) The cause of such discrepancies is not known, though one can speculate that, among other possible explanations, the assumed $[\text{Fe}/\text{H}]$ or $[\text{O}/\text{Fe}]$ values are slightly too high, the gravity and/or temperature dependencies of the adopted color transformations are not quite right, or there are minor problems with, say, the treatment of the diffusion and extra-mixing

physics or of the atmospheric boundary condition.⁵ However, a resolution of this matter is not needed here because discrepancies between the predicted and observed turnoff colors do not affect the derived $\Delta V_{\text{TO}}^{\text{HB}}$ ages, *provided* that the isochrones are corrected for them when the age is evaluated.

This is demonstrated in Figure 9. The middle panel is equivalent to Fig. 7, except that isochrones for the same chemical abundances have been plotted for ages of 10 to 13 Gyr, in steps of 1 Gyr, have not been shifted in the horizontal direction to a common TO color. The models clearly provide a very good match to the observed morphologies of the MS and SGB and, as deduced from the earlier plot, the implied age of M 5 is very close to 11.5 Gyr. In the left- and right-hand panels, the same isochrones have arbitrarily been shifted by 0.015 mag to the red and to the blue, respectively, to force a mismatch between theory and observations. Indeed, if we had not shifted our isochrones by 0.025 mag to the blue (middle panel), their superposition onto the cluster CMD would have looked similar to that shown in the left-hand panel, but appearing even more discrepant. On the other hand, the case shown in the right-hand panel bears considerable similarity to the fits of isochrones to the NGC 3201 and M 30 CMDs that were reported by Dotter et al. (2010). Regardless of how well the models reproduce the colors of real stars, these sorts of discrepancies could easily arise if, for instance, the assumed reddenings are wrong.

It is clearly much more difficult to derive the age of M 5 if the isochrones do not fit the MS and TO observations. Whereas an age near 11 Gyr seems to be indicated by the overlay of the models onto the observed SGB in the left-hand panel, a significantly higher age (at least 12 Gyr) would be favored by the comparison shown in the right-hand panel. These estimates differ from the correct age (for the assumed distance and chemical abundances) by about 0.5 Gyr. The reason why isochrones are compared with observed CMDs is to determine which one provides the optimum match to the locus of stars from just below the turnoff to the beginning of the SGB, as this isochrone is presumably the one that best reproduces the observed turnoff luminosity. This can be evaluated only if each isochrone that is considered is first adjusted in color, if necessary, so that the predicted and observed TO colors agree. The fact that Dotter et al. (2010) failed to do this in the case of NGC 3201 and M 30 is the reason why the ages that they determined for these GCs (and possibly other metal-deficient clusters) are too high for the assumed distances by ~ 0.5 Gyr, judging from the results presented in Fig. 9. [In comparing isochrones with observed CMDs, Dotter

⁵In fact, preliminary work has revealed that evolutionary tracks and isochrones for low metallicities are hotter/bluer by approximately the requisite amount if MARCS model atmospheres (Gustafsson et al. 2008) are attached to the interior structures at the photosphere or at an optical depth $\tau = 100$. Thus, we have good reason to suspect that the treatment of the atmosphere is mainly responsible for this difficulty.

et al. (see their §4.2) applied “minor adjustments” to initial estimates of $[\text{Fe}/\text{H}]$, distance modulus, and reddening from the Harris (1996; 2003 revision) catalog “to improve the fit to the unevolved main sequence first and the RGB second”. As discussed in § 6.1.2, there is no reason to expect that such fine-tuning will lead to improved interpretations of observed CMDs, especially if the resultant overlays of the models onto the TO and SGB observations make it difficult to identify the best-fit isochrone.]

4. The ZAHB-based Distance Scale

It is relatively straightforward to apply the $\Delta V_{\text{TO}}^{\text{HB}}$ method described above to at least 30 of the GCs in the Sarajedini et al. (2007) sample, less so for most of the rest. However, before considering those clusters with the most easily fitted HB populations, it is important to show that the luminosities of our ZAHBs are in satisfactory agreement with observational constraints, as this implies that the derived distance moduli (and hence ages) are reasonably accurate in an absolute sense. The open circles in the top panel of Figure 10, which are connected by the solid curve, give the predicted M_V values for the ZAHB models at each of nine $[\text{Fe}/\text{H}]$ values from -2.40 to -0.80 , assuming $Y = 0.25$. They were evaluated at $\log T_{\text{eff}} = 3.85$, which is characteristic of variable stars near the center of the instability strip (see, e.g., Sandage 1990a, Cacciari 2013). Since the mean magnitude of the RR Lyrae stars in GCs that have $[\text{Fe}/\text{H}] \approx -1.5$ is about 0.10 mag brighter than the ZAHB (Sandage 1993), the dotted curve, which is obtained if the solid curve is shifted upwards by 0.10 mag, should be compared with empirical determinations of RR Lyrae luminosities at similar metal abundances.

From an analysis of > 100 RR Lyraes in the Large Magellanic Cloud (LMC), Clementini et al. (2003) obtained $\langle V_0 \rangle = 19.064 \pm 0.064$ at $[\text{Fe}/\text{H}] = -1.5$, together with $\Delta M_V / \Delta [\text{Fe}/\text{H}] = 0.214 \pm 0.047$. These findings, which are based on stars that have $-1.8 \lesssim [\text{Fe}/\text{H}] \lesssim -1.2$ (with only a few outliers), are represented by the dashed line and the attached errorbar if it is assumed that the true distance modulus of the LMC is 18.50 mag (Freedman & Madore 2010, Laney, Jonek, & Pietrzyński 2012, Molinaro et al. 2012). Both the slope and the zero-point clearly agree quite well with the predictions of our models. However, based on new astrometric data for five field RR Lyrae variables from the Fine Guidance Sensors on the *HST*, Benedict et al. (2011, see their table 10) derived $M_V = 0.45 \pm 0.05$ at the reference metallicity. This is just barely consistent at the 1σ level with the Clementini et al. results (see Fig. 10), although the differences are negligible in the case of RR Lyr, which is the star with the smallest errorbar in the Benedict et al. sample. For this variable, the latter obtained $M_V = 0.54 \pm 0.07$, which places it on the dashed line if it has the metallicity that

they adopted ($[\text{Fe}/\text{H}] = -1.41$). On the other hand, UV Oct ($M_V = 0.35 \pm 0.13$, $[\text{Fe}/\text{H}] = -1.47$) is brighter than RR Lyr by nearly 0.2 mag, which leads one to wonder if it is in an advanced evolutionary stage that is much more luminous than the ZAHB for its metal abundance. (This is quite possible since, for instance, about 14% of the RR Lyrae pulsators in M 3 are overluminous according to Cacciari, Corwin, & Carney 2005.) Just one such star would have an impact on the Benedict et al. determination of the mean value of M_V and its uncertainty because their sample contains only a few stars. On the other hand, improved consistency between the Benedict et al. and Clementini et al. results would be obtained if the LMC has $(m - M)_0 > 18.50$.

Statistical parallax and Baade-Wesselink studies have favored considerably fainter absolute magnitudes for RR Lyrae stars. Using the first of these two methods, Gould & Popowski (1998) obtained $M_V = 0.77 \pm 0.13$ at $[\text{Fe}/\text{H}] = -1.60$, which may be compared with $M_V = 0.74 \pm 0.14$ at $[\text{Fe}/\text{H}] = -1.53$ (Fernley et al. 1998) from the application of the second technique. These results, which are represented, in turn, by the open and filled triangles in Fig. 10, would imply rather short distance scales and high ages (greater than the age of the universe) if they are accurate. However, the errorbars are large enough that they do not present a problem at a $\gtrsim 1-2\sigma$ level. From our perspective, it is encouraging that the dotted curve provides a reasonable compromise of all of the above results, though its uncertainty in the vertical direction is quite large ($\sim \pm 0.10$ mag).

Insofar as the slope of the variation of $M_V(\text{RR})$ with $[\text{Fe}/\text{H}]$ is concerned, we (and Benedict et al. 2011) are inclined to favor the value derived by Clementini et al. (2003) because it is based on so many variable stars. Worth mentioning is the fact that BASTI models (Pietrinferni et al. 2006) and those reported by Catelan, Pritzl, & Smith (2004) predict almost the same slopes as our models. Although not shown here, the former are ~ 0.07 mag brighter than ours at $[\text{Fe}/\text{H}] = -1.5$, while the latter are fainter by ~ 0.03 mag, but both run roughly parallel to the dotted and dashed loci in the upper panel of Fig. 10. It should be kept in mind, however, that there is also significant support for $\Delta M_V / \Delta [\text{Fe}/\text{H}] > 0.214$ (see the recent review by Cacciari 2013).

Further support for our models is provided in the bottom panel of Fig. 10. This compares the predicted luminosities (at $\log T_{\text{eff}} = 3.85$) from the same ZAHB models that were plotted in the upper panel with the values derived by De Santis & Cassisi (1999) for seven GCs from an analysis of the pulsational properties of member *ab*-type variables. Although De Santis & Cassisi adopted a different metallicity scale in their investigation, they state that the uncertainties in this scale do not significantly affect their evaluation of $\log L_{3.85}^{\text{ZAHB}}$. Consequently, we have adopted the latest $[\text{Fe}/\text{H}]$ values from CBG09, as assumed throughout this study, in preparing this plot. Except in the case of NGC 1851, which is more luminous

than the theoretical locus at its metallicity by $> 3\sigma$, the solid curve provides a satisfactory fit to the data. (A possible explanation of the relatively high luminosity of the NGC 1851 HB is that this system has a somewhat higher helium abundance than the other GCs considered by De Santis & Cassisi.) On the other hand, it could be argued from these data that the dependence of $\log L_{3.85}^{ZAHB}$ on $[\text{Fe}/\text{H}]$ is somewhat shallower than that predicted by our ZAHB models.

To conclude this section, a few remarks concerning subdwarf-based distances are warranted. As already mentioned in § 2, our isochrones reproduce the properties of local subdwarfs with accurate distances from *Hipparcos* quite well (see Vandenberg et al. 2010). In fact, they do so without requiring any T_{eff} or color shifts whatsoever, if the temperatures derived for them by Casagrande et al. (2010) and the color- T_{eff} relations based on the latest MARCS model atmospheres (Gustafsson et al. 2008) are assumed. Yet, as shown in the next section, the same isochrones must be adjusted to the blue by ~ 0.02 mag, on average, in order for them to match the observed turnoffs of GCs when our ZAHBs are used to determine the cluster distance moduli. The direction of these offsets is such that, were we to use the field subdwarfs to evaluate the cluster distances through the MS-fitting technique, we would obtain larger values of $(m - M)_{APP}$ by ≈ 0.10 mag (on average). However, the local field subgiant HD 140283 suggests that, if anything, our ZAHB-based distances are already too high (see Vandenberg et al. 2002, Bond et al. 2013). This apparent inconsistency has yet to be resolved, though it may indicate, for instance, that GC metallicities, which are based primarily on bright giants, are not on precisely the same scale as those of the nearby field halo dwarfs, that there are some important differences in the chemical abundances of cluster and field stars of similar $[\text{Fe}/\text{H}]$, or ...

This problem is not new, as the same difficulty was reported by Bergbusch & Vandenberg (2001) in their analysis of field subdwarfs using temperatures that were derived for them primarily by Gratton, Carretta, & Castelli (1996). The Gratton et al. and Casagrande et al. T_{eff} scales are quite similar: both are considerably hotter than, e.g., the Alonso, Arribas, & Martinez-Roger (1996) scale, and the assumption of either one enables our models to satisfy the subdwarf constraint. In principle, we *should* adopt $[\text{Fe}/\text{H}]$ values for the GCs which are close to those reported by Carretta & Gratton (1997) (instead of those given by CBG09) since they are based on the hot T_{eff} scale of Gratton et al, but doing so would increase the difficulty of matching the turnoff colors. That is, the assumption of more metal-rich isochrones in fits to a given CMD would require even larger blueward color offsets in order to reproduce the observed photometry. This is obviously a complex and important problem that needs to be resolved as soon as possible. In any case, because distances based on local subdwarfs are much more dependent on the assumed T_{eff} and $[\text{Fe}/\text{H}]$ scales than ZAHB-based distances (see, e.g., the caption of Fig. 8), we have chosen to rely on the latter.

However, the associated distance moduli uncertainties are at least $\sim \pm 0.10$ mag.

5. Globular Cluster Age Determinations

Although the number of globular clusters that contain multiple, chemically distinct, discrete stellar populations appears to be increasing with time, they are *obviously* present in the optical CMDs of only a few of them, including ω Cen (e.g., Bellini et al. 2010), NGC 2808 (Piotto et al. 2007), NGC 1851 (Milone et al. 2008), and M 22 (Marino et al. 2009). They have been found in several others, but the use of ultra-violet (e.g., broad-band U) or specialized filters (e.g., see the investigations of M 4, NGC 288, and M 2 by Marino et al. 2008, Roh et al. 2011, and Lardo et al. 2012, respectively) and/or very careful and precise photometry near the cluster centers has been required to discover them; see, the studies of 47 Tuc by Anderson et al. (2009) and Milone et al. (2012b), of NGC 6752 by Milone et al. (2010), and of NGC 6397 by Milone et al. (2012a). The pioneering Strömngren work that F. Grundahl carried out more than 10 years ago should also be acknowledged since the measured c_1 indices in every GC that he observed revealed the existence of large star-to-star variations in the abundance of nitrogen at sufficiently faint magnitudes on the giant branch (see Grundahl et al. 2000, Grundahl & Briley 2001) that they must have been present in the gas out of which the current MS and lower RGB stars formed. In fact, C–N and O–Na anticorrelations appear to be a universal property of all globular clusters (Carretta et al. 2010b).

For the vast majority of the GCs, such chemical abundance variations do not have a significant impact on the optical CMD analyses presented here. With few exceptions, the total [(C+N+O)/Fe] abundances in the cluster stars appear to be constant to within the observational errors (e.g., Smith et al. 1996), despite the omnipresence of CN-weak and CN-strong stars, and the [Fe/H] variations are known to be very small (Kraft 1994, CBG09). In fact, it is to be expected that the *HST* CMDs considered here generally will exhibit relatively little scatter because the adopted color index, $(m_{F606W} - m_{F814W})$ is similar to Johnson-Cousins $V - I_C$ in not being particularly sensitive to metallicity. Such CMDs can discriminate between stellar populations that have significantly different helium and C+N+O abundances because these elements affect the H-R diagram locations and morphologies of isochrones, but *uv* photometry (preferably narrow-band, perhaps centered on a suitable spectral feature) appears to be needed to detect CMD splittings due to O–Na or Mg–Al anticorrelations (see Sbordone et al. 2011, Cassisi et al. 2013). It is still of some interest to compare isochrones and ZAHB loci for normal He and CNO abundances with the CMDs of GCs that are known to have enhanced abundances of these elements in order to obtain a visual impression of how well such models reproduce the observations. Consequently, such

comparisons are presented below for, e.g., NGC 1851 and NGC 2808, but not for ω Cen, which is dropped from further consideration because of the wide range in $[\text{Fe}/\text{H}]$ that is found in this system. (We note, however, that a detailed investigation of *HST* photometry of ω Cen, using the same Victoria-Regina isochrones as those employed here, and of its chemical evolution, has been recently carried out by Herwig et al. 2012.)

Section 5.1 presents and discusses our results for 24 GCs that are more metal-poor than $[\text{Fe}/\text{H}] = -1.0$, according to CBG09, and that have HB morphologies which can be fitted most reliably by our models. Because this procedure does involve some level of subjectivity, the University of Victoria participants in this project (DAV, RL, and KB) independently determined the cluster distance moduli and ages following the methods described in § 3. In general, the three estimates of the ages so obtained agreed to within ± 0.25 Gyr: no cases were found where the derived ages differed by > 0.5 Gyr. (These age differences, which provide a measure of the internal uncertainty of our age-dating procedure, are listed in the summary table in § 6.) Similar good agreement was found for 10 clusters that have $[\text{Fe}/\text{H}] > -1.0$ (see § 5.2), once it was decided how best to fit a ZAHB with an appreciable vertical component at the red end to the observed HB “clump” that is characteristic of metal-rich systems. Most of the remaining GCs in our sample are considered in § 5.3, where the difference in color between the turnoff and the lower giant branch is used as the primary age constraint. The CMDs of a few clusters, including those associated with the Sagittarius dwarf galaxy, are analyzed in § 5.4. Section 6, tabulates the ages that have been derived for all 55 GCs that have been considered in this study, describes the resultant age–metallicity and age versus Galactocentric distance relations, reconciles our findings with those reported by MF09, and compares various properties of the globular clusters in an attempt to understand why the most metal-deficient clusters appear to be split into two groups.

5.1. Metal-poor ($[\text{Fe}/\text{H}] < -1.0$) Globular Clusters with Easily Fitted HB Populations

Figure 11 illustrates that our ZAHB models provide a good match to the luminosities and colors of the HB populations that belong to six of the most metal-deficient GCs (those with $[\text{Fe}/\text{H}] < -2.2$) on the assumption of the distance moduli and reddenings that are specified in the upper left-hand corner of each panel. Except for the fact that the observed RGBs tend to be somewhat bluer than the model predictions, the isochrones also reproduce the cluster CMDs quite well, yielding ages that range from 12.0 Gyr, in the case of M 68 (NGC 4590), to 12.75 Gyr, in the case of M 92 (NGC 6341), M 15 (NGC 7078), and M 30 (NGC 7099). The other two clusters are predicted to have intermediate ages, resulting in a

mean age of 12.5 Gyr for the entire group. The adopted $E(B - V)$ values are identical to those found from the Schlegel et al. (1998) dust maps, though a somewhat smaller value may be applicable to M 15 given that it may otherwise be hard to explain why the $\delta(\text{color})$ value, which is the discrepancy between the predicted and observed turnoff colors, is significantly larger for this cluster than for M 92 or M 30, which have very similar metallicities (unless, perhaps, M 15 has a higher helium abundance). If the $E(B - V)$ value of M 15 were reduced by about 0.02 mag, improved overall consistency would be obtained insofar as all of the best-fit isochrones would have to be adjusted to the blue by 0.015–0.020 mag in order to match the observed TO colors.

The difficulty of obtaining accurate *absolute* ages is highlighted by the fact that recent determinations of the age of M 92 do not agree particularly well. For instance, Brown et al. (2012), who were primarily interested in the ages of three ultra-faint dwarf (UFD) galaxies *relative* to that of M 92, derived an age of 13.7 Gyr for the latter. The higher age, by nearly 1 Gyr compared with our estimate, is due to their adoption of a shorter distance modulus by about 0.03 mag as well as a lower (absolute) oxygen abundance by 0.24 dex. Similarly, differences in the assumed distances are the main reason why VandenBerg et al. (2010) and di Cecco et al. (2010) obtained ages of 13.5 Gyr and 11.0 Gyr, respectively, for M 92. However, the adopted distance scale in the present study is consistent with that implied by the RR Lyrae standard candle (though the uncertainties are large; see the previous section). In addition, we favor a moderately high [O/Fe] value because the latest non-LTE analyses of the spectra of extremely metal-deficient field halo stars have yielded [O/Fe] ~ 0.6 at [Fe/H] $\lesssim -2$ (Ramírez et al. 2012; see their Fig. 3), and because a relatively high oxygen abundance appears to be needed for ZAHB models to match the reddest HB stars in M 15.

In fact, it is apparent in Fig. 11 that our ZAHB models do not extend far enough to the red to match those stars, which suggests that M 15 may have an even higher O abundance than we have assumed — see, e.g., VandenBerg & Bell 2001, who have investigated the impact of varying the O abundance on computed ZAHB loci for extreme Population II stars. (The reddest HB stars in the other five GCs considered in this figure are likely evolved stars given their small numbers and somewhat elevated luminosities.) Whether or not M 15 and M 92 have significantly different oxygen abundances is not known, but just as the measured O abundances in field stars at a given [Fe/H] show a scatter of ~ 0.2 dex (e.g., Fabbian et al. 2009), there could well be similar cluster-to-cluster variations.

Similar analyses are presented in Figure 12 for GCs that have $-1.50 > [\text{Fe}/\text{H}] \geq -2.20$. It is not necessary to say very much about these results, given that each panel is self-explanatory. The most robust ages are those which have been determined for clusters with low reddenings and/or that have substantial red HB populations. For the seven clusters

with $[\text{Fe}/\text{H}]$ values between -1.50 and -1.80 , the derived mean age is 11.7 Gyr. Higher ages are predicted for the two more metal-poor systems in this sample, but most of the clusters in the $-1.80 > [\text{Fe}/\text{H}] \geq -2.20$ metallicity bin have extremely blue HBs. Their ages are determined in § 5.4. As in the previous figure, Schlegel et al. (1998) $E(B - V)$ values have been adopted, except for NGC 3201, where a higher reddening by 0.04 mag has been assumed in order to accommodate the location of the bluest HB stars while preserving a good fit to the lower bound of the distribution of red HB stars. It is a concern that the $\delta(\text{color})$ offsets, which are needed for the best-fit isochrones to match the observed turnoffs, vary as much as they do (from -0.011 to -0.040), but what this means is not clear. It is possible that the variations in $\delta(\text{color})$ arise from errors in the adopted $[\text{Fe}/\text{H}]$ values. Alternatively, it may be the assumed reddenings that need to be revised.

Suppose, for instance, that the actual reddening of NGC 5286 is lower than the Schlegel et al. value by 0.010 mag. In order to achieve a comparable fit to the blue HB as that shown in Fig. 12, the apparent distance modulus would have to be increased by 0.10 mag, resulting in a significantly reduced age (to 11.0 Gyr). Although not shown here, that isochrone provides an equally good fit to the turnoff observations, assuming $\delta(\text{color}) = -0.025$ mag, as that obtained by the 12.0 Gyr isochrone if $(m - M)_{APP} = 15.94$ and $\delta(\text{color}) = -0.040$ mag. However, if the higher distance modulus is more accurate, then all of the stars near the red end of the densest part of the HB population in NGC 5286 would lie well above the ZAHB; i.e., they would all have to be evolved stars. This seems less likely than in the adopted fit, wherein the faintest of these stars are adjacent to the ZAHB, simply because there are so many stars in this group: the densest concentration of HB stars should be near the ZAHB where the evolutionary timescales are the longest. Regardless of which variation of the $\Delta V_{\text{TO}}^{\text{HB}}$ method is implemented, the ages that are inferred for some GCs will depend on the assumption that is made concerning the evolutionary state of the HB stars that are observed.⁶

There are no such difficulties when globular clusters contain prominent red HB populations, such as those that are the subject of Figure 13. Indeed, the $\Delta V_{\text{TO}}^{\text{HB}}$ ages for most of the clusters in this group should be especially robust. The exceptions are NGC 2808 which, as already noted, contains discrete stellar populations, and M 107 (NGC 6171), which suffers

⁶Our ZAHB models were sufficiently relaxed/evolved over many short timesteps that they should mark the beginning of the slowest part of the core He-burning phase. Still, it would be much more instructive to compute synthetic HB distributions for comparisons with the observed HB populations (see, e.g., Cassisi et al. 2004, Catelan et al. 2004) as they have the potential to discriminate between different possible interpretations of the data. Such work will be carried out once a subroutine to deal with semi-convection has been implemented in the Victoria code.

from significant differential reddening. (The difficulty of selecting the best-fit isochrone in the latter case is most apparent when a much larger plot of its CMD is examined.) The ZAHB does match the morphology of the HB populations of NGC 2808 quite well on the assumption of the Schlegel et al. (1998) reddening, despite the known chemical abundance variations in it. Furthermore, its ZAHB-based distance should be of quite high precision given that the lower bound to the distribution of its reddest HB stars is so well-defined. In any case, if the two problematic clusters are ignored, the mean age of the remaining GCs, which have $-1.07 \geq [\text{Fe}/\text{H}] \geq -1.44$, is 11.6 Gyr. Interestingly, the ages of NGC 6362, NGC 6717, and NGC 6723 (12.5, 12.5, and 12.25 Gyr, respectively) are similar to those found for the most metal-deficient GCs, while most of other $[\text{Fe}/\text{H}] \approx -1.3$ clusters have ages of $\lesssim 11.0$ Gyr, which are less than any of the ages that have been determined at lower metallicities.

Given the compelling evidence that NGC 2808 contains stars with different helium abundances (perhaps up to $Y = 0.40$, see Piotto et al. 2007), it is perhaps not surprising that isochrones for $Y = 0.25$ require an especially large blueward color correction in order to match the turnoff color of this cluster. (On the other hand, most of the spread in its CMD occurs below the turnoff; consequently, the median TO color, to which the best-fit isochrones are matched, could well be representative of the dominant, normal- Y sub-population.) In fact, even larger $\delta(\text{color})$ values would have been obtained for M 4 (NGC 6121) and M 107 had we adopted Schlegel et al. (1998) $E(B - V)$ values for them. However, in these two cases, it seems more likely that such large color offsets are due to an over-estimation of the dust-map reddenings, which are very high ($\gtrsim 0.45$ mag), than to some other explanation. Hence, we decided to adopt smaller $E(B - V)$ values for M 4 (see Hendricks et al. 2012) and M 107 by 0.03–0.05 mag in order that the resultant $\delta(\text{color})$ values are much more consistent with those obtained for nearly unreddened GCs of similar metallicity. NGC 6723 is the only other cluster in this group where the Schlegel et al. reddening, $E(B - V) = 0.177$, was not adopted. Indeed, such a high value is unrealistic since, if the distance modulus is determined from the horizontal part of the distribution of HB stars, the location of the blue tail can be matched by the same ZAHB *only* if $E(B - V) \approx 0.07$. (Since the dust maps provide “line of sight” reddenings, it may be possible to reconcile these, or similar, discrepancies if a large fraction of the absorbing gas/dust is behind the GC in question, rather than being entirely in front of it.)

No attempt has been made here (but see Piotto et al. 2007, Milone et al. 2012c) to try to fit isochrones for higher Y to the CMD of NGC 2808, in part because the photometry that we have used does not separate the observations into discrete main sequences. However, as shown by Piotto et al., the latter merge into a relatively narrow, single locus of stars near the turnoff, resulting in a well-defined (single) SGB. This morphology is fully consistent with the predicted behavior of isochrones for a large range in helium abundance, but essentially the

same age (see VBD12). In view of this, we expect that our fit of isochrones to the median turnoff color and to the distribution of SGB stars just redder than the TO will have yielded quite a good estimate of the cluster age (11.0 Gyr, see Fig. 13). In the case of NGC 1851, the double subgiant branch discovered by Milone et al. (2008) is clearly present in our data and we have fitted isochrones to the dominant, brighter population (although this is not apparent at the scale of the plot in the top right-hand corner). The reduced luminosity of the fainter SGB population is most easily explained if the stars in that sequence have higher C+N+O abundances than in the majority of the clusters stars (see Cassisi et al. 2008).

5.2. Globular Clusters that have $[\text{Fe}/\text{H}] \geq -1.0$

The most well-studied GC in the metal-rich group is 47 Tucanae. In addition to being nearly unreddened, its distance modulus has been determined to relatively high precision by Thompson et al. (2010), who obtained $(m - M)_V = 13.35 \pm 0.08$ from their analysis of the eclipsing binary member V69. As this estimate depends on the assumed reddening and adopted color– T_{eff} calibration, we used their derived radii, masses, colors, and magnitudes for V69, along with $E(B - V) = 0.032$ (Schlegel et al. 1998) and $[\text{Fe}/\text{H}] = -0.76$ (CBG09), to obtain an apparent distance modulus for 47 Tuc of $(m - M)_V = 13.35$ if the color–temperature relations of Casagrande et al. (2010) are employed, or 13.33 if the MARCS transformations, which are also been used to transpose our isochrones from the theoretical to the observed plane, are adopted instead. The difference between these estimates is much smaller than the uncertainty, and arguments can be presented in support of both transformations. However, we are inclined to favor the larger value of $(m - M)_V$ because the Casagrande et al. transformations are based on direct measurements of real stars.

Accordingly, we adopted $(m - M)_V = 13.35$, which, for $E(B - V) = 0.032$, is equivalent to $(m - M)_{F606W} = 13.34$, since $A_{F606W} \approx 2.80 E(B - V)$ (Siriani et al. 2005) as compared with $A_V \approx 3.07 E(B - V)$ (McCall 2004). Assuming this distance modulus, together with $E(B - V) = 0.032$, we produced the fit of a ZAHB to the HB population of 47 Tuc that is shown in Figure 14. Although there is considerable evidence for helium abundance variations ($\delta Y \lesssim 0.03$) in this system (e.g., Nataf et al. 2011, Gratton et al. 2013), the faintest and reddest HB stars presumably have normal helium contents, and it is to these stars that the ZAHB has been fitted. As indicated, the models assume $[\text{Fe}/\text{H}] = -0.76$ and an initial helium abundance corresponding to $Y = 0.257$. Moreover, with these choices for the cluster properties, the age of 47 Tuc is predicted to be 11.75 Gyr. We decided to adopt an independent estimate of the 47 Tuc distance because there is some ambiguity in how a ZAHB should be compared with the type of HB morphology that is characteristic of metal-

rich systems. Previous work (e.g., Dorman, Vandenberg, & Laskarides 1989) suggested that the slightly sloped line which defines the lower boundary of the faintest HB stars in 47 Tuc does not coincide with the observed ZAHB, but rather that the latter is located along the upturn that is predicted to occur near the red end.

The same thing is indicated by the particular comparison that is shown in Fig. 14. According to these results, stars arriving on the HB after undergoing the helium flash populate only that part of a ZAHB between its red end and the short horizontal line just below it, which has been drawn at the minimum luminosity of the observed HB clump. Because masses tend to “pile up” when a ZAHB approaches its minimum T_{eff} (maximum color), before bending back to the blue, the mass range in this small region of the ZAHB is considerable. To be specific, the reddest ZAHB model that has been plotted has a mass which is consistent with the neglect of mass loss over the preceding evolution, while the point that is defined by the intersection of the short horizontal line with the ZAHB has a lower mass by $0.20M_{\odot}$. (The ranges in luminosity and color encompassed by the entire HB population must therefore be a reflection of the tracks that are followed during post-ZAHB evolution; see the paper by Dorman et al. 1989.) Thus, differences in the adopted distance have implications for the inferred mass loss that occurred in the stars prior to reaching the ZAHB.

It is clearly fortuitous that the ZAHB for the adopted abundances provides such a good fit to the observations, given all of the parameters at play. In fact, the models that have been used to fit the CMD of 47 Tuc do not reproduce the properties of the binary (V69) as well as one would like. Figure 15 plots the components of V69 on the mass–radius plane, together with the predicted variations of radius with mass along isochrones for ages that vary in 0.5 Gyr increments from 10.0 to 12.0 Gyr in some panels, or from 10.5 Gyr to 12.5 Gyr in others (as specified just above the abscissa of each panel). The upper left-hand panel contains the isochrones from the previous figure: they favor an age of 11.0 ± 0.5 Gyr for V69 (and hence 47 Tucanae), which is 0.75 Gyr less than the age that was derived from the turnoff photometry. The other panels illustrate the impact of varying each of the chemical abundance parameters in turn. Higher ages by about 0.5 Gyr are obtained if Y is reduced by 0.005 or if the assumed $[\text{Fe}/\text{H}]$ value is increased by 0.06 dex. Although not shown, the implication of the lower left-hand panel is that a higher age (by about the same amount) would also be the result of increasing $[\alpha/\text{Fe}]$ by 0.11 dex.

Whether or not 47 Tuc stars have such large enhancements of the α -elements is presently uncertain. Whereas Carretta et al. (2013) obtained $[\text{Mg}/\text{Fe}] = 0.53$ and $[\text{Si}/\text{Fe}] = 0.44$ from their spectroscopic survey of about 100 cluster giants, Gratton et al. (2013) derived $[\text{Mg}/\text{Fe}] = 0.39$ and $[\text{Si}/\text{Fe}] = 0.26$ from a similar investigation of 110 HB stars. For the initial oxygen abundance, the situation is further complicated by the O–Na anticorrelation, though

we suspect that the best estimate is close to the upper end of the observed range. In the investigation by Carretta et al., the mean and upper envelope $[\text{O}/\text{Fe}]$ values for their sample of stars are 0.26 and ≈ 0.40 , respectively. A much higher average value of $[\text{O}/\text{Fe}]$ ($= 0.60$) was derived Koch & McWilliam (2008) from 8 RGB stars that have $0.48 \leq [\text{O}/\text{Fe}] \leq 0.66$. These determinations may be compared with $[\text{O}/\text{Fe}] \approx 0.50$ in thick-disk field stars that have $[\text{Fe}/\text{H}] \sim -0.8$ (Ramírez et al. 2012). Regardless, just as an increase in $[\alpha/\text{Fe}]$ would tend to reduce the difference between the ages inferred from the CMD and the binary, the age discrepancy would be exacerbated if the models assumed lower α -element abundances (see the bottom, left-hand panel of Fig. 15). (Note that different choices for the chemical abundance parameters would affect the corresponding ZAHB-based distances, but only slightly given that the adopted variations are small. Nevertheless, this effect on the CMD age has not been taken into account.)

Another way of reconciling the binary mass-radius age with the CMD age is to increase the model temperatures. It is quite possible that the predicted T_{eff} scale is too cool because of deficiencies in, for instance, our treatment of the atmospheric boundary condition, convection, or diffusive processes. The impact of such a problem on the M-R diagram is illustrated by the short- and long-dashed curves in the upper left-hand panel. These show, in turn, how the location of the 11.0 Gyr isochrone that is represented by the solid curve would be affected if the predicted temperatures were increased, or decreased, by 75 K. The effect on the inferred age is apparently ± 0.25 Gyr, respectively. Thus, it would be possible to obtain ages from both the M-R diagram and the CMD that agree to within 1σ if the models were hotter by about 75 K. It turns out that, at the masses of the binary components, the temperatures along 11.0–11.75 Gyr isochrones are cooler than those obtained from the radii and colors of V69, but within ≈ 60 K. Since an upward revision in the predicted temperatures would improve the agreement, it seems likely that this is the correct way to obtain the best consistency between Figs. 14 and 15. Note that improved consistency would not be obtained if we simply adopted an increased distance modulus by a few hundredths of a magnitude. Because the components of V69 have measured magnitudes, models that match the observed radii, in combination with the predicted temperatures, also imply a particular value of the apparent distance modulus. Since our adopted modulus is already at the high end of the range indicated by the uncertainties in the properties of the binary, any arbitrary increase in $(m - M)_V$ will cause even larger discrepancies with the distance based on the binary.

As already mentioned, other potential solutions include lowering the helium abundance and/or increasing the $[\text{Fe}/\text{H}]$ value, and we are considering such adjustments in a much more detailed study of 47 Tuc and its binary V69 (K. Brogaard et al., in preparation). However, for the present study we have chosen to adopt the CBG09 metallicity scale and a particular variation of Y with $[\text{Fe}/\text{H}]$ for the entire GC sample. Even if it is possible to argue for

adjustments of these choices for a given cluster, it is not known whether they are unique to that cluster or whether they should be applied to the entire sample. Therefore, no such variations have been explored here, especially as our main goal is to obtain the best estimates of *relative* GC ages.

With the adopted composition and apparent distance modulus, the implied mass loss agrees rather well with that determined by Miglio et al. (2012) in the case of the super-metal-rich open cluster NGC 6791 using asteroseismology. These investigators found a mean mass difference of $0.09M_{\odot}$ between the lower RGB and the red HB clump, which suggests that the red HB stars in NGC 6791 have masses that do not differ by more than $\approx 0.18M_{\odot}$. Such a dispersion in the mass loss is also supported by the analysis of the cluster CMD carried out by Brogaard et al. 2012.) To within the uncertainties, this is the same as the value of $\approx 0.20M_{\odot}$ found here from our fit of a ZAHB to the HB population of 47 Tuc⁷

Given the apparent near constancy of the difference in the mass of the most and least massive stars that populate the red HBs of NGC 6791 and 47 Tuc, whose metallicities bracket those of the GCs in the metal-rich group under consideration, we believe that it is quite reasonable to assume that the same result applies to the latter. Thus, to determine the distance modulus of each metal-rich GC in our sample, we have determined which ZAHB model has a mass that is $0.20M_{\odot}$ less than the RGB tip mass for the adopted age (ignoring mass loss along the giant branch): that model is identified by the intersection of a short horizontal line with the ZAHB. Then the dereddened cluster photometry is shifted in the vertical direction until that horizontal line coincides with the faintest HB star in the cluster HB population, resulting in the adopted value of $(m - M)_{APP}$. If the maximum amount of mass loss that occurs prior to the ZAHB were, for instance, as small as $0.10M_{\odot}$ or as large as $0.30M_{\odot}$, the derived distance modulus of 47 Tuc (and the other metal-rich GCs in our sample) would be larger, or smaller, than our adopted modulus by only ≈ 0.05 mag. This is not insignificant, but neither does it completely overwhelm other uncertainties.

When distance moduli are derived in this way for the GCs that have $[\text{Fe}/\text{H}] \geq -1.0$, the ZAHBs and isochrones generally provide satisfactory matches to the observed photometry, as shown in Figure 16. The least reliably determined ages are those for NGC 5927, NGC 6304, NGC 6624, and M 69 (NGC 6637), as their CMDs appear to be affected by significant differ-

⁷Even in low metallicity clusters, the range in mass spanned by HB stars may be quite similar. For instance, our fit of ZAHB models to the horizontal branch of M92 (see Fig. 11) suggests that its lowest mass HB star is only $\sim 0.16M_{\odot}$ less massive than a 12.75 Gyr star that has evolved to the HB without undergoing any mass loss whatsoever during its previous evolution. However, such estimates will be quite uncertain given the strong sensitivity of HB models to the assumed chemistry. For an excellent review of mass loss and its implications for the HB phase, see Catelan (2009).

ential reddening and/or substantial field-star contamination. Note that, in none of the nine GCs, is the $E(B - V)$ value less than 0.10 mag. Except in the case of NGC 6366, where the HB stars are offset to the blue of their expected location relative to the ZAHB (possibly due to a chemical abundance effect), the HB populations are quite well matched by the ZAHBs — though this is partly by design. Schlegel et al. (1998) reddenings have been assumed for all of the clusters except those considered in the top row as well as M 71 (NGC 6838). In order to obtain a similar fit to their HB populations as those found for the other five clusters, it was necessary to adopt reduced reddenings by as little as 0.02 mag (NGC 6304) to as much as 0.08 mag (NGC 5927). An important consequence of making such revisions is that the resultant $\delta(\text{color})$ values become much more similar for all of the GCs in the sample. The mean age of this group, including 47 Tuc, is 11.1 Gyr, implying that metal-rich GCs are about 1.5 Gyr younger than the most metal-deficient systems. This finding is at odds with the conclusion reached by MF09, who found little or no difference in their ages. A resolution of these conflicting results is provided in § 6.1.1.

5.3. MSTO-to-RGB Color Constraints on Relative GC Ages

It is readily appreciated that the $\Delta V_{\text{TO}}^{\text{HB}}$ method cannot be used to determine very precise ages for globular clusters that have extremely blue HBs. In those systems in which the horizontal-branch populations are nearly vertical on the CMD, even small offsets in color (due, e.g., to reddening uncertainties) would have a big effect on the distances, and therefore ages, that are derived from fits of computed ZAHBs to the observations. In such cases, the relative age technique described by VandenBerg et al. (1990; hereafter VBS90) can be used to provide much tighter constraints on their absolute ages if, in particular, it is used to compare the CMDs of two clusters that have similar chemical abundances but one of them has a red HB that is amenable to a $\Delta V_{\text{TO}}^{\text{HB}}$ analysis. The essence of the VBS90 procedure is to superimpose the principal photometric sequences of two GCs, simply by applying the necessary vertical and horizontal shifts to one of them, so that both have the same turnoff color and the same magnitude at a point on the upper MS that is 0.05 mag redder than the TO. Then whatever separation of their RGBs is found at, say, 2.8 mag above the latter fiducial point will be a direct measure of the difference in the age of the two clusters. In effect, relative GC ages are found from the difference in color between the MSTO and the RGB at a pre-selected, arbitrary point on the giant branch. This relative age diagnostic, which will henceforth be referred to as $\Delta H_{\text{TO,RGB}}$, where the “H” represents “horizontal” just as the “V” in $\Delta V_{\text{TO}}^{\text{HB}}$ can be thought of as indicating “vertical”, is independent of distance, reddening, and the zero-point of color calibrations.

Marín-Franch et al. (2010, also see MF09) have stated that this so-called “horizontal method” of determining relative ages is sensitive to the assumed value of the mixing-length parameter (α_{MLT}), or more generally, the treatment of super-adiabatic convection, as well as the adopted color– T_{eff} relations. They say that, as a consequence, this approach is “strongly model dependent”. However, these are valid concerns only if the $\Delta H_{\text{TO,RGB}}$ method is used to determine *absolute* ages; indeed, VBS90 advised against such a practice in the paper that introduced this new *relative*-age-dating technique. The latter relies only on how the color of the RGB, at a fixed magnitude, is affected by variations in age. Because it involves such a narrow range in RGB colors and because it has no dependence on the zero-points of the color transformations, errors in the color– T_{eff} relations will be inconsequential.

To support these assertions we have used the $\Delta H_{\text{TO,RGB}}$ method to evaluate the relative ages of two hypothetical GCs whose RGBs differ in color by 0.015 mag at 2.8 mag above the ordinate zero-point when their CMDs have been registered to one another according to the directions given by VBS90 (see above). Suppose both clusters have $[\text{Fe}/\text{H}] = -1.4$ and normal helium and α -element abundances for that metallicity, and let us consider two sets of isochrones, for the same chemical abundances, which are otherwise identical except that one assumes $\alpha_{\text{MLT}} = 1.50$ while the other assumes $\alpha_{\text{MLT}} = 2.007$. When similarly registered to one another, the isochrones based on the smaller value of the mixing-length parameter predict a *much* larger difference in color at 2.8 mag above the ordinate zero-point than those which assume $\alpha_{\text{MLT}} = 2.007$. In fact, depending on which of the two grids of isochrones is used to evaluate the age corresponding to a given (observed) MSTO-to-*RGB* color difference, absolute ages that differ by $\gtrsim 3$ Gyr would be obtained. (Clearly it is very risky to derive the absolute ages of star clusters in this way.)

However, for relative ages, it is only the difference in color between the *RGB* segments that matters. At the same magnitude offset from the ordinate zero-point, the difference in color between, say, 11 and 13 Gyr isochrones is 0.0221 mag if derived from the models for $\alpha_{\text{MLT}} = 1.50$, versus 0.0195 mag in the case of those which assume $\alpha_{\text{MLT}} = 2.007$. That is, the former predict a variation in color with age of 0.0109 mag/Gyr as opposed to 0.0097 mag/Gyr for the latter. (Such slopes are not strictly constant as the difference in color, at a fixed luminosity between, e.g., 11 and 12 Gyr isochrones will generally be slightly larger than that found for 12 and 13 Gyr isochrones — but this is a second-order effect.) Returning to the example of two clusters whose *RGBs* differ in color by 0.015 mag, the isochrones for $\alpha_{\text{MLT}} = 1.50$ predict an age difference of 1.55 Gyr, while those for $\alpha_{\text{MLT}} = 2.007$ yield 1.38 Gyr. Thus, despite using isochrones with very different color offsets between the *TO* and the *RGB*, the derived relative ages are nearly the same.

Even though this analysis considered isochrones that were computed for very different

values of α_{MLT} , we do not believe that there is compelling evidence that this parameter varies *significantly* with mass, metallicity, or evolutionary state. If it did, we would not obtain such good agreement between isochrones that assume a constant value of α_{MLT} and the observed CMDs of GCs that span at least 2 dex in $[\text{Fe}/\text{H}]$ (see, e.g., Figs. 11–14, 16). In fact, models based on the same physics have been just as successful in explaining the observations of the old, super-metal-rich open cluster NGC 6791 (Brogaard et al. 2012), whose properties have been especially tightly constrained through analyses of a few of the detached, eclipsing binary stars that it contains. The Vandenberg et al paper also showed that Victoria-Regina isochrones reproduce to within ~ 10 K (in the mean) the temperatures derived by Casagrande et al. (2010) using the infrared-flux method for field subdwarfs that have $-2.2 \lesssim [\text{Fe}/\text{H}] \lesssim -0.5$ and accurate *Hipparcos* parallaxes. Similar results have been obtained in the past (Vandenberg, Bergbusch, & Dowler 2006), and importantly, no significant dependence of the mixing-length parameter on metallicity has been found in empirical calibrations of infrared photometry for giants in 28 GCs that have $-2.2 \lesssim [\text{Fe}/\text{H}] \lesssim -0.2$ (Ferraro et al. 2006, also see Palmieri et al. 2002).

These results are completely at odds with the recent findings of Bonaca et al. (2012, also see Basu et al. 2012), who concluded that α_{MLT} increases by ≈ 0.5 per dex in $[m/\text{H}]$ from their analysis of asteroseismic data for a sample of dwarfs and subgiants in the Kepler field. To resolve this dilemma, work needs to be undertaken to compare the photometric and spectroscopic T_{eff} scales, to study the extent to which star-to-star differences in the detailed heavy element abundances affect the results, to evaluate the impact of stellar models that neglect (in the Bonaca et al. study) convective core overshooting and diffusive processes, and to carefully examine other sources of systematic error. In this paper, we can only point out that comparisons of modern isochrones with photometric data for star clusters do not support a steep dependence of α_{MLT} on metallicity.

For example, since isochrones for $\alpha_{\text{MLT}} = 2.005$ provide a superb fit to the CMD of NGC 6791 (see Brogaard et al. 2012), the Bonaca et al. results would suggest that models relevant to 47 Tuc, which is ≈ 1 dex more metal-poor than NGC 6791, should assume $\alpha_{\text{MLT}} \approx 1.5$. To examine the implications of this choice, this (low) value of the mixing-length parameter has been adopted in the computation of a grid of models for $Y = 0.257$ and $[\text{Fe}/\text{H}] = -0.76$ (i.e., the same chemical abundances that were assumed in the models plotted in Fig. 14). Although not shown, these calculations predict temperatures that are 320 K and 390 K cooler near the base and the tip of the RGB, respectively, than those shown in that figure. Furthermore, because of the steep dependence of the bolometric corrections and colors on T_{eff} in the case of cool giants, both the location and the slope of the predicted RGB are very discrepant relative to the observed giant branch. To be sure, the uncertainties are such that a small variation of α_{MLT} with mass, metallicity, and/or evolutionary state

cannot be ruled out, but even if this parameter varied by $\sim 10\text{--}15\%$ across the H-R diagram, which would require some compensating adjustments to the atmospheric boundary conditions and/or to the color– T_{eff} relations in order to obtain comparable fits to observed CMDs, our isochrone-fitting procedure would yield essentially identical ages (as shown in Fig. 5).

While, in principle, it should be possible to obtain rather precise relative ages using the VBS90 technique, the results do depend quite critically on whether or not the clusters whose CMDs are intercompared have the same chemical abundances. For instance, Vandenberg & Stetson (1991) pointed out early on that the same value of $\Delta(B - V)_{\text{MS,RGB}}$ would be obtained for two GCs if they had identical metal abundances but differed in age by $\approx 10\%$, or if they were coeval but had different $[\text{O}/\text{Fe}]$ values by ~ 0.3 dex (assuming no other chemical differences). Indeed, it turns out that cluster-to-cluster variations in Y or in the abundances of several of the other metals (notably Ne, Mg, or Si; see VBD12), would complicate the interpretation of $\Delta H_{\text{TO,RGB}}$ measurements, especially at higher metallicities. This is shown in Figure 17, where 12 Gyr isochrones for $[\text{Fe}/\text{H}] = -2.0$ and 11 Gyr isochrones for $[\text{Fe}/\text{H}] = -1.0$ have been plotted with, and without, the assumed chemical abundance variations that are indicated in the top left-hand corner of each of the six panels that comprise this plot. The isochrones, which have been taken from VBD12, have been registered to one another using the VBS90 prescription: the zero-point of the abscissa coincides with the TO color, while the magnitude at the point on the upper MS that is 0.05 mag redder than the turnoff defines the zero-point of the ordinate (note the location of the filled circle on the 12 Gyr isochrones).

The insert in the upper left-hand panel plots the relative locations of the RGB segments of isochrones for the two values of $[\text{Fe}/\text{H}]$, and ages from 10.5 to 13.5 Gyr in 1.0 Gyr steps. They were arbitrarily moved to the region enclosed by the dotted rectangle (simply for display purposes) from original ordinate values ranging from ≈ -2.4 to -3.2 . By comparing these results with the predicted color offsets of the RGBs (at an ordinate value of ~ -2.8) that arise from chemical composition variations, one finds, for instance, that a 0.4 dex increase in the value of $[\text{O}/\text{Fe}]$ at $[\text{Fe}/\text{H}] = -2.0$ (right-hand plot, top row) mimicks the effect on the RGB location that is comparable to the shift produced by about a 1 Gyr increase in age. Similarly, a higher value of $[\text{Mg}/\text{Fe}]$ by 0.4 dex at $[\text{Fe}/\text{H}] = -1.0$ (middle panel, bottom row) apparently causes a redward offset of the RGB (relative to the TO) that is approximately equivalent to that predicted for a ~ 1.5 Gyr reduction in age. These are just rough estimates: Fig. 17 has been included here mainly to illustrate qualitatively how cluster-to-cluster differences in age and chemical abundances affect the $\Delta H_{\text{TO,RGB}}$ parameter.

In fact, the observed variations in the abundances of individual metals in clusters of similar $[\text{Fe}/\text{H}]$ are closer to $\delta[m/\text{Fe}] = 0.1\text{--}0.2$ dex (Carretta et al. 2009b) than to 0.4 dex, so

the concerns that are raised by Fig. 17 are not nearly as serious as this plot suggests. Moreover, since the majority of the GCs that have extremely blue HBs have $[\text{Fe}/\text{H}] \lesssim -1.6$, the only abundance variations that appear to have detectable consequences for $\Delta H_{\text{TO,RGB}}$ -based estimates of their relative ages are those of helium and/or oxygen. Fortunately, differences in Y can be distinguished from differences in $[\text{O}/\text{Fe}]$ because the former have bigger effects on the slope of the subgiant branch than the latter. This is most easily seen when isochrones are superimposed according to the VBS90 procedure (compare the plots in the upper left- and right-hand panels). It is worth reiterating that, as discussed by VBD12, the age-sensitive parts of isochrones *for low metallicities* depend almost entirely on the absolute C+N+O abundances (or $[\text{CNO}/\text{H}]$ coupled with the CNO abundances in the adopted solar mixture). The $[\text{Fe}/\text{H}]$ value is a useful way of “tagging” GCs because, with few exceptions, it does not vary significantly from star-to-star within a given cluster (as already mentioned). It also provides a good “label” for isochrones given that a given metals mixture, with or without some adjustments to the solar m/Fe number abundance ratios, is normally scaled to any desired $[\text{Fe}/\text{H}]$ value. However, the iron abundance is far less important than the $[\text{O}/\text{H}]$ ($= [\text{Fe}/\text{H}] + [\text{O}/\text{Fe}]$) value at low Z .

Although Fig. 2 showed that the morphology of isochrones (for $[\text{Fe}/\text{H}] \leq -1.4$) in the vicinity of the turnoff is nearly independent of age, there is some age dependence of the luminosity, and slope, of the SGB at the lowest metallicities. As illustrated in Figure 18, 11–13 Gyr isochrones for $[\text{Fe}/\text{H}] = -2.40$ begin to deviate from one another just past the turnoff, while those for higher metallicities do so at colors, relative to the TO, that become steadily redder as the $[\text{Fe}/\text{H}]$ value increases. (Note that the intercomparisons of isochrones presented in Figs. 2–5 minimized the differences between them at a color that is 0.05 mag redder than the TO, both above and below the turnoff. As a consequence, the differences between their SGB segments are considerably smaller in those plots than in Fig. 18.) While these differences are still rather small, they nevertheless resemble the effects of enhanced Y on the SGB at a fixed age (see the top left-hand panel of Fig. 17). This should be kept in mind when interpreting any cluster-to-cluster differences in the morphologies of their CMDs that are found when the latter are registered to one another according to the directions given by VBS90.

It is obviously important to apply the $\Delta H_{\text{TO,RGB}}$ method to the GCs that have already been considered, in order to check that the relative ages of clusters with similar metallicities are consistent with the differences in their $\Delta V_{\text{TO}}^{\text{HB}}$ ages. However, we will first turn our attention to a few “second-parameter” clusters and then consider several systems with extremely blue HBs. The advantage of proceeding in this way is that the latter appear to provide some valuable insights (or at least “food for thought”) concerning the second-generation stars in GCs that may be relevant to a subset of the $[\text{Fe}/\text{H}] \lesssim -1.6$ clusters that were the subject of

§ 5.1.

5.3.1. *M3 and M13*

Figure 19 illustrates the fiducial sequences that have been derived for M3 and M13. Why these clusters have such different HB morphologies, despite having similar metallicities, is still an open question even though extensive efforts have been made during the past 40 years to try to solve this puzzle (see, e.g., the review by Catelan 2009). Since age and/or chemical abundance differences, notably of He or the CNO elements, are the most likely second parameters (after $[\text{Fe}/\text{H}]$, which is the first parameter), it is possible that variations in the properties of the multiple stellar populations that all GCs appear to contain are responsible for this phenomenon. Furthermore, given that age, Y , and $[\text{CNO}/\text{Fe}]$ affect isochrones in different ways (see Fig. 17), the differences between the CMDs of M3 and M13 for turnoff to lower-RGB stars should provide vital clues concerning the identification of the second parameter, or of their relative importance if there is more than one.

Accordingly, considerable care has been taken to accurately determine the median photometric sequence through the MS, SGB, and lower RGB of each cluster. To do this, we sorted the photometry into 0.10 mag bins, determined the median magnitude and color in each bin, and then (for the lower RGB) performed a least-squares cubic fit to the 18-20 points so obtained. To determine the turnoff color, the median points for three bins both above and below the TO were fitted by a least-squares quadratic, which was then evaluated over small intervals of M_{F606W} to determine the bluest color. A similar process was used to derive the magnitude at the color on the upper MS which is 0.05 mag redder than the TO color, using the median points from 8 neighboring bins. (Approximate distance moduli and the adopted cluster reddenings have been assumed in constructing Fig. 19 so that the same regions of both CMDs are displayed, thereby facilitating visual comparisons.)

Unfortunately, the age-dependent $\Delta H_{\text{TO,RGB}}$ parameter is also predicted to be a fairly sensitive function of $[\text{Fe}/\text{H}]$ at a fixed age (see Fig. 3). Although the VBS90 registration procedure was not used to produce the latter, it is quite obvious that nearly the same figure would have been obtained had it been employed: the isochrones plotted therein would require only slight vertical shifts in order for them to pass through the usual registration zero-points for the x - and y -axes. From suitable plots, we find that a 0.1 dex difference in the relative metal abundances of two GCs whose CMDs are intercompared would affect the inferred age difference by 0.25–0.5 Gyr. This can be taken as the uncertainty of relative age estimates based on the horizontal method since most $[\text{Fe}/\text{H}]$ determinations are uncertain by ± 0.05 – 0.10 dex in a relative sense (versus $\gtrsim \pm 0.10$ – 0.20 dex in an absolute sense). To obtain the

best consistency with $\Delta V_{\text{TO}}^{\text{HB}}$ ages, it is, in fact, necessary (see § 5.3.3) to take metallicity differences into account when using MSTO-to-RGB colors to evaluate relative GC ages.

How we have done this is illustrated in the upper left-hand panel of Figure 20, which plots the the fiducial sequences of M3 and M13 after they have been registered to one another. (To minimize space requirements, only the region from just below the TO to the lower RGB has been plotted.) The dashed lines plot the RGB segments of 10.5 to 13.5 Gyr isochrones, in 0.5 Gyr steps, for $Y = 0.25$ and $[\text{Fe}/\text{H}] = -1.50$ (i.e., for chemical abundance parameters that we have adopted for M3). However, we could have opted to plot the giant-branch loci for a somewhat higher or lower metallicity without any misgivings because the age-dependent separations of the RGBs vary only weakly with $[\text{Fe}/\text{H}]$ (see Fig. 18). Given the uncertainties that were discussed in the previous paragraph, it does not matter that the horizontal displacement between the giant branches of, say, 10.5 and 11.0 Gyr isochrones is slightly larger than that of 12.5 and 13.0 Gyr isochrones; consequently, it is not necessary to assume a specific age (in Gyr) for one of the GCs and then deduce the absolute age of the other cluster from the overlap of its giant branch onto the isochrone RGBs. In fact, it is our usual practice to adjust the location of the grid of dashed lines by whatever color offset is needed so that the giant branch of one of the clusters coincides with the third or fourth isochrone. Then, just by inspection of the observed separation of the GC giant branches relative to the dashed lines, which differ in age by 0.5 Gyr (in the direction from “younger” to “older”, as indicated), the difference in the cluster ages is readily evaluated.

The length of the horizontal line which connects the small filled circle at an ordinate value of -2.8 to the short solid line that has the same slope as the dashed loci represents the correction to the color of the M3 RGB that should be applied to it to remove the effect on the $\Delta H_{\text{TO,RGB}}$ parameter of the difference in the cluster metallicities. Thus, whereas the separation of the solid and dashed curves suggests that the two GCs differ in age by about 0.5 Gyr, the models actually predict an age difference closer to 1.0 Gyr if the nearly 0.1 dex difference in their $[\text{Fe}/\text{H}]$ values is taken into account. However, according to the right-hand panel of Fig. 18, the cluster SGBs should overlay one another if age is the main distinguishing property of M3 and M13. This is clearly not the case. Indeed, the top right-hand panel of Fig. 20 indicates that a difference in Y is a much more viable way of explaining the offset in the cluster subgiant branches.

The lower left-hand panel shows that, if M3 has $Y = 0.25$ and an age of 11.75 Gyr (which will be justified shortly), it is then possible to reproduce the observations in the panel just above it if M13 has $Y = 0.29$ and an age of 12.0–12.25 Gyr. We initially thought that similar consistency could be obtained if M13 had an age of $\gtrsim 11.75$ Gyr, $Y = 0.29$, and an enhanced O abundance by $\delta[\text{O}/\text{Fe}] \approx 0.3$ dex, since the effect of the latter is to

displace the RGB for a fixed age to somewhat bluer colors *relative to the turnoff* (see the lower right-hand panel). [It is, of course, the C+N+O abundance that is important; i.e., the same results would be found if N, instead of O, were enhanced by a sufficient amount that $\delta[\text{CNO}/\text{Fe}] \approx 0.3$. In fact, this alternative is arguably the favored one given that helium-rich stars in ω Cen (see, e.g., Johnson & Pilachowski 2010, Marino et al. 2011) and in NGC 2808 (Bragaglia et al. 2010) have low oxygen, and rather high nitrogen, abundances.]

However, the main effect of increasing the C+N+O abundance on isochrones is to reduce the age at a given turnoff luminosity (or equivalently, to displace an isochrone for a fixed age to a lower TO luminosity). This tends to increase the separation between the MSTO and the giant branch; compare the dashed and dotted curves in the lower right-hand panel. To obtain a reduced separation, either the helium enhancement must be large enough to overwhelm the effects of increased CNO, or alternatively, the abundances of the CNO elements should be reduced. In the latter case, fits of the corresponding models to the observed SGB on an absolute magnitude versus color plane would imply a higher age. The main conclusion to be drawn from Fig. 20 is that M 13 appears to have a higher helium abundance than M 3, as there does not appear to be any other way of explaining the differences in the morphologies of their CMDs between the turnoff and the RGB. (The same solution of this problem was first proposed by Johnson & Bolte 1998.) It is certainly very fortunate that variations in the abundance of helium can be detected in this way — if the model predictions can be relied upon — in view of the fact that Y is normally very difficult to determine in cool stars, due to the lack of detectable He lines in their spectra.

This does not necessarily imply, however, that there are no significant star-to-star variations of Y in either cluster. The more general conclusion to be drawn from Fig. 20 is that the *average* helium content of M 13 appears to be higher than that of M 3 (by, say, $\delta Y \sim 0.04$). In fact, the possibility that all of the stars in M 13 had the same high value of Y when they formed presents some difficulties for the interpretation of the cluster CMD. Suppose, for instance, that M 13 has an age of 12.25 Gyr and $Y = 0.29$, versus 11.75 Gyr and $Y = 0.25$ for M 3; i.e., that their properties differ in ways that are compatible with the results shown in Fig. 20. As illustrated in Figure 21, the isochrone for the adopted parameters is able to reproduce the turnoff of M 13 only if the apparent distance modulus is 14.40, assuming $E(B - V) = 0.017$ (Schlegel et al. 1998). In fact, that isochrone provides an especially agreeable fit to the MS-to-RGB populations, including, in particular, the slope of the subgiant branch. However, the fully consistent ZAHB locus is clearly too bright relative to the observed HB stars with $M_{F606W} \lesssim 1.5$.

One way of achieving a satisfactory simultaneous fit of the models to the entire CMD of M 13 is to assume that this cluster has two or more chemically distinct stellar populations

characterized by different helium (and possibly CNO) abundances. The left-hand panel of Figure 22 shows that the lower bound to the distribution of HB stars can be matched quite well by a ZAHB for $Y = 0.25$ and $[\text{Fe}/\text{H}] = -1.58$ if M 13 has $(m - M)_{APP} = 14.45$. Since, on this color plane, the location of the blue HB tail is insensitive to the value of Y , it is not possible to distinguish between the high- and low- Y HB populations if the former evolve to ZAHB structures that are well to the blue of the instability strip. The brightest/reddest HB stars may be either evolved stars from zero-age locations along the blue tail or they may be near-ZAHB stars with $Y \sim 0.29$ (given their proximity to the dashed curve), especially if they also have high CNO abundances, which tends to drive HB stars of a given mass to redder colors (see, e.g., Pietrinferni et al. 2009). [Sandquist et al. (2010) also suggested that the reddest HB stars in M 13 are probably evolved stars, in part because this is implied by the distance modulus that is obtained using the RGB-tip standard candle (Bellazzini et al. 2004).]

The observed widths of the M 13 MS and RGB certainly appear to be large enough to accommodate a large spread in helium abundance, as indicated by the 12.0 Gyr isochrones for $Y = 0.25$ (solid curve) and $Y = 0.33$ (dashed curve). In fact, the widths of the principal photometric sequences (also in the case of M 3, see the right-hand panel) are artificially broadened due to photometric errors arising from crowding and other effects, which can be expected to be especially severe in the most populous clusters. Although we generally selected stars with tabulated errors of < 0.01 mag, a large fraction of the stars, especially those on the giant branch, appear to have been measured only once (based on our limited examination of the impact of culling the data in various ways). If we further restrict the number of stars to those with 4 or more observations in both m_{F606W} and m_{F814W} , the resultant CMDs for the main sequences of M 3 and M 13 are tightened considerably, though the MS widths still remain somewhat larger than the difference between the solid and dashed loci in the left-hand panel of Fig. 22. We are unsure as to whether or not this is the true intrinsic width, but we have assumed that it is. Moreover, it is our impression that the tightest CMDs that we are able to obtain for the most massive clusters are broader, with thicker subgiant branches (~ 0.10 – 0.15 mag, at a given color), than those of lower mass, but further work is needed to do a proper evaluation. In any case, this is an important caveat that should be kept in mind.

M 3 could well have appreciable star-to-star helium abundance variations as well, though comparisons of HB models with observations of M 3 on various Strömgen CMDs and on the $(\log T_{\text{eff}}, \log g)$ -plane suggest that there is little or no variation in Y along its entire horizontal branch (Catelan et al. 2009). Of course, for a difference in Y to be the main cause of the different SGB morphologies (see Fig. 20), it is only necessary that M 13 have a higher Y , *in the mean*, than M 3 by about 0.04. A very similar suggestion, based in part

on a consideration of the location of the RGB luminosity function bump in the two clusters, was put forward by Caloi & D’Antona (2005), who noted that a large variation in Y might be expected in M 13 if it has a much higher proportion of second-generation stars than M 3. Further support for $Y(\text{M 13}) - Y(\text{M 3}) \sim 0.02\text{--}0.04$ is provided in the very recent analysis of far- uv /optical CMDs by Dalessandro et al. (2013). Clearly such a difference would also provide a natural way of explaining why the HB in M 13 is so much bluer than that of M 3.⁸

As shown in Fig. 22, our preferred fits of isochrones to the CMDs of these two clusters suggest they are nearly coeval: the difference in their ages is estimated to be 0.25 ± 0.25 Gyr. We note, as well, that the thickness of the SGB (in both GCs) suggests that something other than, or in addition to, Y is varying since the location of the subgiant branch at a fixed age has very little dependence on the assumed helium abundance (see, e.g., the isochrones that have been plotted in the left-hand panel). Presumably this is caused by a variation in the CNO abundances and/or age, although Cohen & Meléndez (2005a) have concluded from their spectroscopic analyses that both clusters have the same, constant value of $[\text{CNO}/\text{Fe}]$, even at the tip of the RGB of M 13 where some stars have super-low oxygen abundances. A final point worth mentioning is that, if our distance estimates are accurate, the RGB bump in M 13 is intrinsically ≈ 0.1 mag brighter than that of M 3, (assuming the apparent V magnitudes of the bump given by Nataf et al. 2013), which would be consistent with M 13 having somewhat higher helium and/or lower CNO abundances than M 3 (for recent predictions of the RGB bump luminosity, see VandenBerg 2013).

5.3.2. *M 5, M 12, NGC 288, and NGC 362*

According to CBG09, M 5 and M 12 (NGC 6218) have $[\text{Fe}/\text{H}] = -1.33$, while NGC 288 and NGC 362 have $[\text{Fe}/\text{H}] = -1.32$ and -1.30 , respectively. Despite having virtually identical metallicities, NGC 362 has a very red horizontal branch, the HB populations of NGC 288 and M 12 are well to the blue of the instability strip, and the HB of M 5 spans a wide color range that the other three GCs sample only partially. These four GCs thus provide an even better example of the second-parameter phenomenon than M 3 and M 13. Since the $\Delta V_{\text{TO}}^{\text{HB}}$ method has already been used to derive reliable ages for M 5 (11.5 Gyr, see Figs. 8, 9) and NGC 362

⁸Interestingly, calibrations of the helium-sensitive R parameter ($= N_{\text{HB}}/N_{\text{RGB}}$, where N_{HB} is the number of horizontal-branch stars and N_{RGB} is the number of red giants that are brighter than the luminosity level of the HB) do not indicate that the helium abundances of these two clusters are appreciably different (e.g., Sandquist 2000, also see Sandquist et al. 2010). In fact, they suggest that Y is very nearly constant for *all* GCs, with no statistically significant dependence on $[\text{Fe}/\text{H}]$ (Salaris et al. 2004). However, such calibrations cannot be expected to apply to clusters that contain multiple stellar populations.

(10.75 Gyr, see Fig. 13), a comparison of the CMD of M 5 (which is better defined than that of NGC 362) with those of NGC 288 and M 12 via a $\Delta H_{\text{TO,RGB}}$ analysis should help to explain why the latter have much bluer HBs than the former.

As in the case of M 3 and M 13, we begin with a plot of the photometric data. Figure 23 illustrates the CMDs of NGC 288 and M 12 from the upper MS to the lower RGB, along with the fiducial sequences that have been derived to represent those observations (using the methods described in connection with Fig. 19). The densities of stars along the cluster giant branches are less than ideal, but the least-squares fits (the solid curves) appear to provide satisfactory representations of the RGB data. The result of registering these mean fiducial loci to that of M 5 (in the usual way) is shown in Figure 24. Interestingly, the cluster subgiant sequences are coincident to within their uncertainties, which suggests that all three GCs have the same helium abundances (recall the upper left-hand panel of Fig. 17). It is also somewhat surprising to find that there is no indication of an age difference between NGC 288 and M 5, while the latter seems to be ~ 2 Gyr younger than M 12.⁹

The issue of whether or not an age difference is primarily responsible for the very different HB types of NGC 288 and NGC 362 has been extensively debated in the scientific literature. Some studies (e.g., Stetson, Vandenberg, & Bolte 1996, also see Vandenberg 2000) have argued that the two clusters are nearly the same age, while others (Bellazzini et al. 2001, Catelan et al. 2001) have concluded that they differ in age by 2 ± 1 Gyr. While the result obtained here lies approximately midway between these findings, it is based on the assumption that both clusters, as well as M 5, have the same abundances of iron and the other heavy elements. This may not be the case. Figure 25 compares isochrone and ZAHB loci with the CMD of NGC 288, on the assumption that its age is 11.5 Gyr, which requires that $(m - M)_{APP} = 14.90$ if $E(B - V) = 0.012$ (Schlegel et al. 1998). Comparing this plot with its counterpart for M 5 in the left-hand panel of Fig. 8 reveals that the RGB of NGC 288 has a noticeably shallower slope than that of M 5 (or, incidently, that of NGC 362, which is morphologically very similar to the giant branch of M 5).

The simplest explanation of this difference is that NGC 288 has a higher abundance of Fe, Mg, or Si given that these are the main elements that affect the predicted temperatures of giants (see VBD12). Some support for this possibility is provided by Shetrone & Keane (2000): according to their tabulated spectroscopic results, NGC 288 has $<[\text{Mg}/\text{Fe}]>$

⁹Because the fiducial sequence that we derived for M 5 appears to be especially well determined, a plot to illustrate how well it reproduces the cluster photometry has not been included here. As a additional space-saving measure, a $\Delta H_{\text{TO,RGB}}$ analysis of NGC 362 has been omitted, as well, because it serves only to confirm that NGC 362 is ≈ 0.75 Gyr younger than M 5, as found using the $\Delta V_{\text{TO}}^{\text{HB}}$ technique. This implies, of course, that NGC 288 is older than NGC 362 by only ≈ 0.75 Gyr.

$= 0.43 \pm 0.03$ and $\langle[\text{Si}/\text{Fe}]\rangle = 0.43 \pm 0.03$ (where the uncertainty is the standard error of the mean), as compared with $\langle[\text{Mg}/\text{Fe}]\rangle = 0.36 \pm 0.03$ and $\langle[\text{Si}/\text{Fe}]\rangle = 0.35 \pm 0.04$ in the case of NGC 362. Whether the former has a higher Mg+Si+Fe abundance than the latter depends on their relative $[\text{Fe}/\text{H}]$ values — something that appears to be quite uncertain. For instance, although Shetrone & Keane concluded from their work that NGC 288 has a lower iron abundance than NGC 362 by 0.06 dex (in close agreement with the findings of Kraft & Ivans 2003), CGB09 reported a difference of only 0.02 dex (in the same sense), while Carretta & Gratton (1997) found that NGC 288 had a *higher* $[\text{Fe}/\text{H}]$ value by 0.08 dex.

If NGC 288 does have a higher Mg+Si+Fe abundance, then one would expect that its SGB should be slightly flatter than those of NGC 362 and M 5 (see Figs. 4 and 24, which indicate that this effect is expected to become important at $[\text{Fe}/\text{H}] \approx -1.3$). Since this effect is opposite to that produced by a higher helium abundance, it is possible that Fig. 24 is giving us the misleading impression that M 5 (and NGC 362) have the same helium abundances as NGC 288 (and M 12). That is, NGC 288 may actually have higher abundances of helium *and* Fe, Mg, and/or Si. Furthermore, isochrones for the same age and metal abundances, but higher Y , have somewhat reduced RGB slopes (compare the solid and dashed isochrones in the left-hand panel of Fig. 22). If our estimated relative ages are accurate, then a helium abundance difference may be the best way of explaining most of the differences in the HB morphologies of NGC 288, NGC 362, and M 5. [Curiously, Shetrone & Keane (2000) found from their spectroscopic analyses that NGC 288 has a somewhat higher oxygen abundance than NGC 362, which goes in the wrong direction to help explain the differences in their HBs. On the other hand, the earlier investigation by Dickens et al. (1991) had found nearly identical Fe and C+N+O abundances in these two clusters.]

While the same concerns may apply to M 12, the differences in the MSTO-to-RGB colors of M 5 and M 12 are too large (see Fig. 24) to be explained solely in terms of a helium abundance variation, as there is no evidence from the superposition of the cluster SGBs to support this possibility. Some difference in the helium abundance or in the mixture of the heavy elements cannot be excluded, but the simplest interpretation of Fig. 24 is that M 12 is significantly older than M 5. If its age is 13.0 Gyr, making it one of the oldest GCs in our sample, the relevant isochrone and ZAHB fit to the observed CMD will be that shown in the right-hand panel of Figure 26. To obtain a satisfactory fit of the ZAHB to the cluster HB stars, it is necessary to adopt $(m - M)_{APP} = 14.05$ and $E(B - V) = 0.225$, which is higher than the reddening derived from the Schlegel et al. (1998) dust maps by ≈ 0.05 mag. Although a rather large color offset must be applied to the isochrone in order to reproduce the turnoff color, the isochrone provides a better fit to the photometry than one for, say, 11.5 Gyr (see the left-hand panel). Both the slope of the SGB and the location of the RGB are less problematic if the higher age is assumed. Perhaps the main argument in support of this

possibility is that the fit of stellar models to the MS and the RGB in the right-hand panel is of comparable quality to that obtained for M 5 (see Fig. 8). In cases like M 12, which has a steeply sloped, extremely blue HB, as well as a relatively high (and possibly uncertain) reddening, the HB stars clearly do not provide a very tight constraint on the cluster distance, and hence its age.

5.3.3. *Low Metallicity ($[\text{Fe}/\text{H}] < -1.4$) Globular Clusters*

The horizontal method, or the approach used by MF09, to determine the relative ages of GCs that have similar metallicities is clearly preferable to the $\Delta V_{\text{TO}}^{\text{HB}}$ technique when the clusters possess blue or extremely blue HBs. It is a concern, however, that the $\Delta H_{\text{TO,RGB}}$ diagnostic is sensitive to metal abundance differences, as already pointed out. Consequently, it is important to intercompare the CMDs of clusters that have as close to the same $[\text{Fe}/\text{H}]$ value as possible so that the effects of the observed $[\text{Fe}/\text{H}]$ differences on the measured cluster-to-cluster variations in the $\Delta H_{\text{TO,RGB}}$ parameter are small. For this reason, we initially selected M 5, M 3, NGC 4147, and M 53 (NGC 5024), which have well-determined $\Delta V_{\text{TO}}^{\text{HB}}$ ages, to be the reference clusters at their metallicities ($[\text{Fe}/\text{H}] = -1.33, -1.50, -1.78,$ and -2.06 , respectively, according to CBG09). However, during the course of our investigation, we discovered that, whereas the aforementioned GCs appear to have subgiant branches with similar slopes, despite spanning a wide range in metallicity, approximately half of the target clusters had more steeply sloped SGBs. In fact, the differences in the MSTO-to-RGB morphologies of the two groups of clusters appear to resemble those of M 3 and M 13; recall the discussion in § 5.3.1.

The upper left-hand panel of Figure 27 reproduces the comparison of the M 3 and M 13 fiducials from Fig. 20, together with that derived for NGC 4147 to show that the latter looks much more “M 3-like” than “M 13-like” insofar as the slope of its SGB is concerned. (We are interested only in the part of each CMD from just past the turnoff to an abscissa value of ≈ 0.13 , as the location of the base of the RGB in a cluster will depend on its age.) The fact that the turnoffs and the SGBs of NGC 4147 and M 3 are nearly coincident, despite having $[\text{Fe}/\text{H}]$ values that differ by 0.28 dex, indicates that the differences between the solid and dashed loci are approximately independent of metallicity (at least in the range spanned by these two clusters). Moreover, since the slope of the SGB, at a fixed $[\text{Fe}/\text{H}]$ value, has no more than a slight dependence on age (see Fig. 18), the near overlap of the NGC 4147 and M 3 fiducials suggests that they have similar helium abundances. The remaining panels in the top two rows of Fig. 27, which consider GCs with $[\text{Fe}/\text{H}]$ values within 0.15 dex of those of M 3 and M 13 likewise suggest that NGC 6584 and M 70 (NGC 6681) have approximately the

same Y as M 3 while NGC 6752 probably has an enhanced helium abundance comparable to that previously deduced for M 13 (see § 5.3.1). Indeed, support for this possibility is provided by the very recent discovery of three distinct sequences in *HST*/WFC3 CMDs of NGC 6752, which are characterized by ΔY values ranging from 0.01 to 0.03 (see Milone et al. 2013).

The bottom row of Fig. 27 presents similar analyses of the TO and subgiant CMDs of two somewhat more metal-deficient GCs using NGC 4147 and NGC 4833 as the adopted reference clusters. The M 13 fiducial has been included in the left-hand panel to show that its SGB slope is quite similar to that of NGC 4833. Curiously, M 53, which is about 0.3 dex more metal-poor than NGC 4147, appears to belong to the same “family” as NGC 4147 (and M 3) given that their SGBs have nearly the same slope, while the appreciably steeper subgiant branch of NGC 5286 is a shared property with NGC 4833 (and M 13). In the first (submitted) version of this paper, additional plots similar to those in Fig. 27 were included for all of the GCs that have $[\text{Fe}/\text{H}] \lesssim -1.5$. They showed, among other things, that M 92 and M 15 appear to have steep SGBs which resemble those of NGC 4833 and M 13, and that NGC 5466 has the connection of a relatively flat SGB via M 53 and NGC 4147 to M 3.

This is especially interesting in view of the fact that Shetrone et al. (2010) have found little evidence for star-to-star variations in the abundances of the light elements in NGC 5466, which suggests that the latter consists almost entirely of first-generation stars. This would be consistent with our working hypothesis that those metal-poor clusters with the flattest SGBs have close to the primordial helium abundance and presumably, therefore, a much smaller fraction of second-generation stars than GCs that have steeper subgiant branches and (possibly) higher Y . An example of a cluster that is chemically very different from NGC 5466 is M 15, which happens to be one of the most massive clusters in the Milky Way. Cohen, Briley, & Stetson (2005) have found that the C and N abundances in its subgiant and lower RGB stars vary by ~ 1.5 and ~ 2.5 dex, respectively. Although they did not measure the abundance of oxygen, C+N was found to increase as C decreases, which requires (as noted by them) the incorporation of ON-processed material. Because these stars are too faint for deep mixing to alter surface abundances (see Denissenkov & Vandenberg 2003), Cohen et al. concluded that there must have been an extended period of star formation in M 15 involving at least two generations of massive stars. (Variations in Y and $[\text{CNO}/\text{H}]$ could well be the reason why its horizontal branch extends to both very blue and very red colors.)

Until the effects of differential reddening (when it is important) and chemical abundance variations have been quantified and disentangled, it is not possible to determine the relative ages of the different stellar populations in M 15, or in any other GC that has a “thick” SGB. At this stage, we are thus unable to say anything about O (or CNO) variations when

attempting to interpret the photometric data. However, because the slope of the subgiant branch appears to be a fairly sensitive function of the helium abundance, and not much else, this diagnostic may enable us to separate the GCs with $[\text{Fe}/\text{H}] \lesssim -1.5$ into low- and higher- Y groups. However, a valid question to ask is how accurately can the SGB slopes be determined, and indeed, one of the referees of this paper urged us to find a way of attaching an errorbar to the derived slopes so as to provide a measure of the significance of the results. In response to this recommendation, we decided to retain only the few comparisons of fiducial sequences that are shown in Fig. 27 and to evaluate the SGB slopes using the linear least-squares subroutine “FIT” from *Numerical Recipes* (Press et al. 1986), as it yields both the slope and its uncertainty for the best-fit line through data.

Some care must be taken in selecting the part of the SGB that is fitted by a straight line since there is obvious curvature near the turnoff and near the lower RGB. Based on an inspection of isochrones and the observed GC CMDs, we opted to perform a least-squares fit to those SGB stars from 0.045 mag redder than the TO to 0.13 mag redder than the TO, in the case of clusters with $[\text{Fe}/\text{H}] < -1.9$. Because more metal-rich GCs have shorter subgiant branches, the adopted color range was slightly reduced at higher metallicities to include only those stars from 0.05 mag redder than the TO to 0.125 mag redder than the TO. Except for this slight difference in the selection criteria, all clusters were treated in the same way. Figure 28 shows some examples of the observed CMDs in which dashed rectangles delineate the regions of the SGBs that have been subjected to a linear least-squares analysis. These CMDs are not the best, nor the worst, ones in our data base insofar as the star-to-star scatter is concerned. The two clusters in the left-hand panels have nearly the same $[\text{Fe}/\text{H}]$, as do those in both right-hand panels, to within 0.03 dex according to CBG09, and it is apparent even from a visual inspection that M 15 has a steeper SGB than NGC 5466 and NGC 6752 has a steeper subgiant branch than NGC 6934. The derived slopes and their uncertainties are indicated in each panel.

Note that the median fiducial sequences which have been determined for the MS and TO stars (the filled circles) are very smooth, as in similar plots which have already been discussed (see Figs. 19 and 23). We investigated whether these sequences depended on the photometric errors by deriving them for CMDs that included only those stars with errors in the tabulated magnitudes < 0.01 mag, or < 0.02 mag, or < 0.03 mag and, although we made such tests for only a limited number of the clusters, the resultant fiducial sequences were always nearly identical. There were slight shifts of the median points for just a few bins in some clusters, but regardless of whether the CMD was well populated and tightly defined (e.g., M 13), had relatively few stars and considerable scatter (like NGC 288), or was especially broad due (likely) to differential reddening (as in the case of NGC 5986), the curves defined by the median points did not differ significantly for the different data sets.

Recall from Fig. 3 that the slope of the SGB at a fixed age tends to increase inversely with $[\text{Fe}/\text{H}]$.

Figure 29 plots the slopes, and their uncertainties, for the GCs in our sample with $[\text{Fe}/\text{H}] \lesssim -1.5$. (Because the slope of the SGB becomes quite a sensitive function of $[\text{Fe}/\text{H}]$ at higher metallicities, as already discussed, little is to be gained by extending the analysis to more metal-rich clusters.) The dashed line represents the best-fit line through all of the points, as derived from the *Numerical Recipes* FIT subroutine. This separates the clusters into groups that have relatively steep or shallow SGBs (the filled and open circles, respectively): the few GCs that straddle the line and hence have intermediate SGB slopes are depicted as open circles with black dots at their centers. The clusters comprising each of the three groups are identified in Table 1, which also lists the information that has been plotted. For the most part, the derived slopes support the division of the GCs into “M 3-like” or “M 13-like” as found in our initial analysis, which was based on comparisons of median SGB sequences like those shown in Fig. 27. Only in a few cases have the classifications changed from our initial determinations, but this is to be expected given the size of the 1σ errorbars for several cases. Indeed, at the 2σ level, most of the errorbars would intersect, which shows that the cluster-to-cluster differences in their SGB slopes are really quite subtle.

Before examining whether these two groups can be differentiated in other ways, it is necessary to determine the ages of those clusters which are not amenable to a $\Delta V_{\text{TO}}^{\text{HB}}$ analysis (since age may be one of the distinguishing characteristics). It is unfortunate that the MSTO-to-RGB color difference is a function of the metallicity since a ± 0.1 dex uncertainty in the relative $[\text{Fe}/\text{H}]$ values implies an error bar of $\sim \pm 0.25\text{--}0.5$ Gyr in the age difference that is derived using the VBS90 approach. For instance, we found that M 3 is $\lesssim 0.25$ Gyr younger than NGC 4147, while M 53 is ≈ 1 Gyr older than NGC 4147, if the $\Delta H_{\text{TO,RGB}}$ technique is used to estimate their relative ages. However, these results are at odds with those already obtained: according to Figs. 12 and 22, M 3, NGC 4147, and M 53 have ages of 11.75, 12.25, and 12.25 Gyr, respectively. It is possible to reconcile the relative ages of the three clusters from the horizontal and vertical methods if the $[\text{Fe}/\text{H}]$ value of NGC 4147 is close to -1.9 (instead of -1.78 , as reported by CBG09) and either M 53 is slightly more metal-rich than our adopted value of $[\text{Fe}/\text{H}]$ and/or it is ~ 0.25 Gyr older the $\Delta V_{\text{TO}}^{\text{HB}}$ estimate. (It would be very encouraging, indeed, if future spectroscopic studies confirm these predictions.)

Fortunately, such cases were found to be in the minority; in general, there was reasonably good consistency of the relative $\Delta H_{\text{TO,RGB}}$ ages of a given GC when determined with respect to both higher and lower metallicity reference clusters. Nevertheless, in view of the M 3–NGC 4147–M 53 example, the 1σ uncertainties of ages that are based solely on the horizontal method must be at least ± 0.5 Gyr. As a result of this example, and a few others that

showed similar discrepancies (see below), considerable time and effort was spent examining the impact on the inferred ages of using different reference clusters and of checking the degree of consistency with the $\Delta V_{\text{TO}}^{\text{HB}}$ ages, even if the latter had not been derived previously. It is helpful to consider, in particular, if isochrones for the adopted ages provide fits to the cluster turnoffs and giant branches of comparable quality as those reported in § 5.1 irrespective of how well the ZAHBs match up with the HB populations. Blindly accepting the $\Delta H_{\text{TO,RGB}}$ ages without such cross-checks would have resulted in different ages for several of the GCs, though the net effect on the mean age–[Fe/H] relation that is derived in this study would not have been very large, given that the number of age determinations that are based primarily on the horizontal method is $< 20\%$ of the total.

Figure 30 presents the application of the $\Delta H_{\text{TO,RGB}}$ method to those clusters for which the horizontal approach is deemed to be more reliable than the $\Delta V_{\text{TO}}^{\text{HB}}$ technique, along with some counter-examples. In each panel, the solid and dashed curves represent, in turn, the lower giant-branch portions of the fiducial sequences of the reference and target GCs, which are identified in the upper left-hand corner. These sequences were registered to the usual abscissa and ordinate zero-points (as in, e.g., Fig. 24 and Figs. 27–29), but only the comparison of their RGB segments are shown, together with a set of isochrones for the metallicity of the reference cluster, since nothing more is needed to derive the difference in their ages. Thus, considering the top row, and noting the corrections that should be applied to the solid curve to account for metallicity differences, one finds that M 3 is predicted to be 0.25–0.5 Gyr older than M 5, $\lesssim 0.25$ Gyr older than NGC 3201 (though the CMD of the latter is very poorly defined), coeval with NGC 6584, and ~ 1.5 Gyr younger than M 70. Except for M 70, which was not considered in § 5.1, these results are consistent to within ± 0.25 Gyr with the differences in the absolute cluster ages previously derived using the $\Delta V_{\text{TO}}^{\text{HB}}$ method. Indeed, the same conclusion is reached in the case of NGC 6934 (see the left-hand panel in the second row from the top) and M 72 (not shown, but which is clearly coeval with M 3).

In the next five panels, M 13 is the adopted reference cluster and the target clusters include several of those systems which, like M 13, appear to have steeper SGBs than M 3. For three of them (M,10, NGC 6752, and M 2), the level of consistency with the results of $\Delta V_{\text{TO}}^{\text{HB}}$ analyses is quite satisfactory. As a space-saving measure, plots showing fits of isochrones and ZAHB loci to the CMDs of clusters with blue HBs have generally not been included in this paper, though they have been produced and carefully examined. Indeed, in the case of NGC 6752, which has a relatively low and well-determined reddening ($E(B - V) = 0.056$; Schlegel et al. 1998), the fit of a ZAHB for [Fe/H] = -1.55 (see CBG09) to the cluster HB stars yields $(m - M)_{\text{APP}} = 13.23$, implying an age of 12.50 Gyr (i.e., 0.50 Gyr older than M 13, which is also favored by the comparison shown in Fig. 30). However, the M 13–NGC 5286 and M 13–NGC 5986 intercomparisons suggest that M 13 is younger than either of

the other clusters by $\gtrsim 1.25$ Gyr. The age of NGC 5286 was previously found to be 12.25 Gyr (see Fig. 12, which is unlikely to be wrong by more than 0.5 Gyr; consequently, we suspect that the much older age that is suggested by Fig. 30 is due, in part, to the assumption of a metallicity that is too low. If the difference in the adopted $[\text{Fe}/\text{H}]$ values is reduced, the inferred ages of M 13 and NGC 5286 would be more similar. The same explanation may apply to NGC 5986, though the CMD of this system is clearly affected by differential reddening, which may affect the determination of its mean photometric sequence. Stellar populations effects may also complicate the interpretation of the CMDs of NGC 5286 and NGC 5986 if our suspicion that age and chemical abundance variations are greater in the group of GCs that has been classified as “M 13-like” is correct.

NGC 4833 is another cluster that presented some difficulties when its CMD is compared with those of other clusters that have similar $[\text{Fe}/\text{H}]$ values. Hence, for the next group of GCs in Fig. 30, NGC 5286 was chosen to be the reference cluster. With this choice, the ages of NGC 6144, NGC 6541, M 22, and M 56 relative to that of NGC 5286 were found to be in satisfactory agreement with the differences in their absolute ages as derived from the $\Delta V_{\text{TO}}^{\text{HB}}$ technique. In the case of NGC 4833, an age of 12.50 Gyr has been adopted, which represents a compromise of the ages that are found from the two methods. The results shown in the remaining panels of Fig. 30 were all found to be in acceptable agreement with those based on fits of isochrones and ZAHBs to the observed CMDs. For none of them were the derived age differences from the $\Delta H_{\text{TO,RGB}}$ and $\Delta V_{\text{TO}}^{\text{HB}}$ analyses > 0.50 Gyr. For instance, whereas Fig. 11 indicates that M 92 and M 30 are coeval, Fig. 30 suggests that they differ in age by 0.50 Gyr. Accordingly, we have adopted an age of 13.0 Gyr for M 30 and thereby achieved consistency with both determinations to within ± 0.25 Gyr. As noted in § 6, similarly averaged ages (sometimes taking a subjective assessment of the reliability into account) have been taken to be the “best” estimates of the ages of a few other GCs.

Aside from a few problematic cases, our age determinations appear to be quite well constrained — though one must continue to be wary of the $\Delta H_{\text{TO,RGB}}$ -based results given their very considerable sensitivity to metal abundances. Not surprisingly, the ages also depend on whether or not we have correctly classified a given cluster into one of the two groups of GCs that are distinguished by different SGB slopes, and on whatever is responsible for that distinction. (Helium abundance differences, which could arise as a consequence of cluster-to-cluster variations in the chemical properties of the stellar populations that they contain, have been tentatively identified as the cause of such morphological differences, but there may be other, as yet unidentified, factors at play.) Figure 31 shows, for example, that much older ages ($\gtrsim 13$ Gyr) would have been derived for NGC 6752 and M 56 had we used M 3 and M 53 as the reference clusters, respectively (instead of M 13 and NGC 5286, which appear to belong to the same “family”). Indeed, the oldest clusters in the group in which

M13 has been taken to be the prototype would have predicted ages as old, or older, than the age of the universe if the $\Delta H_{\text{TO,RGB}}$ method were used to obtain their ages relative to that of M3. By the same token, the oldest GCs in the M3 group would have been found to have younger ages by ~ 0.5 Gyr than our adopted estimates had their fiducial sequences for the MSTO-to-RGB stars been compared with that of M13.

5.3.4. Higher Metallicity ($[\text{Fe}/\text{H}] \geq -1.4$) Globular Clusters

Because the effects of variations in the abundances of the heavy elements on isochrones become larger as the metallicity increases (see VBD12), relative age determinations based on the horizontal method will be especially uncertain at higher $[\text{Fe}/\text{H}]$ values. Fortunately, the red HBs of metal-rich systems are more easily fitted by computed ZAHBs than the blue horizontal branches that are typical of metal-poor GCs, and since the $\Delta V_{\text{TO}}^{\text{HB}}$ technique has a reduced dependence on the metal abundance (see § 3.2 for an instructive discussion of this point), the vertical method is clearly the “method of choice” when determining ages (particularly cluster-to-cluster differences in in age) at higher values of $[\text{Fe}/\text{H}]$. For these reasons, no attempt has been made to apply the $\Delta H_{\text{TO,RGB}}$ method to GCs that have $[\text{Fe}/\text{H}] \geq -1.4$. We note, as well, that we were unable to detect any SGB slope variations in the CMDs of metal-rich clusters; see, e.g., the comparisons of the fiducial sequences of M5, NGC 288, and M12 that are shown in Fig. 24. It may, in any case, be difficult to determine whether such variations exist because the slope of the SGB is predicted to be an increasingly sensitive function of the metal abundance at $[\text{Fe}/\text{H}]$ values above ~ -1.4 (see Fig. 4). Consequently, the effects on the SGB due to a metal abundance increase could be comparable to, and compensate for, those caused by a moderate helium abundance enhancement, and vice versa.

5.4. Six Additional Globular Clusters, Including Four Associated with the Sagittarius Dwarf Galaxy

Although there are 64 GCs in the Sarajedini et al. (2007) data set, the CMDs for several of them are not sufficiently well defined to permit the derivation of accurate fiducial sequences. This is especially true in the case of the $[\text{Fe}/\text{H}] \sim -0.45$ clusters NGC 6388 and NGC 6441, due to field-star contamination and/or the effects of significant differential reddening. (Since they are among the most massive and tightly-bound clusters in the Milky Way, stellar populations effects likely contribute to the breadth of their photometric sequences as well. In fact, distinct sub-populations of stars have been discovered in them

by Bellini et al. 2013.) NGC 2298 ($[\text{Fe}/\text{H}] = -1.96$) and NGC 6093 ($[\text{Fe}/\text{H}] = -1.75$) were found to be similarly problematic, in that their stellar distributions in the vicinity of the turnoff are clearly asymmetric, which makes the determination of the turnoff color, the slope of the SGB, and the value of the $\Delta H_{\text{TO,RGB}}$ parameter in either cluster quite uncertain. Furthermore, our attempt to fit ZAHB loci to their blue HBs suggests that the reddenings given by the Schlegel et al. (1998) dust maps are too low by $\gtrsim 0.04$ mag. Among those GCs without NGC numbers, the paucity of stars in the CMDs of E 3 and Pal 1, and the ambiguous location of the subgiant branch and the very broad giant branch in the CMD of Lynga 7, preclude the possibility of precise age determinations for these systems. In view of these difficulties, we decided to drop these seven clusters from our sample, along with Terzan 7, because our model grids do not extend to sufficiently high metal abundances to produce isochrones and ZAHBs for its metallicity ($[\text{Fe}/\text{H}] = -0.12$, according to CBG09).

Up to this point, ages have been derived for 50 of the remaining 55 globular clusters. For the rest, the observed CMDs and the derived $\Delta V_{\text{TO}}^{\text{HB}}$ ages are presented in Figure 32. [In order to have two complete rows of three panels, an isochrone fit to the CMD of M 70 is included, even though its age was previously determined using the horizontal method. This particular cluster was selected because, despite its very blue HB, the ZAHB-based distance that is obtained on the assumption of the reddening given by Schlegel et al. (1998) implies an age which agrees well with that inferred from the $\Delta H_{\text{TO,RGB}}$ approach; see Fig. 30. By assessing the consistency of the results from the two age-dating methods, we have obtained an age for M 70 that appears to be quite well constrained. Similar assessments have been made for other clusters with blue HBs, but with varying degrees of success.] Because NGC 6535 has such a sparsely populated CMD, the best estimate of its age is obtained using the $\Delta V_{\text{TO}}^{\text{HB}}$ method. However, unlike the example of M 70, it is not possible to obtain a satisfactory fit of stellar models to the photometric data unless the Schlegel et al. reddening estimate is increased by about 0.07 mag. With such an adjustment (see the top left-hand panel), the ZAHB for the observed $[\text{Fe}/\text{H}]$ value provides a satisfactory match to the few HB stars that are present and, in particular, the best-fit isochrone reproduces the MS, SGB, and lower RGB stars about as well as we have been able to achieve for most of the GCs.

Ibata, Gilmore, & Irwin (1995) discovered that M 54 (NGC 6715), Arp 2, and Terzan 8 are associated with the Sagittarius dwarf galaxy, while a similar origin of Pal 12 was deduced by Dinescu et al. (2000) from an analysis of its orbit. In support of previous age determinations (e.g., VandenBerg 2000), Pal 12 appears to be an unusually young system, with an age near 9 Gyr. However, the ages derived here for M 54, Arp 2, and Terzan 8 are all quite similar to those found for other globular clusters of similar metallicities. As CBG09 did not determine the mean iron abundance of stars in Ter 8, its $[\text{Fe}/\text{H}]$ value has been taken from the spectroscopic study by Mottini, Wallerstein, & McWilliam (2008), who obtained

–2.34 from their analysis of Fe I and Fe II lines. This estimate would appear to be on nearly the same scale as the one by CBG09 given that Mottini et al. also determined that Arp 2 has $[\text{Fe}/\text{H}] = -1.77$ (from Fe I lines), which is in very good agreement with the CBG09 determination of -1.74 . Only in the case of Pal 12 have models for $[\alpha/\text{Fe}] = 0.0$ (e.g., Brown, Wallerstein, & Zucker 1997) been used to fit the cluster CMD. According to Mottini et al., the observed α -element enhancements in Arp 2 and Ter 8 are “not too different” from those found in Galactic GCs at similar $[\text{Fe}/\text{H}]$ values, and we have assumed that this conclusion also applies to M 54. To be specific, models for $[\alpha/\text{Fe}] = 0.46$ have been fitted to the CMDs of Arp 2, Ter 8, and M 54.

Interestingly, Mottini et al. derived $[\text{O}/\text{Fe}] = 0.21 \pm 0.22$ for Arp 2 and 0.71 ± 0.17 for Ter 8. These differences have not been taken into account. However, it is very difficult to measure the oxygen abundances in metal-poor stars (see, e.g., Ramírez et al. 2006) and the assumed value, $[\text{O}/\text{Fe}] = 0.50$, which appears to be close to the best estimate of the mean oxygen overabundance in stars of low metallicity (see, e.g., Ramírez et al. 2012), is just outside the 1σ uncertainties of the derived values. It is surprising that a ZAHB for $[\text{Fe}/\text{H}] = -1.44$ provides such a good fit to the HB population of M 54 given that Carretta et al. (2010a) have found a ~ 0.2 dex dispersion in its metallicity. Although an 11.75 Gyr isochrone for $[\text{Fe}/\text{H}] = -1.44$ provides a reasonably good match to its CMD, M 54 is clearly a complex system that could well have somewhat younger or older components. No attempt has been made here to explore the impact of age and/or chemical abundance variations, though our derived age is expected to be a reasonably accurate estimate for its dominant stellar population.

6. Globular Cluster Ages and Their Correlations with Other Properties

The ages that have been derived in this investigation for the 55 GCs that comprise our sample are listed in the fourth column of Table 2. The first two columns identify the clusters, and the third column lists the adopted $[\text{Fe}/\text{H}]$ values from the study by CBG09 (or, in the case of Terzan 8, from Mottini, Wallerstein, & McWilliam 2008). The letters “V” or “H” in the fifth column indicate, in turn, whether the adopted age is based primarily on the vertical, or the horizontal, method. For those clusters in which the letter “A” appears in the fifth column, the $\Delta V_{\text{TO}}^{\text{HB}}$ and $\Delta H_{\text{TO,RGB}}$ results have been averaged in order to obtain the tabulated age. To support these age estimates, at least one plot is provided for each GC: the sixth column contains the reference(s) to the relevant figure(s). The last five columns list, in the direction from left to right, the HB type (from Mackey & van den Bergh 2005), the Galactocentric distance (in kpc), the absolute integrated visual magnitude (both R_G and

M_V have been taken from the 2010 edition of the catalog by Harris 1996), the central escape velocity (in km/s), and the common logarithm of surface density of stars at the cluster center (in \mathcal{M}_\odot/pc^2). (The calculation of the last two quantities is described in § 6.2.) In this study, the HB type is defined to be $(B-R)/(B+V+R)$, where B, V, and R represent the number of stars that lie blueward of the instability strip, the number of variable (RR Lyrae) stars, and the number of stars that are on the red side of the instability strip, respectively.

The ΔV_{TO}^{HB} ages that were independently determined by the UVic participants in this collaborative project (i.e., DAV, KB, and RL) spanned the age ranges that are specified in the seventh column. (If, as in a few cases, exactly the same age was found, only a single number is reported.) In general, these estimates agreed to within 0.25–0.50 Gyr, which is the basis for adopting ± 0.25 Gyr uncertainties for what we consider to be the best determined ages. (These are *internal* uncertainties; i.e., they do not include the effects of distance or chemical abundance errors. As the Victoria models appear to satisfy the constraints provided by standard candles reasonably well, we believe that the derived distance moduli are accurate to within ± 0.10 mag, which implies an age uncertainty of $\approx \pm 1$ Gyr. As shown by VBD12, turnoff luminosity versus age relations for low metallicity stars are strong functions of primarily the helium and oxygen abundances. Although our adopted values of Y and $[O/Fe]$ represent current best estimates, there may well be cluster-to-cluster variations in these quantities, in the mean, that impact age determinations at the level of 0.5–1.0 Gyr. For instance, a ± 0.15 dex uncertainty in the assumed $[O/Fe]$ value corresponds to an age uncertainty of ± 0.5 Gyr.) As is widely appreciated, relative ages are more secure than absolute ages.

Because they depend quite sensitively on the adopted metallicity, ages based primarily on the horizontal method have generally been considered to be uncertain by ± 0.50 Gyr, though this error bar was reduced to ± 0.38 Gyr (i.e., midway between ± 0.25 and ± 0.50 Gyr) if the two age-dating methods that we have employed yielded fully consistent results (as in the case of, e.g., M 70). A larger uncertainty (i.e., ± 0.75 Gyr) was ascribed to the derived ages of only two clusters, NGC 5986 and M 107, in view of the fact that their CMDs are especially problematic (broad and asymmetric stellar distributions). Note that, because the ZAHB-based distances are uncertain by at least ± 0.01 – 0.02 mag, even in the most favorable cases, our final age estimates have been rounded to the nearest 0.25 Gyr. Note, as well, that the adopted age is always within the range that is listed in the seventh column (when one is specified), though not necessarily in the middle of that range. After ΔV_{TO}^{HB} ages had been independently derived by DAV, KB, and RL, the different fits of isochrones and ZAHBs to the observed CMDs that had been obtained by the three investigators were carefully scrutinized and the one that was judged to be the most agreeable comparison between theory and observations was selected. These cases are the ones that have been

reproduced in Figs. 11–14 and Fig. 16.

6.1. The Age–Metallicity and Age–Galactocentric Distance Relations

Figures 33 and 34 show how the ages that we have determined vary, in turn, with $[\text{Fe}/\text{H}]$ and with Galactocentric distance, R_G . The first of these plots bears more than a passing resemblance to a similar diagram that was constructed by VandenBerg (2000, see his Fig. 40). In fact, it should not be a surprise that the age–metallicity relation (AMR) obtained here is qualitatively very similar to the one produced 13 years ago because the same $\Delta V_{\text{TO}}^{\text{HB}}$ technique was used in both studies to derive the ages and, more importantly, the respective ZAHB models predict nearly the same dependence of $M_V(\text{RR Lyrae})$ on $[\text{Fe}/\text{H}]$. It is to be expected that there will be, and are, differences in the absolute ages given that, in particular, the current Victoria-Regina isochrones take the diffusion of helium and the latest nuclear reactions into account. In addition, there are some significant differences in the adopted chemical abundances. However, for the GCs in common to the two studies, the predicted ages differ by $\lesssim 1$ Gyr, which is well within the error bars due to distance and $[\text{O}/\text{Fe}]$ uncertainties. To be sure, the present results are more robust because they have been derived from a much larger sample of GCs with superior photometry using improved stellar models that allow for variations in the abundances of helium and several metals. The availability of models for different values of Y , in particular, have enabled us to determine that the morphological variations that are seen in the CMDs of clusters with similar metallicities cannot be explained solely in terms of age differences.

According to Fig. 33, GCs more metal-poor than $[\text{Fe}/\text{H}] \sim -1.7$ have a mean age of ≈ 12.5 Gyr with a dispersion of $\sim \pm 0.5$ Gyr. At higher $[\text{Fe}/\text{H}]$ values, one has the visual impression that the AMR is bifurcated, with one branch running from approximately 12.5 Gyr at $[\text{Fe}/\text{H}] = -1.7$ to 11 Gyr at $[\text{Fe}/\text{H}] = -1.2$, while the other is offset to higher metallicities by ≈ 0.6 dex at a fixed age. Remarkably, it turns out that most of the clusters in the latter sequence, which include M 12, NGC 6362, NGC 6717, and 47 Tuc, have disk-like kinematics according to Dinescu, Girard, & van Altena (1999a), and it is possible that the other two $[\text{Fe}/\text{H}] < -1.0$ GCs in this small group (NGC 6717 and NGC 6723) do so as well, but we have been unable to find any orbital information for them. In contrast, the intermediate-metal-poor clusters that constitute the other branch (including M 2, M 3, M 5, M 13, NGC 288, and NGC 362, and a few others) seem to have mostly (exclusively?) halo-type orbits (also see Dinescu et al. 1999b). Although Pal 12 does not appear in this plot (because its age is outside the range of the ordinate), its age (9.0 Gyr) and $[\text{Fe}/\text{H}]$ value (-0.81) would place it close to a linear extension of the left-hand branch of the AMR to

higher metallicities, while the clusters with $[\text{Fe}/\text{H}] > -0.9$, which have long been known to have a flattened spatial distribution (Zinn 1985), lie along a continuation of the right-hand branch.

The split AMR obviously has important implications for the formation/assembly of the GC system belonging to the Milky Way. Since it would be worthwhile to perform an expanded analysis of the cluster kinematics, to compare our AMR with those derived for stars in the solar neighborhood (e.g., Casagrande et al. 2011) and for such dwarf galaxies as Sagittarius and the Large Magellanic Cloud (e.g., Leaman et al. 2013), and to examine the consistency of the results with different formation scenarios (e.g., Elmegreen et al. 2012), further discussion of Fig. 34 has been deferred to a study by Leaman, VandenBerg, & Mendel (2013). However, one issue that should be addressed here is why our results conflict with those of MF09 (and Dotter et al. 2010), who argued that the majority of the Galactic GCs are nearly coeval, aside from a relatively small subset of young, $[\text{Fe}/\text{H}] \lesssim -1.2$ systems that follow a single AMR with a significant slope. In fact, the main point of contention is whether the GCs that have $[\text{Fe}/\text{H}] > -1.0$ are of comparable age as the most metal-deficient clusters, as they reported, or younger by $\approx 1.5\text{--}2$ Gyr, as derived in this investigation. In the next section, an explanation of the main cause of this discrepancy is provided.

However, before turning to that discussion, a few comments should be made concerning Fig. 34. First, considering the entire data set, there is virtually no dependence of the mean age or the dispersion in age on R_G . Second, whereas the clusters in our sample with $[\text{Fe}/\text{H}] \geq -1.0$ are all located within 8 kpc from the center of the Milky Way, those of lower metal abundances are distributed over the entire range in Galactocentric distance that has been plotted. (Pal 12, which has $[\text{Fe}/\text{H}] = -0.81$ and $R_G = 15.8$ kpc, is an “exception to the rule”, and there are likely to be others, but this cluster is believed to have originated in the Sagittarius dwarf galaxy and therefore *may* belong to a different category than the other metal-rich GCs in our sample. Moreover, as noted above, Pal 12 appears to be connected with a different AMR than the other GCs in our sample that have $[\text{Fe}/\text{H}] \sim -0.8$.) Finally, there is quite a striking difference in the ages of the clusters that have $[\text{Fe}/\text{H}] < -1.7$ and those that have $[\text{Fe}/\text{H}] \geq -1.0$, which is, of course, just a reflection of the AMR shown in the previous figure.

Our finding that old, very metal-poor GCs are found at any R_G , while the majority of the metal-rich clusters are younger and located at smaller Galactocentric distances, suggests an “outside-in” scenario for the formation of the Galaxy. Given the evidence of Sagittarius, there is no denying that mergers of dwarf galaxies are responsible for many of the GCs that reside in the Milky Way. However, it also seems very likely that many of them formed during the collapse of a single, massive protogalaxy, perhaps as described by Eggen, Lynden-

Bell, & Sandage (1962, also see Sandage 1990b), or by Hartwick (2009), who suggested that protogalactic filaments first collapsed in a direction perpendicular to their lengths and then along their lengths. To improve our understanding, it would be helpful to include Bulge GCs in the sample, as well as clusters that are located at $R_G \gtrsim 20$ kpc. [In fact, the AMR that is analyzed by Leaman et al. (2013) includes the six outer-halo clusters that were the subject of a paper by Dotter, Sarajedini, & Anderson (2011).]

6.1.1. *Relative Ages Based on the rMSF Method of Marín-Franch et al. (2009)*

It took some careful detective work to understand why the results obtained by MF09 conflict with ours. In fact, the main reasons for the difference is that (i) the rMSF method that was devised, and used, by MF09 is especially sensitive to the adopted metal abundances and (ii) the $[m/H]$ values that they adopted involve some inconsistencies. This can be appreciated by considering the results shown in Figure 35, which plots the age– $[m/H]$ relations that are obtained using the rMSF method on the assumption of different metallicity scales. The top two panels reproduce their Figs. 10 and 11 for a subset of the sample of GCs that they considered: only those clusters with normalized relative ages < 0.75 and those without $[Fe/H]$ determinations by CBG09 have been omitted. Note that we have added “R97” to the labels in the upper left-hand corner of these two panels to emphasize that the metal abundances used by MF09 were obtained from the Rutledge, Hesser, & Stetson (1997, hereafter R97) catalog. In the case of clusters not considered by R97 (those represented by small filled circles), MF09 adopted the metallicities given by Zinn & West (1984, hereafter ZW) and transformed them to the Carretta & Gratton (1997, hereafter CG) scale using the equation given by Carretta et al. (2001).

The results plotted in panel (a), which assume the CG scale of R97, do indicate that there is a population of coeval GCs that spans the entire metallicity range. However, this is not the case if the ZW scale is adopted; see panel (b). Despite the evidence to the contrary, MF09 (see their footnote 14) conclude that the results derived from the two metallicity scales are equivalent, and then proceed to use only the CG results for their subsequent analysis. However, as seen by comparing panels (a) and (b), there are differences between them — and, for the following reason, we believe that the CG scale of R97 is the least trustworthy one. In footnotes to their table of $[Fe/H]$ values, R97 warn the reader that, for several clusters at the metal-rich end, $[Fe/H]$ values on the CG scale have been obtained by extrapolating their Ca II triplet measurements linearly past the most metal-rich cluster that had an $[Fe/H]$ value determined from high-resolution spectra. This is of particular concern because, as discussed by R97, there is an inconsistency between the CG and ZW scales as derived from their

calibration of Ca II triplet line strengths, likely because the Ca II lines lose their sensitivity to $[\text{Fe}/\text{H}]$ at the metal-rich end.

In fact, most of that inconsistency was removed by Carretta et al. (2001) when they obtained and analyzed spectra for stars in two very metal-rich clusters. Had MF09 employed the non-linear equation derived by Carretta et al. to transform *all* of the ZW metallicities to the CG scale, instead of just a subset of them, they would have obtained the AMR shown in panel (c).¹⁰ At the metal-rich end, this resembles the relationship plotted in panel (b) more so than in panel (a) and, importantly, it also looks similar to the AMR shown in panel (d). This is based on the more recent metallicity scale of CBG09 (as adopted in our investigation), where a non-linear relationship between the Ca II triplet measurements and $[\text{Fe}/\text{H}]$ is further supported by high-resolution spectroscopy of two additional high-metallicity clusters. To obtain the results of panels (c) and (d), we used the turnoff magnitudes given by MF09 (from their Table 4) and $[m/\text{H}]$ values that were calculated from the corresponding $[\text{Fe}/\text{H}]$ determinations using their equation (3). To derive the relative ages that are plotted in these panels, we assumed that $d(\text{age})/d([m/\text{H}]) \sim -4.5$ Gyr/dex, which is a good approximation to the predicted variation of age with $[m/\text{H}]$ in their Fig. 7, together with their relative ages and corresponding age zero-point to obtain new absolute ages. These were then transformed back to relative ages using the same zero-point as MF09; namely, the mean age of clusters with $[m/\text{H}] < -1.4$. Indeed, when the same CBG09 metallicities are adopted, relative ages based on the MF09 formalism (panel d) appear to be quite similar to our findings.

The results shown in panels (a) to (d) demonstrate that the MF09 approach is exceedingly sensitive to the adopted chemical abundances (which are likely to undergo further adjustments in the future). However, as pointed out in § 3, the $\Delta V_{\text{TO}}^{\text{HB}}$ method that is the basis of most of our age determinations is not particularly dependent on the assumed $[\text{Fe}/\text{H}]$ scale: the effect of metallicity on the luminosity of the HB is compensated to a significant extent by its effect on the turnoff luminosity at a given age. This is a huge advantage. Even if we had adopted the CG/R97 abundance scale, we would not have obtained an age-metallicity relation that is similar to the one reported by MF09. Also worth emphasizing is the fact that, as acknowledged by MF09, the rMSF technique is sensitive to the abundances of such elements as Mg and Al, which have been observed to vary from cluster-to-cluster (see Carretta et al. 2009b). These, and several other abundant heavy elements affect the color

¹⁰In constructing this panel, we discovered that the $[\text{Fe}/\text{H}]$ values given by MF09 (in their Table 1) for NGC 6144, NGC 6584, NGC 6652, and M 56 are incorrect, though the $[m/\text{H}]$ values that are given for these same clusters in their Table 4 are fine. We also found that the transformation equation from Carretta et al. was not used to derive the CG/R97 $[m/\text{H}]$ values of M 3 and M 92: the $[\text{Fe}/\text{H}]$ values for these clusters were presumably taken directly from Carretta & Gratton (1997).

offset between the MSTO and the RGB at a fixed age much more so than the luminosity of the turnoff (see VBD12 and our Fig. 17). At low metallicities, the turnoff luminosity versus age relations are strong functions of the helium and oxygen abundances, and little else. (It is also a clear disadvantage of the $\Delta H_{\text{TO,RGB}}$ method of determining relative ages that it is a sensitive function of $[\text{Fe}/\text{H}]$ and the detailed heavy-element mixture. This method, which should be applied *only* to clusters that have the same metal abundances, is clearly of limited usefulness.)

A further concern with the MF09 results is that, if the CBG09 metallicities are correct, there is a 0.65 dex difference in the $[m/\text{H}]$ values of the reference clusters that were used for the two most metal-rich groups of GCs. Coupled with the likelihood that the clusters with high $[\text{Fe}/\text{H}]$ values are more metal-rich and younger than assumed by MF09, the errors in the inferred ages from the rMSF method will be increased. Consider, in particular, their Fig. 6 (or our Fig. 4), which shows that the lower MS slopes of computed isochrones vary significantly with $[\text{Fe}/\text{H}]$, especially at higher metallicities. Such variations make the result of the rMSF method dependent on the exact magnitude range that is used and on the difference in the metal abundances between that of the reference cluster for a given metallicity bin and those of each of the target clusters in that group. In fact, the self-consistency test that they show in their Fig. 6 considers only relatively small variations in $[m/\text{H}]$: the impact of varying the age was not examined. Moreover, their test does not extend above $[m/\text{H}] = -0.5$, where the difficulties will be exacerbated.

MF09 found from their consideration of a few different grids of evolutionary models that their results were essentially independent of this choice. This is probably to be expected given that it is the differences between the isochrones for different ages that matter rather than their location on the CMD in an absolute sense. As shown in Figure 36, both the DSEP and the BASTI (Pietrinferni et al. 2006) isochrones predict similar, though not identical, separations between the isochrone RGBs for different ages at a fixed $[\text{Fe}/\text{H}]$ (left-hand panels), and for variations in $[\text{Fe}/\text{H}]$ at a given age (right-hand panels) when the isochrones are registered to the usual abscissa and ordinate zero-points. These results compare quite well with those derived from the Victoria-Regina isochrones used in this investigation (see the right-hand panels of Fig. 2 and Fig. 3, respectively). There are certainly some morphological differences between the three sets of models, and the separation of the giant branch from the MSTO is obviously much larger in the case of the BASTI isochrones than in the DSEP or Victoria-Regina predictions. This is probably caused primarily by the neglect of diffusive processes in the BASTI computations, though differences in the treatment of convection, the atmospheric boundary condition, the adopted color- T_{eff} relations, or the detailed heavy-element mixture may also be partially responsible for this. (Since the giant branches of the best-fit Victoria-Regina isochrones tend to be on the red side of observed RGBs when the predicted and

observed turnoffs are matched, the published BASTI isochrones can be expected to be more discrepant, if the same distance and metallicity scales are adopted.)

To conclude: we believe that we have provided compelling arguments that the MF09 findings are suspect, particularly for metal-rich GCs. In this regard, the importance of the binary in 47 Tuc should not be overlooked, as it indicates a clear preference for a relatively young cluster age (recall Fig. 15). (Any increase in the assumed helium abundance of this system would only serve to reduce the derived age.) In addition, the rMSF method, but not our implementation of the $\Delta V_{\text{TO}}^{\text{HB}}$ method, requires that the TO luminosity be determined as accurately as possible. This quantity is very hard to define in the CMDs of metal-rich GCs, in particular, given that they tend to be nearly vertical over a ~ 0.2 mag range in the vicinity of the turnoff, and it is likely to be especially ambiguous in clusters containing multiple stellar populations. Regardless of this practical difficulty, a compelling reason to avoid using the TO luminosity was provided by Mazzitelli, D’Antona, & Caloi (1995), who showed that interpolations within grids of evolutionary tracks that differed only in the treatment of superadiabatic convection yielded isochrones with different TO luminosity versus age relations. This was attributed to the effects of *interpolating* in tracks that were morphologically quite different since, as their work also demonstrated, the TO luminosities of evolutionary tracks (as opposed to isochrones) have no more than a slight dependence on how the convective gradient is determined in surface convection zones. In addition, because of the strong sensitivity of the rMSF technique to the assumed [Fe/H] determinations — something which was properly examined by MF09 and not studied at all by Marín-Franch et al. (2010) — coupled with the uncertainties and the errors (albeit small errors, see § 3.1) inherent to the actual fitting process, we dispute the claim made by Marín-Franch et al. (2010) that their approach is “much more suitable than other techniques for retrieving relative GC ages”.

6.1.2. *Cautionary Remarks Concerning the Fitting of Isochrones to Observed CMDs*

In this investigation, globular cluster ages have been determined using what we believe is the most robust, objective, and least model-dependent method currently in use, as it places almost no reliance on predicted temperatures and colors and it has less of a dependence on metal abundances than other techniques. To derive the best estimate of the age of a given GC, for the assumed distance and chemical abundances, our isochrones have been adjusted in color by whatever amount is necessary (typically by ~ 0.02 mag) in order to match the observed turnoff color, thereby facilitating the identification of that isochrone which reproduces the observed CMD *just* in the vicinity of the TO. The morphology from ≈ 1 mag below the TO through to the beginning of the SGB (where the subgiants have

colors that differ from the median turnoff color by $\lesssim 0.05$ mag) is predicted to be essentially independent of age, helium and metal abundances, and even the value of the mixing-length parameter (see Figs. 2, 3, and 5) — at least for values of these quantities relevant to GCs. In general, our isochrones for ages that have been derived in this way provide reasonably satisfactory fits to the entire CMDs, except that the predicted RGBs tend to lie on the red side of the observed giant branches. The uncertainties in the inferred ages primarily reflect the uncertainties in the adopted distances and chemical abundances.

It is important to appreciate that discrepancies between predicted and observed colors are of little concern for the ages so obtained. Indeed, isochrones will generally fail to provide the best possible match to an observed CMD when well-supported estimates of the distance, reddening, and metal abundances are assumed because, e.g., the adopted cluster parameters (which have significant uncertainties) may not be quite right, the color- T_{eff} relations suffer from small zero-point or systematic errors, or there are problems with the stellar models concerning, among other things, the treatment of convection, diffusion, and/or the atmospheric boundary conditions. There is, in particular, no justification for favoring that isochrone which provides the best simultaneous fit to the observed MSTO and the RGB, or for making small adjustments to the cluster $(m - M)_0$, $E(B - V)$, $[\text{Fe}/\text{H}]$, Y , or $[\alpha/\text{Fe}]$ values if they are made solely to improve the quality of the fit to the CMD — because both approaches assume that the models *should* reproduce the photometric data. This is not necessarily the case.

For instance, super-adiabatic convection is usually treated using the mixing-length theory (Böhm-Vitense 1958), which involves the free parameter α_{MLT} (and a few others). It is unlikely that this parameter is a constant (i.e., independent of mass, chemical composition, and evolutionary state), even though it is treated as such. (Although studies of GCs appear to rule out large variations of α_{MLT} , as discussed in § 5.3, the uncertainties associated with the basic properties of stars are still too large to rule out variations at, say, the ~ 10 – 15% level.) In fact, Trampedach & Stein (2011) have argued, from their 3-D simulations of surface convection in solar abundance stars (the only metallicity that they considered in their initial investigation), in support of a particular variation of α_{MLT} with T_{eff} and gravity. (As far as we are aware, the implications of these predictions for stellar models have yet to be determined.) A free parameter, D_{turb} also appears in formulations of the extra mixing (see Richard et al. 2002, VBD12) that appears to be needed below outer convection zones in order for diffusive models to account for the low abundance of lithium in the Sun and to successfully predict the near independence of the Li abundance with T_{eff} at the hot end of the “Spite plateau” (Spite & Spite 1982). It could turn out that, when the models incorporate a better treatment of convection or of turbulent mixing, the resultant isochrones will provide improved fits to observed CMDs. If the physics in current models is lacking in some way,

some discrepancies between theoretical models and observations *should* be expected.

For the same reasons, suggestions that a more objective, least-squares or maximum likelihood numerical method should be used to select which isochrone best represents an observed CMD are indefensible. A few studies over the years have even advocated that some kind of global optimization method be employed to derive such cluster properties as their distances, reddenings, and metallicities, as well as their ages (e.g., Monteiro & Dias 2011). As long as free parameters are used in some of the physics ingredients of stellar models, one must continue to be wary of relying on the latter (primarily the predicted T_{eff} and color scales) in an absolute, or even relative, sense. Even if the physics were more robust than it is at present, there will continue to be uncertainties in the opacities and nuclear reactions, as well as in the observed properties of stellar populations. Many things must be known to very high accuracy in order to obtain “perfect” fits of models to photometric data. It is, in fact, quite encouraging that current models reproduce observed CMDs as well as they do.

Analyses of observations of complex stellar populations, such as those found in dwarf galaxies or in the Galactic Bulge, or those which are so distant that only giant branch, and possibly HB, stars can be observed clearly require well-constrained stellar models in order to obtain the best possible interpretations of the data. For such studies, it is important to “calibrate” the isochrones (e.g., suitably adjust the color– T_{eff} relations) to fit the observations of nearby open and globular star clusters, so that the inferred ages and other properties of the target system are then determined *relative* to those of the calibrating objects. This is the approach taken by, e.g., Brown et al. (2004). Sophisticated statistical methods that use, e.g., Monte Carlo or Bayesian techniques to analyze observed CMDs should *only* be employed after the stellar models that are used have been thoroughly tested and corrected, as necessary, in order to satisfy empirical constraints as well as possible.

6.2. On the Separation of the $[\text{Fe}/\text{H}] \lesssim -1.5$ GCs into Two Groups

Our discovery that the majority of the most metal-deficient GCs can be divided into two distinct groups, depending on the slope of the subgiant branch in their observed CMDs (see Table 1), is the most intriguing result of this investigation. It is also surprising that the total number of clusters with $[\text{Fe}/\text{H}] \lesssim -1.5$ is almost evenly divided into the two groups (see below). Such a near fifty-fifty split brings to mind the work of van den Bergh (1993), who speculated from his analysis of GC orbits that there may have been a merger of a massive object (or objects) containing M3-like stellar populations with the protoGalaxy. (Such a merger, if it happened, could only have occurred very early in the evolution of the Milky Way, since the Galaxy appears to have had a relatively quiescent history since

thick-disk formation; see Hammer et al. 2007.) He noted, for instance, that these systems predominately have “plunging” (highly elongated) and/or retrograde orbits (also see Rodgers & Paltoglou 1984), as well as below-average luminosities, especially if they are located at large Galactocentric distances. However, orbital information was not available at that time for many of the GCs in our sample and, in the case of a few clusters in common to the two studies, the orbits were classified by van den Bergh as “indeterminate” (see his Table 6).

Fortunately, the orbital characteristics of many of the metal-poor GCs considered here are given by Dinescu et al. (1999a): we have extracted from their paper the information that is given in Table 3. While there is a tendency for the M 3-like clusters to have larger eccentricities (e) and (especially) apoGalactic distances (R_a), and to reach greater heights above the plane (z_{\max}), than the clusters in the group containing M 13, there are notable exceptions no matter what orbital property is considered. For instance, M 92 has a higher eccentricity than most of the GCs that have relatively flat SGBs, and M 13 has significantly higher values of e , R_a , and z_{\max} than M 3. Moreover, as shown by Dinescu et al. (see their Fig. 6), metal-poor clusters with red or blue HBs are not segregated in any way on the total energy versus orbital angular momentum plane.

Admittedly, we were beginning to question whether the division of the metal-poor GCs into two groups was real . . . until we produced Figure 37. This shows that the clusters which have similar SGB slopes as M 3 (those represented by *open circles*) are predominately low-luminosity systems that have relatively large values of R_G (and R_a , as already mentioned).¹¹ The clusters belonging to the group represented by M 13 (those plotted as *filled circles*) are intrinsically bright objects and, with the exception of M 13, their orbits do not extend beyond ~ 10 kpc from the Galactic center (see Table 3). Note that composite symbols have been used for three GCs to indicate that they have intermediate SGB slopes for their metallicities and, consequently, could not be assigned to either of the aforementioned groups.

The upper panel of Figure 38 plots the HB types of the same sample of clusters as a function of $[\text{Fe}/\text{H}]$, using the same symbols as in the previous figure. Not unexpectedly, the M 13-like clusters have exclusively blue HBs, but it is also apparent that there are many GCs with very blue horizontal branches (especially at $-2.1 < [\text{Fe}/\text{H}] < -1.7$) that apparently belong to the other group. The middle panel, reveals that, at $[\text{Fe}/\text{H}] \gtrsim -2.1$, there is no

¹¹While this appears to confirm the results obtained by van den Bergh (1993), it should be appreciated that his definition of an M 3-like cluster is not the same as ours. In his investigation, GCs that either have a relatively red HB, like that of M 3, or belong to Oosterhoff class I were considered to be M 3-like. Such systems as NGC 6101 and M 70, which have blue or very blue HBs, would not have been included in that group, and yet we have classified them as M 3-like on the basis of their SGB slopes. Thus, while the respective cluster samples are quite similar, there are some important differences.

separation of the two groups insofar as their ages are concerned. Hence, differences in age are not responsible for the observed variations in the HB types at a fixed metal abundance. Only at the lowest $[\text{Fe}/\text{H}]$ values is there an indication of a correlation of HB type with age, but even here, the 1σ error bars on the derived ages overlap one another. Moreover, as shown in the classic paper by Lee, Demarque, & Zinn (1994), much larger age differences (≈ 2 Gyr) are needed to explain the wide variation in the HB types at similar metallicities if age is the controlling second parameter. If we are correct in attributing the differences between the M3 and M13 families of GCs to helium abundance variations, these results imply that the most important second parameter is Y . (However, the possibility should be kept in mind that cluster-to-cluster variations in the total C+N+O abundance at a given metallicity may be present, which could impact both the observed HB morphologies and the predicted ages. Unfortunately, the extent of such variations between clusters and within each GC are not presently known for the majority of the clusters in our sample.)

A recent examination of several of the global properties of ~ 150 GCs was carried out by van den Bergh (2011), who showed, among other things, that their central concentrations ($c = \log r_t/r_c$, where r_t and r_c are, respectively, the tidal and core radii) are independent of metallicity, that clusters with collapsed cores tend to be located close to the center of the Galaxy, and that there is no more than a weak correlation between $[\text{Fe}/\text{H}]$ and R_G . He also found no unambiguous correlation of the cluster ellipticity with other parameters. We have not subjected our small sample of 28 metal-poor clusters to the same analysis, though we were motivated to check whether the ellipticity, which is presumably a tracer of the orbital, and perhaps stellar, rotational velocities, provided any discrimination between the two groups. It is known (see, e.g., Peterson 1983, and references therein) that the horizontal-branch stars in GCs that have anomalously blue HBs for their metallicity, such as M13, rotate significantly faster than those found in systems with intermediate or red HB types. Increased mass loss during the giant-branch phase, which would promote bluer HBs, could well be an important consequence of higher rotational velocities (Fusi Pecci & Renzini 1975), just as the spread in mass that is needed to explain observed HBs is likely to have some connection to star-to-star variations in the stellar rotation rates. The fact that the derived $[\text{O}/\text{Fe}]$ and O/Na abundances vary with luminosity along the RGB of M13 (Johnson & Pilachowski 2012, Kraft et al. 1997), probably due to rotation-driven deep mixing, while such correlations are not seen in M3 giants (Snedden et al. 2004, Cohen & Meléndez 2005a), may be telling us that cluster-to-cluster variations in the rotational properties of their stellar populations are large enough to have far-reaching ramifications.

As shown in the bottom panel of Fig. 38, there is perhaps a slight offset in the mean ellipticity of the clusters that are plotted as filled circles, on the one hand, and those represented by open circles, on the other — at least at $[\text{Fe}/\text{H}] > -2.1$, if the GCs with uncertain

classifications are omitted. (The ellipticities were taken from the table given by van den Bergh 2011.) However, the evidence in support of ellipticity being a useful discriminant is clearly rather weak. What is worth considering in some detail is the extent to which the two groups of clusters are able to retain the gas that is shed by stars as they evolve. This is the subject of the next section.

6.2.1. *On the Retention of Mass-Loss Material by Globular Clusters*

We have suggested that the M13-like GCs have higher helium abundances, in the mean, than those in the group typified by M3. In order for multiple stellar populations to form, the matter which is lost by stars belonging to the first generation (FG) must be able to cool and accumulate in the cluster centers. This cannot occur in *present-day* GCs that have masses $\lesssim 10^5 \mathcal{M}_\odot$. [The current thought is that GC masses were much higher early in their evolutionary histories when the second generation (SG) stars formed: we will return to this point after describing the gas retention properties of the clusters at the present time.] According to the gas-flow models computed by Faulkner & Freeman (1977) under the most conservative of assumptions (i.e., highly centrally concentrated structures, the neglect of photoionization energy input, etc.), steady-state outflows (i.e., GC winds) will be very effective in removing the mass-loss material from low-mass clusters for all gas ejection energies down to ~ 15 km/s, which essentially encompasses all plausible mass-loss mechanisms.

In Figure 39, the masses of several GCs of interest are plotted as a function of their central escape velocities, $v_{e,0}$. The masses were derived from the M_V values listed in Table 2 assuming a mass-to-light ratio $\langle \mathcal{M}/L_V \rangle = 1.6(\mathcal{M}/L_V)_\odot$ (Illingworth 1976; Pryor et al. 1991; Albrow, de Marchi, & Sahu 2002), whereas $v_{e,0}$ was calculated using the method described by VandenBerg & Faulkner (1977, see their §V). (Masses derived in this way are probably uncertain by at least $\sim \pm 25\%$: more massive, centrally concentrated clusters appear to have average mass-to-light ratios closer to 2; see, e.g., the study of M15 by Pasquali et al. 2004.) Interestingly, none of the M13-like GCs (the filled circles), except NGC 6397, have masses $< 10^5 \mathcal{M}_\odot$. For our cluster sample, the apparent overlap of clusters represented by both open and filled circles at a value of $\log M/\mathcal{M}_\odot$ just above 5.1 (the location of the horizontal, dashed line) appears to mark the mean transition mass between lower mass GCs that develop steady-state winds and higher mass systems that could acquire growing gas reservoirs at their centers as a result of gas inflows. (This transition mass is predicted to vary inversely with the value of the concentration parameter, c ; see the paper by VandenBerg & Faulkner)

In support of this possibility, we note that NGC 6752 and M 30 are collapsed-core GCs with $c = 2.50$ (according to the 2010 edition of the catalog compiled by Harris 1996); consequently, it would not be too surprising that they might be able to retain the gas from low-velocity winds when other clusters of similar mass but lower central concentrations (such as NGC 6584 and NGC 6934, which both have $c \approx -1.5$) develop steady-state outflows. NGC 6397 and M 70 are also collapsed-core, $c = 2.50$ GCs, and their present masses, which are less than those of NGC 6752 and M 30, appear to be low enough ($\lesssim 10^5 \mathcal{M}_\odot$) that winds should be able to dissipate the gas which is produced by normal stellar mass-loss processes. Although GCs less massive than M 30, including M 70, apparently have relatively flat SGBs, NGC 6397 seems to be an exception to the rule. Indeed, a double MS has been discovered in its CMD by Milone et al. (2012a), who conclude that this system contains two stellar populations with slightly different helium and light element abundances. This may indicate that NGC 6397 was much more massive when it formed and that it contains two distinct generations of stars, as Milone et al. have argued. However, if that is the correct explanation and if it is generally the case that GCs have lost $\gtrsim 90\text{--}95\%$ of their initial masses over their lifetimes, why do nearly all of the M 13-like clusters lie near or above the horizontal dashed line in Fig. 39?

Crosses mark the locations of clusters in our sample that have $[\text{Fe}/\text{H}] \gtrsim -1.5$, and although only a subset of them have been identified in the plot (for the sake of clarity), the fact that NGC 362 and M 5 have relatively high masses while NGC 288 is a low-mass system could well be relevant to our understanding of the second-parameter phenomenon. In particular, the retention of mass-loss material will be especially difficult in the case of NGC 288 given both its low mass and its low central concentration ($c = 0.99$), and it may have been more difficult than in the case of NGC 362 and M 5 at earlier times as well if its initial mass was also significantly less than those of the latter. (Interestingly, despite having unfavorable properties for the retention of gas *at the present time*, NGC 288 has been found to have discrete sequences of stars in uv CMDs, which are likely caused by differences in the light-element abundances and possibly a small variation in Y ; see Piotto et al. 2013.) The other second-parameter cluster in the same set (see § 5.3.2) is M 12. It is located just below M 56 and NGC 6934 in Fig. 39, and since its mass is within the $\sim 0.1\text{--}0.15$ dex uncertainty associated with the dashed line (see VandenBerg & Faulkner 1977), it may or may not be able to develop a steady-state outflow. Of the GCs that are represented by open circles, the ones that seem to have the most anomalous locations on the mass- $v_{e,0}$ plane are M 3 and M 53.

However, there is another potentially important mechanism for the removal of gas from globular clusters and that is ram-pressure sweeping by the interstellar medium of the Galactic halo. According to Frank & Gisler (1976), the halo density (in g/cm^3) required to sweep a

cluster as a result of the dynamical ram pressure arising from the motion of a GC through the halo medium at a velocity v_{cl} (≈ 200 km/s) is

$$\rho_g(halo) \approx \alpha \sigma_0 v_{e,0} / v_{cl}^2$$

where α is the proportional rate of mass loss from stars (i.e., the global mass loss rate divided by the GC mass; see Faulkner & Freeman 1977) and σ_0 is the surface density of stars at the cluster center (in $\mathcal{M}_\odot/\text{pc}^2$). (Values of $\log \sigma_0$ for all of the GCs in our sample are listed in Table 2: these have been calculated using the relations described by VandenBerg & Faulkner 1977.) If the value of α is taken to be $4 \times 10^{-19} \text{ s}^{-1}$, as adopted by Faulkner & Freeman, ram-pressure sweeping by a halo medium with a density of 10^{-26} g/cm^3 would be effective in clusters that have $\log \sigma_0 v_{e,0} \leq 5.7$. Since $\rho_g(halo)$ is proportional to α , the same constraint may be obtained for lower values of the halo density, which are probably more realistic (e.g., Silk 1974), simply by assuming smaller values of the uncertain parameter α . In fact, a significantly smaller value, $\alpha = 7 \times 10^{-20} \text{ s}^{-1}$, was derived by Priestley, Ruffert, & Salaris (2011) in their recent investigation of GC wind models, and if this determination is adopted, $\log \sigma_0 v_{e,0} = 5.61$ (the location of the vertical dotted line in Figure 40) is obtained if $\rho_g(halo) = 1.5 \times 10^{-27} \text{ g/cm}^{-3}$. Under these assumptions, the majority of the GCs with masses $\gtrsim 10^5 \mathcal{M}_\odot$ (those with higher values of $\sigma_0 v_{e,0}$) should be able to resist the ram-pressure purging of any gas that has accumulated between passages through the Galactic disk. (To avoid ram-pressure stripping by the disk, they would need to have $\log \sigma_0 v_{e,0} > 8$ for any reasonable choices of α .)

Just as there is a transition mass between GCs that will, or will not, develop steady-state gas outflows (the horizontal dashed line), there is an apparent separation between the filled and open circles on the mass– $\sigma_0 v_{e,0}$ diagram (the vertical dotted line). Thus, even though the density of the halo is very low, the ram pressure associated with the passage of GCs through this medium is sufficient to prevent the accumulation of mass-loss material in clusters with $\log \sigma_0 v_{e,0} \lesssim 5.6$. This separation is not perfect, as M 3 lies slightly to the right, while NGC 4833, M 10, and M 56 lie to the left, of the dotted line. However, differences in the orbit and the orbital velocity, among other things, could well explain these few exceptions. (Indeed, some of the clusters may not have been allocated to the right group as the 1σ uncertainties of the SGB slope determinations are quite large; see Table 1 and Fig. 29.) In any case, it is interesting that, of the GCs with masses $> 10^{5.5} \mathcal{M}_\odot$, M 3 and M 53 (in particular) have values of $\sigma_0 v_{e,0}$ that are at the low end of the observed range.

It is remarkable that the clusters which show the strongest evidence for discrete multiple stellar populations are located to the right of the dotted line and above the dashed line (reproduced from Fig. 39), given that the masses and the structural properties of the GCs will have undergone significant changes over their evolutionary histories due to tidal interactions,

the “evaporation” of low-mass stars, and other dynamical effects. Bekki (2011) has argued, for instance, that initial masses of up to $10^7 \mathcal{M}_\odot$ are needed to explain the observed large fraction of second-generation (SG) stars that have been detected in several GCs. It is possible that most of the clusters in the so-called M 3–like group (those plotted as open circles) were never massive enough to form significant numbers of SG stars. This is suggested by the fact that the CMDs of most of these clusters tend to be very tight and well-defined (see, e.g., those for NGC 5053 and NGC 5466 in Fig. 11 or of NGC 4147 in Fig. 12). The star-to-star variations in age or in the abundances of helium or C+N+O in these clusters must be rather small given that the luminosities of their SGB stars at a given color vary so little.

As O–Na anticorrelations have been found in most GCs, including those with masses $10^4 \lesssim \mathcal{M}/\mathcal{M}_\odot \lesssim 10^5$ (Carretta et al. 2010b), they may simply be a property of the gas out of which the FG stars formed. If the clusters that have been plotted as open circles had been able to generate large numbers of SG stars like their more massive cousins, but lost a bigger fraction of their initial stellar populations over time, there should still be enough FG stars in their cores to cause significant spreads in the colors of the MS, SGB, and RGB stars in their observed CMDs. The lack of such spreads suggests that these clusters contain just a single stellar generation, albeit one that shows primordial variations in the abundances of the light elements. A noteworthy cluster in this regard is NGC 7492, which shows the O–Na anticorrelation (Cohen & Meléndez 2005b) despite having $\log \sigma_0 v_{e,0} \approx 3.0$. This outer-halo ($R_G \approx 26$ kpc) cluster is located so far to the left of the dotted line in Fig. 40 that it seems highly improbable that it was ever able to retain any of the mass-loss material from the first (and only?) generation of stars that formed, even if its initial mass were 20 times its current mass (which is $\log \mathcal{M}/\mathcal{M}_\odot \approx 4.46$). Another cluster with a very low value of $\log \sigma_0 v_{e,0}$ (≈ 3.1), but a sufficiently high mass (just under $10^5 \mathcal{M}_\odot$) that it is expected show an O–Na anticorrelation, is NGC 5053. However, as far as we are aware, the necessary spectroscopic studies to determine whether this and associated variations of the light elements are found in this GC have not yet been undertaken.

It may turn out that only those GCs in the upper right-hand corner of Fig. 40 (i.e., those that currently have $\log \mathcal{M}/\mathcal{M}_\odot \gtrsim 5.1$ and $\log \sigma_0 v_{e,0} \gtrsim 5.6$) show appreciable enhancements in helium, and possibly CNO (or other metals), though C+N+O generally appears to be constant in them to within the uncertainties; e.g., see the studies of M 13 by Cohen & Meléndez (2005a) and of NGC 6752 by Carretta et al. (2007). The light element variations that appear to be common to all clusters more massive than $\log \mathcal{M}/\mathcal{M}_\odot \approx 4.5$, and in particular, the large cluster-to-cluster variations in such characteristics as the ratio of CN-weak to CN-strong stars and the degree to which O and Na or Al and Mg are anticorrelated may not indicative of multiple stellar generations, but are possibly due instead to differences in the star formation history and the chemical evolution of the individual protoclusters prior

to the formation of the stars that currently reside in them.¹² The presence of multiple stellar populations is certainly much less conspicuous in bona fide GCs (e.g., Piotto et al. 2012) than in objects that were likely to have been the nucleated cores of dwarf galaxies (ω Cen, M 54, and possibly NGC 2808 and NGC 1851; see, e.g., Bekki & Yong 2012). (A thoughtful discussion of the different manifestations of the multiple stellar populations phenomenon in terms of the initial mass and the progenitor structure is provided by Valcarce & Catelan 2011.)

7. Concluding Remarks

Using an improved version of the venerable $\Delta V_{\text{TO}}^{\text{HB}}$ method, ages have been determined for the majority of the 55 globular clusters considered in this investigation. For the most part, the ZAHBs that are the basis of the derived distances reproduce the morphologies of the observed HB distributions very well, which, together with the fact that they satisfy empirical constraints on the luminosities of RR Lyrae stars to within their 1σ uncertainties, gives us added confidence in them. An important advantage of our implementation of the $\Delta V_{\text{TO}}^{\text{HB}}$ method is that isochrones are fitted to just the turnoff portion of an observed CMD, where the morphology is predicted to be nearly independent of age and metallicity, and that the inferred ages are based on the location of the beginning of the SGB instead of the turnoff luminosity, which is a poorly defined quantity in observed CMDs. Indeed, in high-quality CMDs such as those analyzed here, the uncertainties in the derived ages arising from the fitting procedure are typically at the level of $\lesssim \pm 0.25$ Gyr, which is a small fraction of the uncertainties associated with the adopted distances and chemical abundances ($\sim \pm 1.5$ – 2 Gyr). To be sure, the ages of GCs that have extremely blue HBs, or broad photometric sequences due to the effects of differential reddening and/or the presence of multiple stellar populations are less precise.

There are a few observations/concerns that should be mentioned with regard to the

¹²Support for this possibility is provided by Denissenkov & Hartwick (2013), whose preprint appeared while our paper was being refereed. They have proposed that the observed chemical abundance anomalies in GCs were produced by a very early generation of super-massive stars which polluted the primordial cluster gas. Unlike all other scenarios proposed to date, their model provides an excellent fit to *all* of the observed light-element correlations and anticorrelations, and it naturally explains why GC, but not the field halo, stars have, e.g., high sodium and low oxygen abundances. Moreover, if it is only in compact, highly centrally concentrated systems like GCs where such super-massive stars have contributed to the very early chemical evolution of the gas, the absence of such anomalies in dwarf galaxies can also be explained. Another attractive feature of this model is that it does not require GCs to have been much more massive initially than they are today.

results of this study, which are reported and quite thoroughly discussed in § 6. For one thing, the unusual HB morphology of M 13 (see Figs. 21 and 22) — namely, the dense concentration of stars that begins just at the knee of the HB and extends to bluer colors together with a sparser population that is offset to brighter magnitudes and extending to the reddest colors — is common to many of the GCs that have exclusively blue horizontal branches (e.g., NGC 6101, M 12, NGC 6541, NGC 6752, M 56, and probably NGC 288, NGC 6397, and M 10, if not a few others). Some are low-mass systems, some are not, and while they tend to have ages $\gtrsim 12.5$ Gyr, this is not always the case. It is not at all clear whether the faintest HB stars in all of these clusters have close to the primordial helium abundance or a higher value of Y , and yet our adopted distance moduli are consistent with $Y \approx 0.25$. The main difficulty with the assumption of a higher helium abundance is that the luminosity of the HB is *very* sensitive to Y ; consequently, the adoption of an appreciably higher Y would imply a significantly increased distance modulus and a younger age. However, this would lead to problems with the predicted and observed MSTO-to-RGB color differences.

Indeed, it was necessary to postulate that M 13 stars have helium abundances ranging from $Y \approx 0.25$ to possibly 0.33, with a mean value of ≈ 0.29 , in order to obtain a sufficiently short distance modulus and a high enough age to reconcile its $\Delta H_{\text{TO,RGB}}$ parameter with that of M 3 *and* to explain the observed differences in their SGB slopes (Fig. 20). If all of the M 13 stars had initial helium contents close to $Y = 0.29$, the ZAHB-based distance modulus would have been $(m - M)_{APP} \approx 14.60$, implying an age near 10.25 Gyr, and the overall fit to the observed CMD would have been considerably less agreeable. Thus, we were led to a scenario in which most (all?) of the stars in some GCs (M 3 and lower-mass systems that have similar SGB morphologies) have “normal” helium abundances, while others (M 13 and GCs that share its CMD characteristics) have a higher Y *in the mean*, but which still contain a significant population of stars with $Y \approx 0.25$. On the other hand, if the faintest HB stars in M 13 stars have $Y \approx 0.25$, why are they so much bluer than their counterparts in M 3? Clearly something is missing in our understanding. (If both clusters have nearly the same age, as we and MF09 have concluded, and very similar CNO abundances, differences in the stellar rotation rates would appear to be the next most plausible explanation for their different HB types.)

Another important issue is the extent to which the C+N+O abundances vary, both from cluster-to-cluster and from star-to-star within each GC. With relatively few exceptions (e.g., NGC 1851, see Yong et al. 2009), spectroscopic studies have found little or no variation in the total CNO abundance within GCs, though it is expected that any significant enhancement in Y will be accompanied by increased CNO abundances if mass loss from intermediate-mass AGB stars is the origin of the helium-enriched gas (e.g., Fenner et al. 2004, Karakas et al. 2006). No allowance has been made in this study for such a correlation, even though turnoff

luminosity versus age relations for metal-poor stars depend almost entirely on the absolute C+N+O abundance (see VBD12), because it is not known at the present time whether the observed luminosity widths of the SGBs in clusters that have thick subgiant branches is caused by variations in CNO or age (or both). The most obvious way of explaining why, for instance, M 15 has a much redder HB than M 92 or M 30 (see Fig. 11), despite all three clusters having nearly identical $[\text{Fe}/\text{H}]$ values, is that the former has higher $[\text{CNO}/\text{Fe}]$ than the latter since increased CNO abundances have the effect of driving HB models to lower effective temperatures (and hence redder colors), with minimal effects on their luminosities (Castellani & Tornambè 1977). If this is indeed the case, then M 15 should be somewhat younger than M 92 and M 30, assuming that all of the other parameters which affect age determinations are left unchanged.

Fortunately, the predicted mean luminosity (but not the slope) of the SGB at a fixed age is essentially independent of Y , but to disentangle the age and abundance effects, large spectroscopic surveys of the cluster subgiant populations will be required. However, perhaps the best way of getting a handle on the chemistry of GCs is to search for and identify eclipsing binary members because they can provide tight constraints on the masses and radii of stars at their locations in observed CMDs, as well as on their distances if accurate and precise estimates of their temperatures can be derived. Such work should be given very strong support: this avenue of research is likely to lead to the biggest improvement in our understanding of GCs during the next few years. (A good example of the value and importance of such studies is provided by the binary V69 in 47 Tuc, which provides a compelling case against the possibility that, as found by MF09, this $[\text{Fe}/\text{H}] \sim -0.8$ cluster is coeval with the most metal-deficient GCs.)

The most unanticipated result of this study is the discovery that the most metal-poor GCs (those with $[\text{Fe}/\text{H}] \sim -1.5$) can be divided into two groups on the basis of differences in their SGB morphologies. That nearly the same separation is obtained between clusters that, *at the present time*, are able, or unable, to retain the gas which is lost via normal mass-loss processes through the development of GC winds or which are subject to ram-pressure stripping by the halo interstellar medium is especially surprising. How is it possible that the gas-retention properties of present-day GCs discriminate so well between those systems that show the strongest evidence for multiple stellar populations (specifically a significantly higher Y) and those for which the tightness of the CMD appears to imply little or no variations in Y , $[\text{CNO}/\text{Fe}]$, or age? This may be telling us that the masses of GCs have not changed by a large factor during their lifetimes. If all clusters formed with ~ 10 – 25 times their present masses (as predicted by, e.g., D’Ercole et al. 2008, Conroy 2012), surely the cluster-to-cluster variations in mass loss that occurred since their formation due to 2-body and tidal interactions, which depend on the orbit and various cluster properties, would have

been large enough that the separation of the M 3-like and M 13-like clusters would not have been so clear-cut.

Some support for a much reduced mass loss over the lifetimes of GCs to date is provided by the recent work of Larsen, Strader, & Brodie (2012), who found that the globular clusters in Fornax, which show very similar variations of light-element abundances as those seen in Galactic GCs, contain 20–25% of all of the stars in this dwarf galaxy that have $[\text{Fe}/\text{H}] < -2.0$. Even if all of the field stars that satisfy this inequality came from the clusters, the latter could not have been more massive than 4–5 times their present masses. Although this result may be complicated by the issue of whether or not Fornax is the result of a merger of two dwarf galaxies (e.g., Coleman et al. 2005, Yozin & Bekki 2012), initial-to-final mass ratios of $\lesssim 5$ are also suggested by the results of n -body simulations that attempt to model how an assumed initial mass function (IMF) would have been altered over the evolutionary history of a cluster through the evaporation of low-mass stars and the effects of tidal interactions with the Galaxy (e.g., Baumgardt, de Marchi, & Kroupa 2008; Zonoozi et al. 2011). Interestingly, it seems that the present-day MFs can be reproduced quite well if all clusters have the same IMF, which is suggested to be the case by the work of Leigh et al. (2012). In addition, the great difficulty of finding halo field stars with low oxygen and high sodium abundances is hard to understand if GCs have lost at least 90–95% of their masses over the past 11–13 Gyr. While Ramírez et al. (2012) have reported the discovery of two such dwarfs, those stars have low α -element abundances (see their Fig. 1), which are not typical of GC stars. Where are the field halo stars with high α/Fe ratios and low oxygen abundances? This is clearly less of a problem if GCs were initially much less massive than many studies have proposed.

Inferences concerning the existence of significant populations of second-generation stars in GCs from the morphology of the horizontal branch — in particular, from the length of the blue HB or the existence of gaps along this feature (e.g., D’Antona & Caloi 2008, Gratton et al. 2010) — are quite speculative as well, though it is possible to differentiate between sub-populations on the HB using uv photometry (Dalessandro et al. 2013, Gratton et al. 2013, and references therein). This is demonstrated by the work of Caloi & D’Antona (2011) who suggested that M 53 consists primarily of first-generation stars because (i) it has quite a stubby blue HB for its metallicity, and (ii) Martell, Smith, & Briley (2008) proposed that one way of understanding the small range in the observed C and N abundances in this cluster is that the polluting gas had not been processed through the full CNO-cycle, in which case the Ne-Na cycle would not have been operative either. As a consequence, Caloi & D’Antona predicted that stars in this system would not show the O–Na anticorrelation.

We do not know if the necessary observations have been carried out to test this pre-

diction, but we suspect that an O–Na anticorrelation will be found because its presence has been reported in stars belonging to M 55 (Carretta et al. 2009c), which have nearly the same $[\text{Fe}/\text{H}]$ as their counterparts in M 53 and, what is especially noteworthy, even more uniform CN band strengths (Briley et al. 1993). Both Martell et al. (2008) and Briley et al. suggest that this can be explained if deep mixing has produced low C/Fe ratios in bright giants of both clusters. This could well be the explanation given that a decline in the carbon abundance with increasing luminosity along the upper RGB has been observed in a number of moderate to very metal-deficient clusters, including M 92 (Carbon et al. 1982), M 15 (Treffler et al. 1983), and M 4 and NGC 6752 (Suntzeff & Smith 1991), among others. In the case of M 13, even the oxygen abundance appears to follow a similar trend (Johnson & Pilachowski 2012). This raises the possibility that deep mixing also plays a role in the observed O–Na anticorrelations, which are seen in, e.g., the lowest metallicity ($[\text{Fe}/\text{H}] < -1.6$) stars in ω Cen (Johnson & Pilachowski 2010, see their Fig. 19).

It should also be kept in mind that, as discussed in the extensive review by Gratton, Carretta, & Bragaglia (2012, also see Renzini 2008), current models for the AGB phase and for rapidly rotating massive stars (Decressin et al. 2007, and references therein) are not able to reproduce the observed abundance patterns in a fully satisfactory and consistent way. Although it may turn out that better agreement will be obtained when some of the many parameters that affect the models are fine-tuned, these difficulties (coupled with those mentioned above) may instead be telling us that the scenario which has been developed over the past few years, requiring very high initial GC masses, among other things, is incorrect. In particular, it is still within the realm of possibility that most of the light-element variations that are observed were present in the gas out of which the observed generation(s) of cluster stars formed (see Denissenkov & Hartwick 2013); i.e., that they arose at earlier times in the evolution of protoclusters. As is widely appreciated, there are problems and inconsistencies with every proposal that has been made to date — which is, of course, the reason why a satisfactory solution has not yet been found despite a tremendous effort by many researchers.

We thank Ata Sarajedini for providing us with the ACS photometry that we have used as well as the web site address where helpful information concerning photometric zero-points is given. We also thank Santi Cassisi for sending us his color transformations to the F606W and F814W bandpasses, based on Castelli-Kurucz model atmospheres, as they were used to extend the MARCS transformations to effective temperatures > 8000 K. For many helpful discussions, as well as useful references, we are grateful to Pavel Denissenkov, David Hartwick, and Sidney van den Bergh. Christian Johnson and Caty Pilachowski pointed out some pertinent results in their recent papers in response to our inquiries, while Bruce Elmgreen provided some important clarifications concerning the formation of globular clusters: these

contributions to our understanding are very much appreciated as well. This paper has also benefitted from suggestions provided by Tom Brown, Aldo Valcarce, and, in particular, two helpful referees. KB acknowledges the support received from the Carlsberg Foundation and from the Villum Foundation, while RL acknowledges NSERC Discovery Grant support to Kim Venn and the financial support to the DAGAL network from the People Programme (Marie Curie Actions) of the European Union’s Seventh Framework Programme FP7/2007-2013 under REA grant agreement number PITN-GA-2011-289313. DAV is grateful for the support of a Discovery Grant from the Natural Sciences and Engineering Research Council of Canada.

REFERENCES

- Ade, P. A. R., Aghanim, N., Armitage-Caplan, C., et al. 2013, arXiv:1303.5076.
- Albrow, M. D., de Marchi, G., & Sahu, K. C. 2002, *ApJ*, 579, 660.
- Alonso, A., Arribas, S., & Martinez-Roger, C. 1996, *A&AS*, 117, 227.
- An, D., Pinsonneault, M., Masseron, T., et al. 2009, *ApJ*, 700, 523.
- Anderson, J., Piotto, G., King, I. R., Bedin, L. R., & Guhathakurta, P. 2009, *ApJ*, 697, L58.
- Asplund, M., Grevesse, N., & Sauval, A. J. 2005, *ASP Conf. Ser.*, 336, 25.
- Bahcall, J. N., & Pinsonneault, M. H. 1995, *Rev. Mod. Phys.*, 67, 671.
- Bahcall, J. N., Pinsonneault, M., Basu, S., & Christensen-Dalsgaard, J. 1997, *Phys. Rev. Lett.*, 78, 171.
- Basu, S., Verner, G. A., Chaplin, W. J., & Elsworth, Y. 2012, *ApJ*, 746, 76.
- Baumgardt, H., de Marchi, G., & Kroupa, P. 2008, *ApJ*, 685, 247.
- Bedin, L. R., Cassisi, S., Castelli, F., Piotto, G., Anderson, J., Salaris, M., Momany, Y., & Pietrinferni, A. 2005, *MNRAS*, 357, 1038.
- Bekki, K. 2011, *MNRAS*, 412, 2241.
- Bekki, K., Yahagi, H., Nagashima, M., & Forbes, D. A. 2008, *MNRAS*, 387, 1131.
- Bekki, K., & Yong, D. 2012, *MNRAS*, 419, 2063.
- Bellazzini, M., Fusi Pecci, F., Ferraro, F. R., Galletti, S., Catelan, M., & Landsman, W. B. 2001, *AJ*, 122, 2569
- Bellazzini, M., Ferraro, F. R., Sollima, A., Pancino, E., & Origlia, L. 2004, *A&A*, 424, 199.
- Bellini, A., Bedin, L. R., Piotto, G., Milone, A. P., Marino, A. F., & Villanova, S. 2010, *AJ*, 140, 631.
- Bellini, A., Piotto, G., Milone, A. P., et al. 2013, *ApJ*, 765, 32.
- Benedict, G. F., McArthur, B. E., Feast, M. W., et al. 2011, *AJ*, 142, 187.
- Bergbusch, P. A., & Stetson, P. B. 2009, *AJ*, 138, 1455.

- Bergbusch, P. A., & Vandenberg, D. A. 2001, *ApJ*, 556, 322.
- Böhm-Vitense, E. 1958, *Z. für Astrophys.*, 46, 108.
- Bohlin, R. C. 2007, *Instrument Sci. Rep. ACS 2007-06*.
- Bonaca, A., Tanner, J. D., Basu, S., et al. 2012, *ApJ*, 755, L12.
- Bond, H. E., Nelan, E. P., Vandenberg, D. A., Schaefer, G. H., & Harmer, D. 2013, *ApJ*, 765, L12.
- Bragaglia, A., Carretta, E., Gratton, R. G. 2010, *ApJ*, 720, L41.
- Briley, M. M., Smith, G. H., Hesser, J. E., & Bell, R. A. 1993, *AJ*, 106, 142.
- Brodie, J. P., & Strader, J. 2006, *ARA&A*, 44, 193.
- Brogaard, K., Vandenberg, D. A., Bruntt, H., et al. 2012, *A&A*, 543, A106.
- Brown, J. A., Wallerstein, G., & Zucker, D. 1997, *AJ*, 114, 480.
- Brown, T. M., Tumlinson, J., Geha, M., et al. 2012, *ApJ*, 753, L21.
- Brown, T. M., Ferguson, H. C., Smith, E., Kimble, R. A., Sweigart, A. V., Renzini, A., Rich, R. M., & Vandenberg, D. A. 2004, *ApJ*, 613, L125.
- Buonanno, R., Corsi, C. E., Pulone, L., Fusi Pecci, F., & Bellazzini, M. 1998, *A&A*, 333, 505.
- Cacciari, C. 2013, *IAU Symp. 289, Advancing the Physics of Cosmic Distances*, ed. R. de Grijs (Cambridge Univ. Press: Cambridge), p. 101.
- Cacciari, C., Corwin, T. M., & Carney, B. W. 2005, *AJ*, 129, 167.
- Caloi, V., & D’Antona, F. 2005, *A&A*, 435, 987.
- Caloi, V., & D’Antona, F. 2011, *MNRAS*, 417, 228.
- Carbon, D. F., Langer, G. E., Butler, D., Kraft, R. P., Suntzeff, N. B., Kemper, E., Trefzger, C. F., & Romanishin, W. 1982, *ApJS*, 49, 207.
- Carretta, E., Cohen, J. G., Gratton, R. G., & Behr, B. 2001, *AJ*, 122, 1469.
- Carretta, E., & Gratton, R. G. 1997, *A&AS*, 121, 95. (CG)

- Carretta, E., Gratton, R. G., Bragaglia, A., D’Orazi, V., & Lucatello, S. 2013, *A&A*, 548, A122.
- Carretta, E., Gratton, R. G., Clementini, G., & Fusi Pecci, F. 2000, *ApJ*, 533, 215.
- Carretta, E., Bragaglia, A., Gratton, R. G., Lucatello, S., & Momany, Y. 2007, *A&A*, 464, 927.
- Carretta, E., Bragaglia, A., Gratton, R. G., D’Orazi, V., & Lucatello, S. 2009a, *A&A*, 508, 695. (CBG09)
- Carretta, E., Bragaglia, A., Gratton, R. G., & Lucatello, S. 2009b, *A&A*, 505, 139.
- Carretta, E., Bragaglia, A., Gratton, R. G., et al. 2009c, *A&A*, 505, 117.
- Carretta, E., Bragaglia, A., Gratton, R. G., et al. 2010a, *ApJ*, 714, L7.
- Carretta, E., Bragaglia, A., Gratton, R. G., Recio-Blanco, A., Lucatello, S., D’Orazi, V., & Cassisi, S. 2010b, *A&A*, 516, 55.
- Casagrande, L., Portinari, L., & Flynn, C. 2006, *MNRAS*, 373, 13.
- Casagrande, L., Ramírez, I., Meléndez, J., Bessell, M., & Asplund, M. 2010, *A&A*, 512, 54.
- Casagrande, L., Schönrich, R., Asplund, M., Cassisi, S., Ramírez, I., Meléndez, J., Bensby, T., & Feltzing, S. 2011, *A&A*, 530, 138.
- Cassisi, S., Castellani, M., Caputo, F., & Castellani, V. 2004, *A&A*, 426, 641.
- Cassisi, S., Mucciarelli, A., Pietrinferni, A., Salaris, M., & Ferguson, J. 2013, *A&A*, 554, A19.
- Cassisi, S., Salaris, M., Pietrinferni, A., Piotto, G., Milone, A. P., Bedin, L. R., & Anderson, J. 2008, *ApJ*, 672, 275.
- Castellani, V., & Tornambè, A. 1977, *A&A*, 61, 427.
- Catelan, M. 2009, *Ap&SS*, 320, 261.
- Catelan, M., Bellazzini, M., Landsman, W. B., Ferraro, F. R., Fusi Pecci, F., & Galletti, F. 2001, *AJ*, 122, 3171.
- Catelan, M., Grundahl, F., Sweigart, A. V., Valcarce, A. A. R., & Cortés, C. 2009, *ApJ*, 695, L97.

- Catelan, M., Pritzl, B. J., & Smith, H. A. 2004, *ApJS*, 154, 633.
- Cayrel, R., Depagne, E., Spite, M., et al. 2004, *A&A*, 416, 117.
- Chaboyer, B., Demarque, P., Kernan, P. J., Krauss, L. M., & Sarajedini, A. 1996, *MNRAS*, 283, 683.
- Chaboyer, B., Demarque, P., & Sarajedini, A. 1996, *ApJ*, 459, 558
- Christensen-Dalsgaard, J., Proffitt, C. R., & Thompson, M. J. 1993, *ApJ*, 403, L75
- Clementini, G., Gratton, R. G., Bragaglia, A., Carretta, E., Di Fabrizio, L., & Maio, M. 2003, *AJ* 125, 1309.
- Cohen, J. G., Briley, M. M., & Stetson, P. B. 2005, *AJ*, 130, 1177.
- Cohen, J. G., & Meléndez, J. 2005a, *AJ*, 129, 303.
- Cohen, J. G., & Meléndez, J. 2005b, *AJ*, 129, 1607.
- Coleman, M. G., Da Costa, G. S., Bland-Hawthorn, J., & Freeman, K. C. 2005, *AJ*, 129, 1443.
- Conroy, C. 2012, *ApJ*, 758, 21.
- Dalessandro, E., Salaris, M., Ferraro, F. R., Mucciarelli, A., & Cassisi, S. 2013, *MNRAS*, 430, 459.
- D’Antona, F., & Caloi, V. 2008, *MNRAS*, 390, 693.
- De Angeli, F., Piotto, G., Cassisi, S., Busso, G., Recio-Blanco, A., Salaris, M., Aparicio, A., & Rosenberg, A. 2005, *AJ*, 130, 116.
- Decressin, T., Meynet, G., Charbonnel, C., Prantzos, N. & Ekström, S. 2007, *A&A*, 464, 1029.
- Denissenkov, P. A., & Hartwick, F. D. A. 2013, arXiv:1305.5975.
- Denissenkov, P., & Vandenberg, D. A. 2003, *ApJ*, 593, 509.
- De Santis, R., & Cassisi, S. 1999, *MNRAS*, 308, 97.
- di Cecco, A., Becucci, R., Bono, G., et al. 2010, *PASP*, 122, 991.
- Dickens, R. J., Croke, B. F. W., Cannon, R. D., & Bell, R. A. 1991, *Nature*, 351, 212.

- Dinescu, D. I., Girard, T. M., & van Altena, W. F. 1999a, *AJ*, 117, 1792.
- Dinescu, D. I., van Altena, W. F., Girard, T. M., & López, C. E. 1999b, *AJ*, 117, 277.
- Dinescu, D. I., Majewski, S. R., Girard, T. M., & Cudworth, K. M. 2000, *AJ* 120, 1892.
- Dorman, B., VandenBerg, D. A., & Laskarides, P. G. 1989, *ApJ*, 343, 750.
- Dotter, A., Chaboyer, B., Jevremović, D., Baron, E., Ferguson, J. W., Sarajedini, A., & Anderson, J. 2007, *AJ*, 134, 376. (DSEP)
- Dotter, A., Sarajedini, A., & Anderson, J. 2011, *ApJ*, 738, 74.
- Dotter, A., Sarajedini, A., Anderson, J., et al. 2010, *ApJ*, 708, 698.
- Eggen, O. J., Lynden-Bell, D., & Sandage, A. 1962, *ApJ*, 136, 748.
- Elmegreen, B. G., Malhotra, S., & Rhoads, J. 2012, *ApJ*, 757, 9.
- D’Ercole, A., Versperini, E., D’Antona, F., McMillan, C. L. W., & Recchi, S. 2008, *MNRAS*, 391, 825.
- Fabbian, D., Nissen, P. E., Asplund, M., Pettini, M., & Ackerman, C. 2009, *A&A*, 500, 1143.
- Faulkner, D. J., & Freeman, K. C. 1977, *ApJ*, 211, 77.
- Fenner, Y., Campbell, S., Karakas, A. I., Lattanzio, J. C., & Gibson, B. K. 2004, *MNRAS*, 353, 789.
- Fernley, J., Barnes, T. G., Skillen, I., Hawley, S. L., Hanley, C. J., Evans, D. W., Solano, E., & Garrido, R. 1998, *A&A*, 330, 515.
- Ferraro, F. R., Valenti, E., Straniero, O., & Livia, O. 2006, *ApJ*, 642, 225.
- Frank, J., & Gisler, G. 1976, *MNRAS*, 176, 533.
- Freedman, W. L., & Madore, B. F. 2010, *ARA&A*, 48, 673.
- Fusi Pecci, F., & Renzini, A. 1975, *A&A*, 39, 413.
- Gould, A., & Popowski, P. 1998, *ApJ*, 508, 844.
- Gratton, R. G., Carretta, E., Bragaglia, A., Lucatello, S., & D’Orazi, V. 2010, *A&A*, 517, A81.
- Gratton, R. G., Carretta, E., & Bragaglia, A. 2012, *A&AR*, 20, 50.

- Gratton, R. G., Carretta, E., & Castelli, F. 1996, *A&A*, 314, 191.
- Gratton, R. G., Lucatello, S., Sollima, A., et al. 2013, *A&A*, 549, A41.
- Grevesse, N., & Sauval, A. J. 1998, *Sp. Sci. Rev.*, 85, 161.
- Grundahl, F., & Briley, M. 2001, *Nucl. Phys. A*, 688, 414.
- Grundahl, F., Vandenberg, D. A., Bell, R. A., Anderson, M. I., & Stetson, P. B. 2000, *AJ*, 120, 1884.
- Gustafsson, B., Edvardsson, B., Eriksson, K., Jørgensen, U. G., Nordlund, Å., & Plez, B. 2008, *A&A*, 486, 951.
- Hammer, F., Puech, M., Chemin, L., Flores, H., & Lehnert, M. D. 2007, *ApJ*, 662, 322.
- Han, S.-I., Lee, Y.-W., Joo, S.-J., Sohn, S. T., Yoon, S.-J., Kim, H.-K., & Lee, J.-W. 2009, *ApJ*, 707, 190.
- Harris, W. W. 1996, *AJ*, 112, 1487.
- Hartwick, F. D. A. 2009, *ApJ*, 691, 1248.
- Hendricks, B., Stetson, P. B., Vandenberg, D. A., & Dall’Ora, M. 2012, *AJ*, 144, 25.
- Herwig, F., Vandenberg, D. A., Navarro, J. F., Ferguson, J., & Paxton, B. 2012, *ApJ*, 757, 132.
- Ibata, R., Gilmore, G., & Irwin, M. 1995, *MNRAS*, 277, 781.
- Iben, I., Jr., & Renzini, A. 1984, *Phys. Rep.*, 105, 329.
- Illingworth, G. 1976, *ApJ*, 204, 73.
- Johnson, J. A., & Bolte, M. 1998, *AJ*, 115, 693.
- Johnson, C. I., & Pilachowski, C. A. 2010, *ApJ*, 722, 1373.
- Johnson, C. I., & Pilachowski, C. A. 2012, *ApJ*, 754, L38.
- Karakas, A. I., Fenner, Y., Sills, A., Campbell, S. W., & Lattanzio, J. C. 2006, *ApJ*, 652, 1240.
- Koch, A., & McWilliam, A. 2008, *AJ*, 135, 1551.
- Komatsu, E., Smith, K. M., Dunkley, J., et al. 2011, *ApJS*, 192, 18.

- Kraft, R. P. 1994, *PASP*, 106, 553.
- Kraft, R. P., & Ivans, I. I. 2003, *PASP*, 115, 143.
- Kraft, R. P., Sneden, C., Smith, G. H., Shetrone, M. D., Langer, G. E., & Pilachowski, C. A. 1997, *AJ*, 113, 279.
- Laney, C. D., Joner, M. D., & Pietrzyński, G. 2012, *MNRAS*, 419, 1637.
- Lardo, C., Pancino, E., Mucciarelli, A., & Milone, A. P. 2012, *A&A*, 548, A107.
- Larsen, S. S., Strader, J., & Brodie, J. P. 2012, *A&A*, 544, L14.
- Leaman, R., VandenBerg, D. A., & Mendel, J. T. 2013, *MNRAS*, submitted.
- Leaman, R., Venn, K. A., Brooks, A. M. 2013, *ApJ*, 767, 131.
- Lee, Y.-W., Demarque, P., & Zinn, R. 1994, *ApJ*, 423, 248.
- Leigh, N., Umbreit, S., Sills, A., Knigge, C., de Marchi, G., Glebbeek, E., & Sarajedini, A. 2012, *MNRAS*, 422, 1592.
- Mackey, A. D., & van den Bergh, S. 2005, *MNRAS*, 360, 631.
- Marín-Franch, A., Aparicio, A., Piotto, G., et al. 2009, *ApJ*, 694, 1498. (MF09)
- Marín-Franch, A., Cassisi, S., Aparicio, A., & Pietrinferni, A. 2010, *ApJ*, 714, 1072.
- Marino, A. F., Milone, A. P., Piotto, G., Villanova, S., Bedin, L. R., Bellini, A., & Renzini, A. 2009, *A&A*, 505, 1099.
- Marino, A. F., Milone, A. P., Piotto, G., et al. 2011, *ApJ*, 731, 64.
- Marino, A. F., Villanova, S., Piotto, G., Milone, A. P., Momany, Y., Bedin, L. R., & Medling, A. M. 2008, *A&A*, 625, 640.
- Martell, S. L., Smith, G. H., & Briley, M. M. 2008, *PASP*, 120, 7.
- Mazzitelli, I., D’Antona, F., & Caloi, V. 1995, *A&A*, 302, 382.
- McCall, M. L. 2004, *AJ*, 128, 2144.
- Miglio, A., Brogaard, K., Stello, D., et al. 2012, *MNRAS*, 419, 2077.
- Milone, A. P., Bedin, L. R., Piotto, G., et al. 2008, *ApJ*, 673, 241.

- Milone, A. P., Piotto, G., King, I. R., et al. 2010, ApJ, 709, 1183.
- Milone, A. P., Marino, A. F., Piotto, G., Bedin, L. R., Anderson, J., Aparicio, A., Cassisi, S., & Rich, R. M. 2012a, ApJ, 745, 27.
- Milone, A. P., Piotto, G., Bedin, L. R., et al. 2012b, ApJ, 744, 58.
- Milone, A. P., Piotto, G., Bedin, L. R., Cassisi, S., Anderson, J., Marino, A.F., Pietrinferni, A., & Aparicio, A. 2012, A&A, 537, A77.
- Milone, A. P., Marino, A. F., Piotto, G., et al. 2013, ApJ, 767, 120.
- Molinaro, R., Ripepi, V., Marconi, M., et al. 2012, ApJ, 748, 69.
- Monteiro, H., & Dias, W. S. 2011, A&A, 530, 91.
- Mottini, M., Wallerstein, G., & McWilliam, A. 2008, AJ, 136, 614.
- Nataf, D. M., Gould, A., Pinsonneault, M. H., & Stetson, P. B. 2011, ApJ, 736, 94.
- Nataf, D. M., Gould, A., Pinsonneault, M. H., & Udalski, A. 2013, ApJ, 766, 77.
- Palmieri, R., Piotto, G., Saviane, I., Girardi, L., & Castellani, V. 2002, A&A, 392, 115.
- Pasquali, A., de Marchi, G., Pulone, L., & Brigas, M. S. 2004, A&A, 428, 469.
- Peterson, R. C. 1983, ApJ, 275, 737.
- Pietrinferni, A., Cassisi, S., Salaris, M., & Castelli, F. 2006, ApJ, 642, 797.
- Pietrinferni, A., Cassisi, S., Salaris, M., Percival, S., & Ferguson, J. W. 2009, ApJ, 697, 275.
- Piotto, G., Bedin, L. R., Anderson, J., King, I. R., Cassisi, S., Milone, A. P., Villanova, S., Pietrinferni, A., & Renzini, A. 2007, ApJ, 661, L53.
- Piotto, G., Milone, A. P., Anderson, J., et al. 2012, ApJ, 760, 39.
- Piotto, G., Milone, A. P., Marino, A. F., Bedin, L. R., Anderson, J., Jerjen, H., Bellini, A., & Cassisi, S. 2013, arXiv:1306.5795.
- Press, W. H., Flannery, B. P., Teukolsky, S. A., & Vetterline, W. T. 1986, *Numerical Recipes* (Cambridge Univ. Press: Cambridge), p. 508.
- Priestley, W., Ruffert, M., & Salaris, M. 2011, MNRAS, 411, 1935.
- Pryor, C., McClure, R. D., Fletcher, J. M., & Hesser, J. E. 1991, AJ, 102, 1026.

- Ramírez, I., Allende Prieto, C., Redfield, S., & Lambert, D. L. 2006, *A&A*, 459, 613.
- Ramírez, I., Meléndez, J., & Chanamé, J. 2012, *ApJ*, 757, 164.
- Renzini, A. 2008, *MNRAS*, 391, 454.
- Richard, O., Michaud, G., Richer, J., Turcotte, S., Turck-Chièze, S., & Vandenberg, D. A. 2002, *ApJ*, 568, 979.
- Richer, J., Michaud, G., & Turcotte, S. 2000, *ApJ*, 529, 338.
- Rodgers, A. W., & Paltoglou, G. 1984, *ApJ*, 283, L5.
- Roh, D.-G., Lee, Y.-W., Joo, S.-J., Han, S.-I., Sohn, Y.-J., & Lee, J.-W. 2011, *ApJ*, 733, L45
- Rosenberg, A., Saviane, I., Piotto, G., & Aparacio, A. 1999, *AJ*, 118, 2306.
- Rutledge, G. A., Hesser, J. E., & Stetson, P. B. 1997, *PASP*, 109, 907. (R07)
- Salaris, M., Riello, M., Cassisi, S., & Piotto, G. 2004, *A&A*, 420, 911.
- Salaris, M., & Weiss, A. 2002, *A&A*, 388, 492.
- Sandage, A. 1982, *ApJ*, 252, 553.
- Sandage, A. 1990a, *ApJ*, 350, 603.
- Sandage, A. 1990b, *JRASC*, 84, 70.
- Sandage, A. 1993, *AJ*, 106, 719.
- Sandage, A. 2006, *AJ*, 131, 1750.
- Sandquist, E. 2000, *MNRAS*, 313, 571.
- Sandquist, E., Gordon, M., Levine, D., & Bolte, M. 2010, *AJ*, 139, 2374.
- Sarajedini, A., Bedin, L. R., Chaboyer, B., et al. 2007, *AJ*, 133, 1658.
- Sbordone, L., Saris, M., Weiss, A., & Cassisi, S. 2011, *A&A*, 534, A9.
- Schlegel, D. J., Finkbeiner, D. P., & Davis, M. 1998, *ApJ*, 500, 525.
- Shetron, M. D., & Keane, M. J. 2000, *AJ*, 119, 840.
- Shetrone, M., Martell, S. L., Wilkerson, R., Adams, J., Siegel, M. H., Smith, G. H., & Bond, H. E. 2010, *AJ*, 140, 1119.

- Silk, J. 1974, *Comm. Ap. Space Sci.*, 6, 1.
- Sirianni, M., Jee, M. J., Benitez, N., et al. 2005, *PASP*, 117, 1049.
- Smith, G. H., Shetrone, M. D., Bell, R. A., Churchill, C. W., & Briley, M. M. 1996, *AJ*, 112, 1511.
- Snedden, C., Kraft, R. P., Guhathakurta, P., Peterson, R. C., & Fulbright, J. P. 2004, *AJ*, 126, 2162.
- Spite, F., & Spite, M. 1982, *A&A* 115, 357.
- Stetson, P. B. 2000, *PASP*, 112, 925.
- Stetson, P. B., Vandenberg, D. A., & Bolte, M. 1996, *PASP*, 108, 560.
- Suntzeff, N. B., & Smith, V. V. 1991, *ApJ*, 381, 160.
- Thompson, I. B., Kaluzny, J., Rucinski, S. M., Krzeminski, W., Pych, W., Dotter, A., & Burley, G. S. 2010, *AJ*, 139, 329.
- Trampedach, R., & Stein, R. F. 2011, *ApJ*, 731, 78.
- Trefzger, C. F., Carbon, D. F., Langer, G. E., Suntzeff, N. B., & Kraft, R. P. 1983, *ApJ*, 266, 144.
- Turcotte, S., Richer, J., Michaud, G., Iglesias, C. A., & Rogers, F. J. 1998, *ApJ*, 504, 539.
- Valcarce, A. A. R., & Catelan, M. 2011, *A&A*, 533, A120.
- Vandenberg, D. A. 2000, *ApJS*, 129, 315.
- Vandenberg, D. A. 2013, *IAU Symp.* 289, *Advancing the Physics of Cosmic Distances*, ed. R. de Grijs (Cambridge Univ. Press: Cambridge), p. 161.
- Vandenberg, D. A., & Bell, R. A. 2001, *New Astron. Rev.*, 45, 577.
- Vandenberg, D. A., Bergbusch, P. A., Dotter, A., Ferguson, J. W., Michaud, G., Richer, J., & Proffitt, C. R. 2012, *ApJ*, 755, 15. (VBD12)
- Vandenberg, D. A., Bergbusch, P. A., & Dowler, P. D. 2006, *ApJS*, 162, 375.
- Vandenberg, D. A., Bolte, M., & Stetson, P. B. 1990, *AJ*, 100, 445.
- Vandenberg, D. A., Casagrande, L., & Stetson, P. B. 2010, *AJ*, 140, 1020.

- VandenBerg, D. A., & Faulkner, D. J. 1977, ApJ, 218, 415.
- VandenBerg, D. A., Richard, O., Michaud, G., & Richer, J. 2002, ApJ, 571, 487.
- VandenBerg, D. A., & Stetson, P. B. 1991, AJ, 102, 1043.
- VandenBerg, D. A., Swenson, F. J., Rogers, F. J., Iglesias, C. A., & Alexander, D. R. 2000, ApJ, 532, 430.
- van den Bergh, S. 1993, AJ, 105, 971.
- van den Bergh, S. 2011, PASP, 123, 1044.
- van Leeuwen, F. 2007, A&A, 474, 653.
- Yong, D., Grundahl, F., D’Antona, F., Karakas, A. I., Lattanzio, J. C., & Norris, J. E. 2009, ApJ, 695, L62.
- Yozin, C., & Bekki, K. 2012, ApJ, 756, L18.
- Zinn, R. 1985, ApJ, 293, 434.
- Zinn, R., & West, M. J. 1984, ApJS, 55, 45. (ZW)
- Zonoozi, A. H., Küpper, A. H. W., Baumgardt, H., Hagi, H., Kroupa, P., & Hilker, M. 2011, MNRAS, 411, 1989.

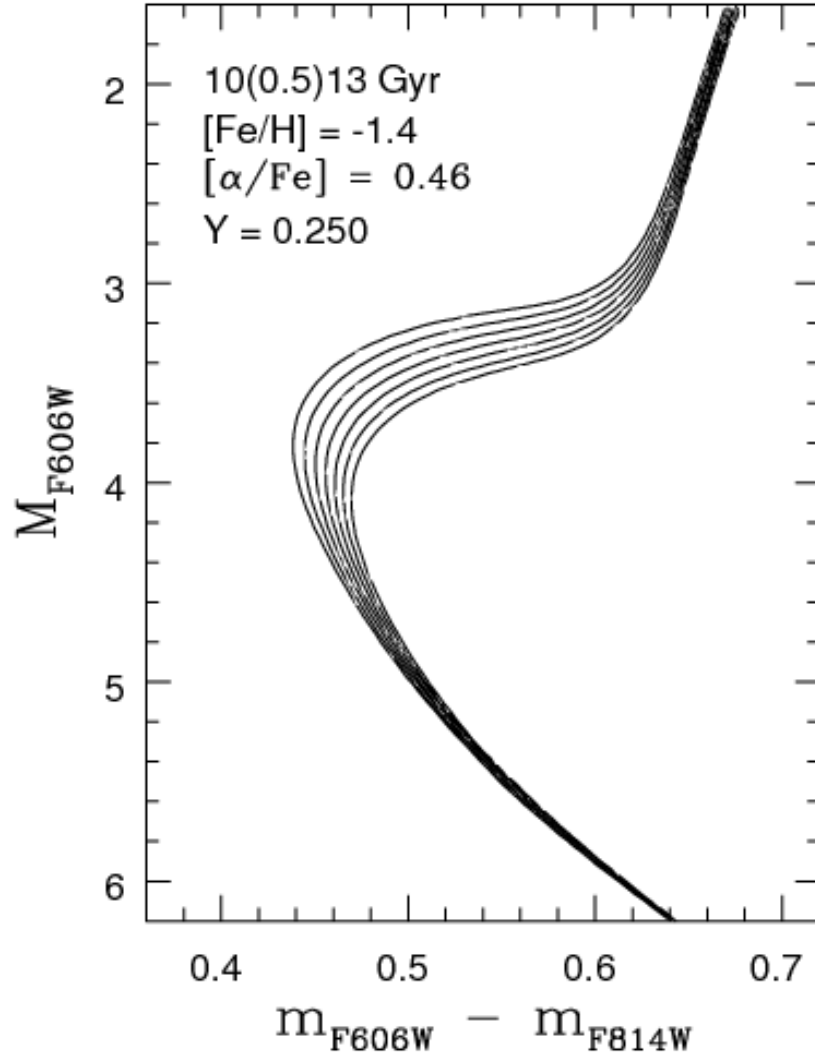


Fig. 1.— Isochrones from Vandenberg et al. (2012, GSCX model series) for the indicated ages and chemical abundances. They have been transposed to the observed plane using color transformations based on the latest MARCS model atmospheres.

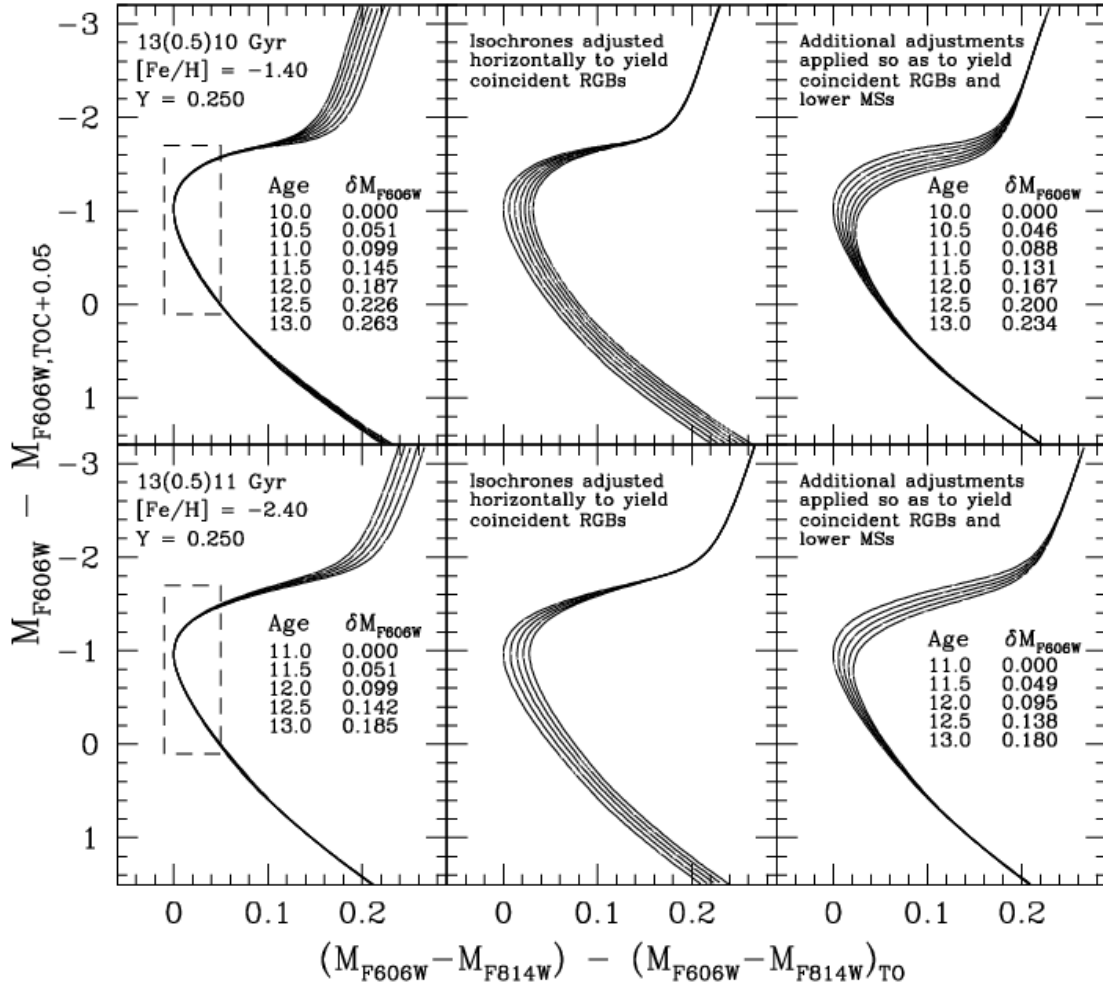


Fig. 2.— *Top row*: isochrones from the previous figure have been shifted in color and magnitude to achieve coincident turnoffs (*left-hand panel*), then adjusted horizontally in color by the amounts that are needed in order for the RGBs of all of the older isochrones to coincide with the location of the giant branch of the 10 Gyr isochrone (*middle panel*), and finally corrected in both magnitude and color (see the text) in order to obtain a simultaneous coincidence of both their giant branches and their lower main sequences (*right-hand panel*). The legends in the *left-* and *right-hand panels* list the differences in the turnoff magnitudes of the isochrones with ages ≥ 10.5 Gyr relative to that of the 10.0 Gyr isochrone. Note that the isochrones superimpose each other nearly exactly in the vicinity of the turnoff (notably the region inside the dashed box that has been plotted in the *left-hand panel*). *Bottom row*: as in the top row, except that 11–13 Gyr isochrones for $[Fe/H] = -2.40$ have been intercompared.

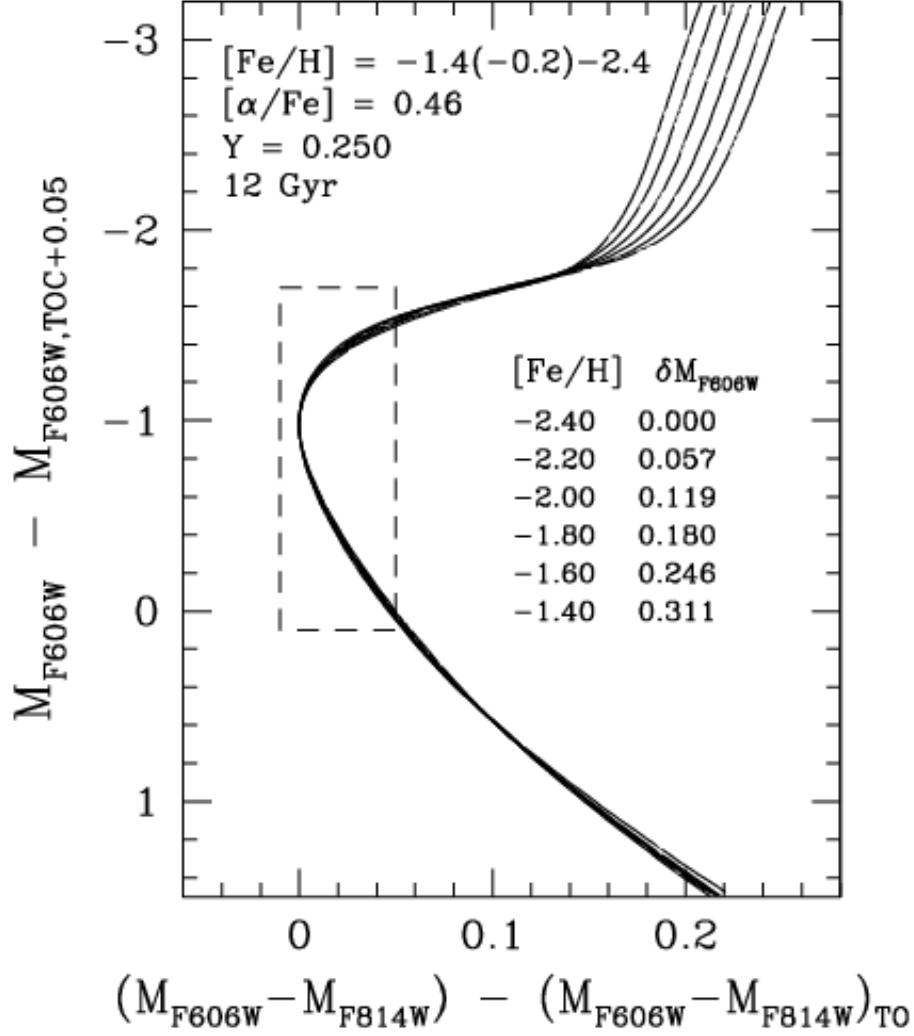


Fig. 3.— As in the left-hand panels of the previous plot, except that isochrones for a range in $[Fe/H]$, instead of age, are intercompared. The table lists the differences in the turnoff magnitudes of the isochrones for $[Fe/H]$ values ≥ -2.20 relative to that of the isochrone for $[Fe/H] = -2.40$. Note that the portions of the isochrones that are contained within the dashed box are morphologically nearly identical, though there is some dependence of the slope of the subgiant branch on $[Fe/H]$, with the lowest metallicity isochrone having the steepest slope.

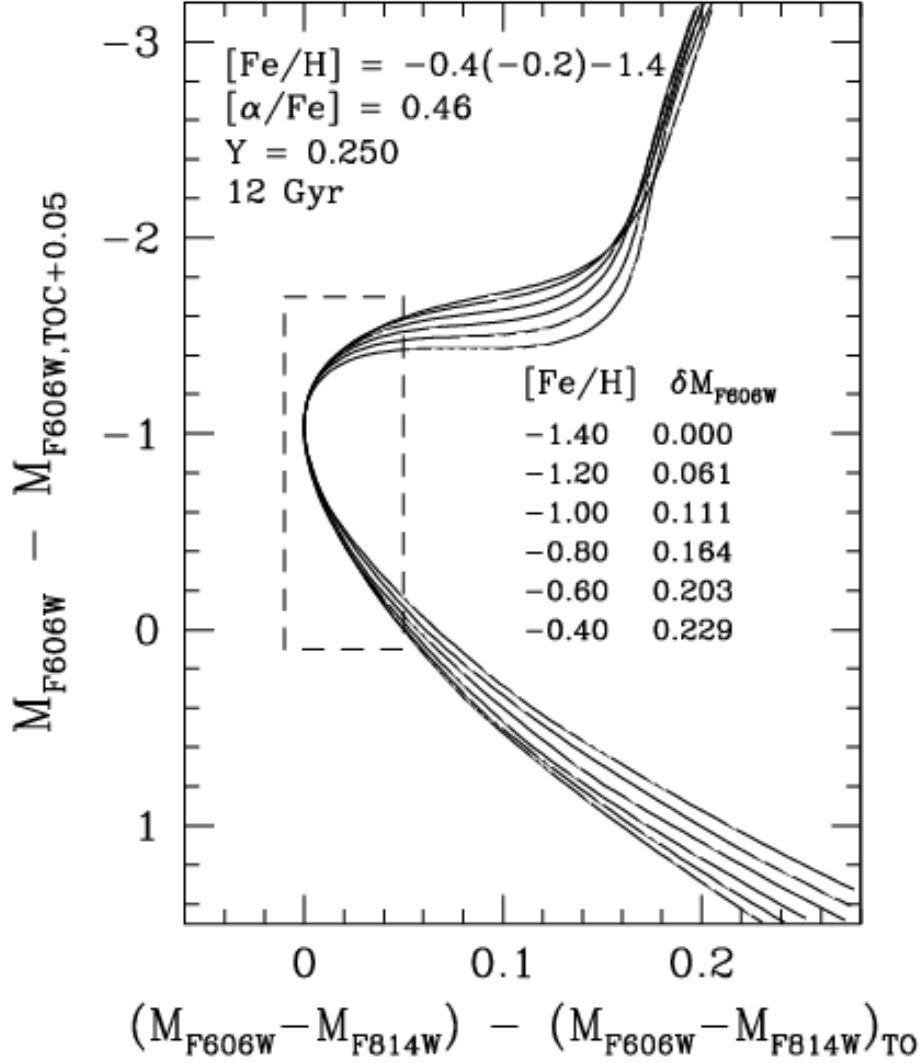


Fig. 4.— As in the previous figure, except that isochrones for $-1.40 \leq [Fe/H] \leq -0.40$ have been intercompared. The table lists the differences in the turnoff magnitudes of the isochrones for $[Fe/H]$ values ≥ -1.20 relative to that of the isochrone for $[Fe/H] = -1.40$.

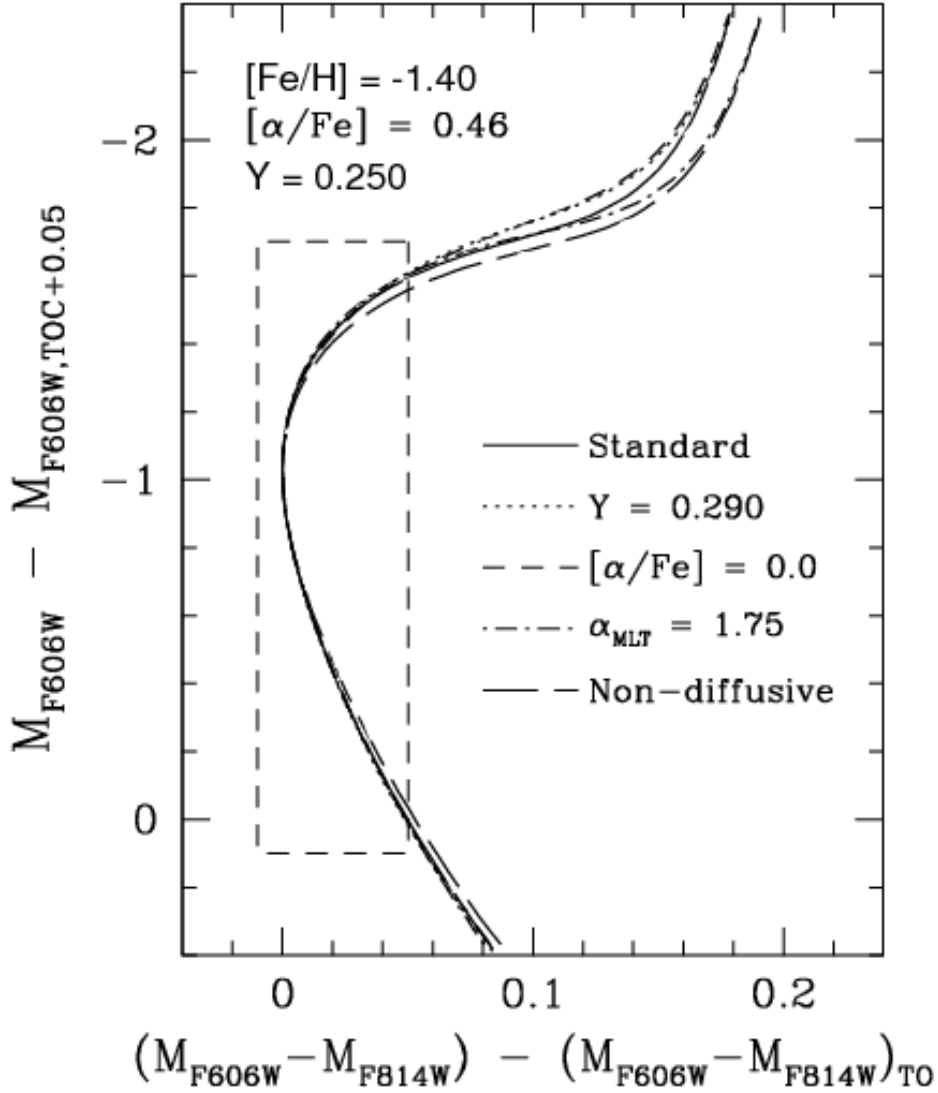


Fig. 5.— As in the previous three figures; in this case, a 12 Gyr isochrone for the chemical abundances specified in the top left-hand corner (the *solid curve*) are compared with those for higher Y (11.3 Gyr, *dotted curve*), lower $[\alpha/\text{Fe}]$ (13.5 Gyr, *short-dashed locus*), a smaller value of the mixing-length parameter by 0.255 (12 Gyr, *dot-dashed curve*), and one in which diffusive processes have been neglected (13.3 Gyr, *long-dashed locus*), as indicated. Different ages have been assumed in order that all of the isochrones have approximately the same turnoff luminosity.

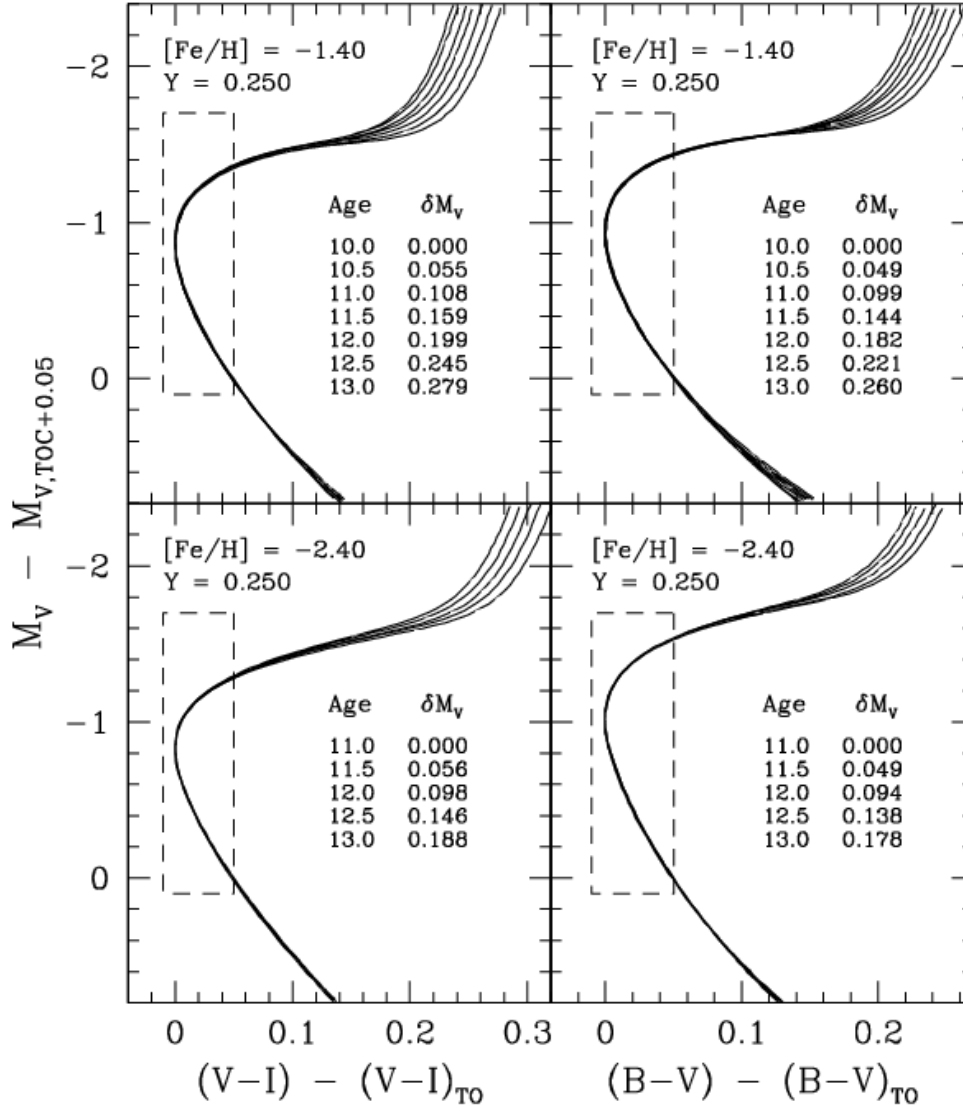


Fig. 6.— As in the left-hand panels of Fig. 2, except that the isochrones are compared on the $V - I$, V and $B - V$, V diagrams.

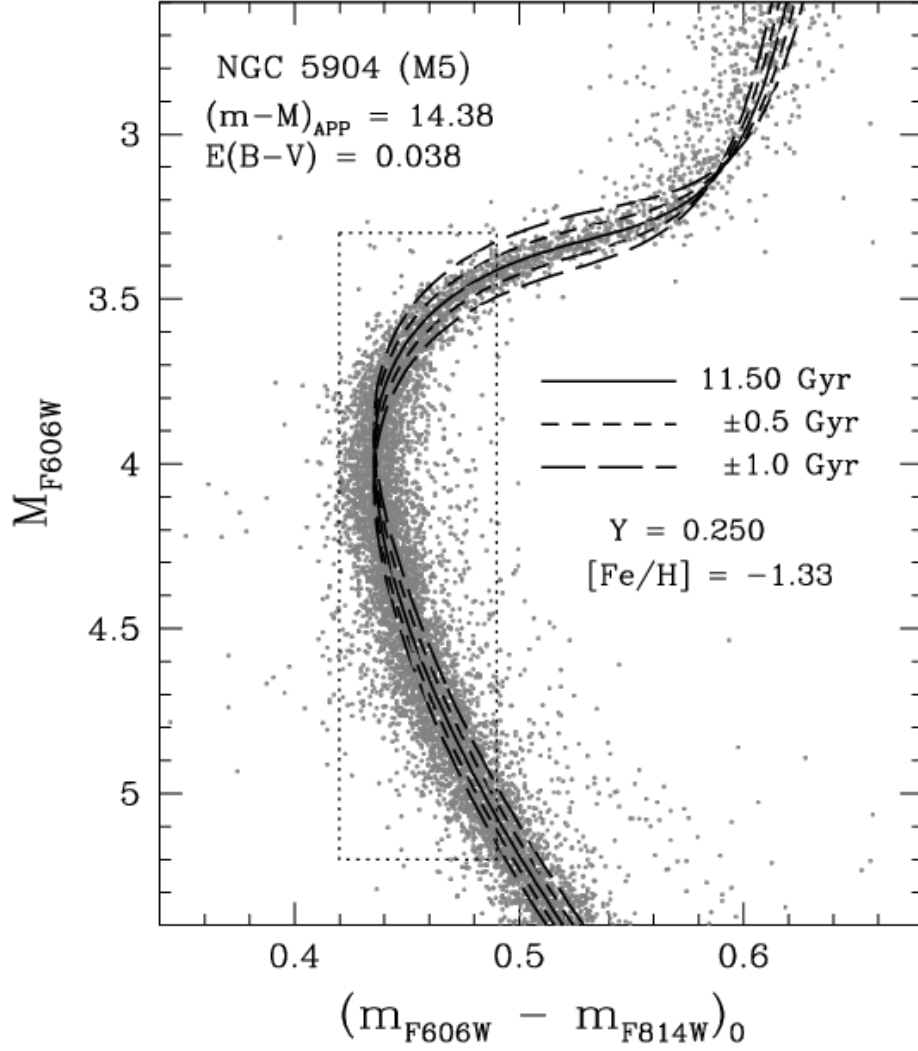


Fig. 7.— A comparison of the CMD of M5 with isochrones for the indicated chemical abundances when an apparent distance modulus of 14.38 and a reddening corresponding to $E(B - V) = 0.038$ are assumed. The *solid curve* represents an 11.5 Gyr isochrone, which provides the best fit to the cluster subgiants (notably those within the dotted rectangle), once it has been corrected by $\delta(\text{color}) = -0.025$ mag, while *dashed loci* represent isochrones that differ in age by ± 0.5 and ± 1.0 Gyr. The latter have also been arbitrarily shifted to the observed TO color: they will provide equally good fits to the turnoff region of the observed CMD if the adopted distance modulus is appropriately adjusted.

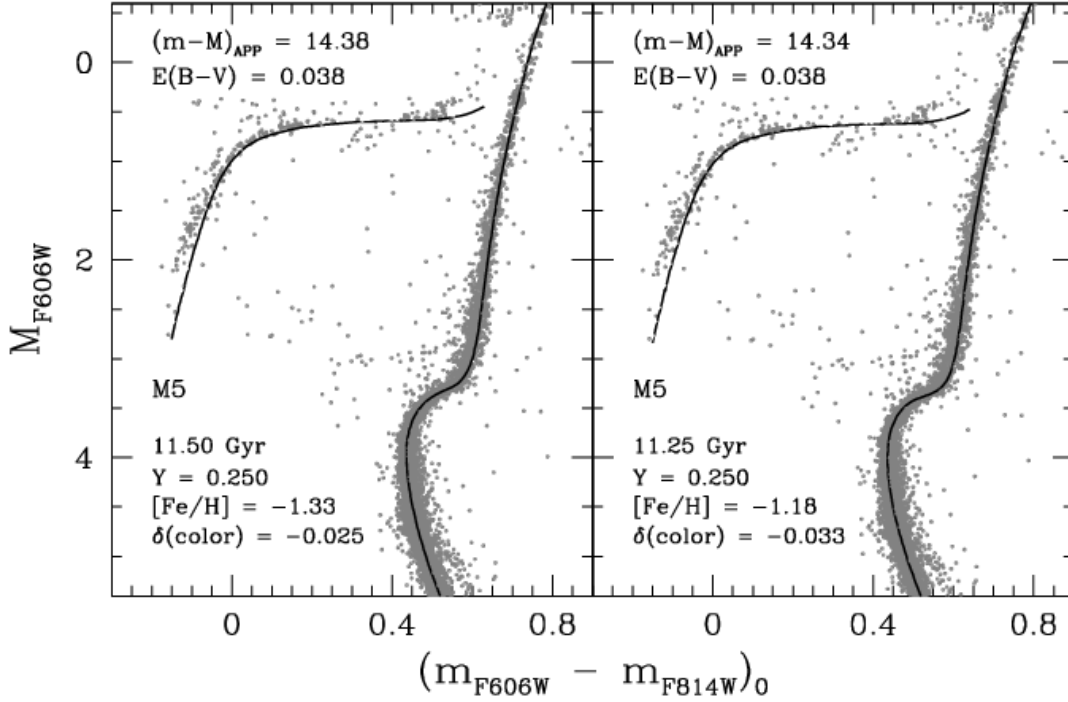


Fig. 8.— Fits of ZAHB loci to the lower bound of the distribution of HB stars in M5, assuming $[Fe/H] = -1.33$ (*left-hand panel*) and $[Fe/H] = -1.18$ (*right-hand panel*), assuming the same values of $E(B - V)$ and Y (as indicated). The models provide an excellent match to the observed HB morphology, except at $M_V > 1.5$ where some discrepancies become apparent. The ZAHB-based apparent distance moduli are 14.38 and 14.34 for the two cases. (The difference in the derived distance modulus would have been nearly a factor of two larger had they been based on fits of the observed CMD to the lower MS segments of the isochrones given that they differ by 0.069 mag at a fixed color.) To match the observed turnoff color, it was necessary to shift the best-fit isochrones for 11.50 and 11.25 Gyr horizontally by -0.025 and -0.033 mag, respectively. These color offsets were not applied to the ZAHB models.

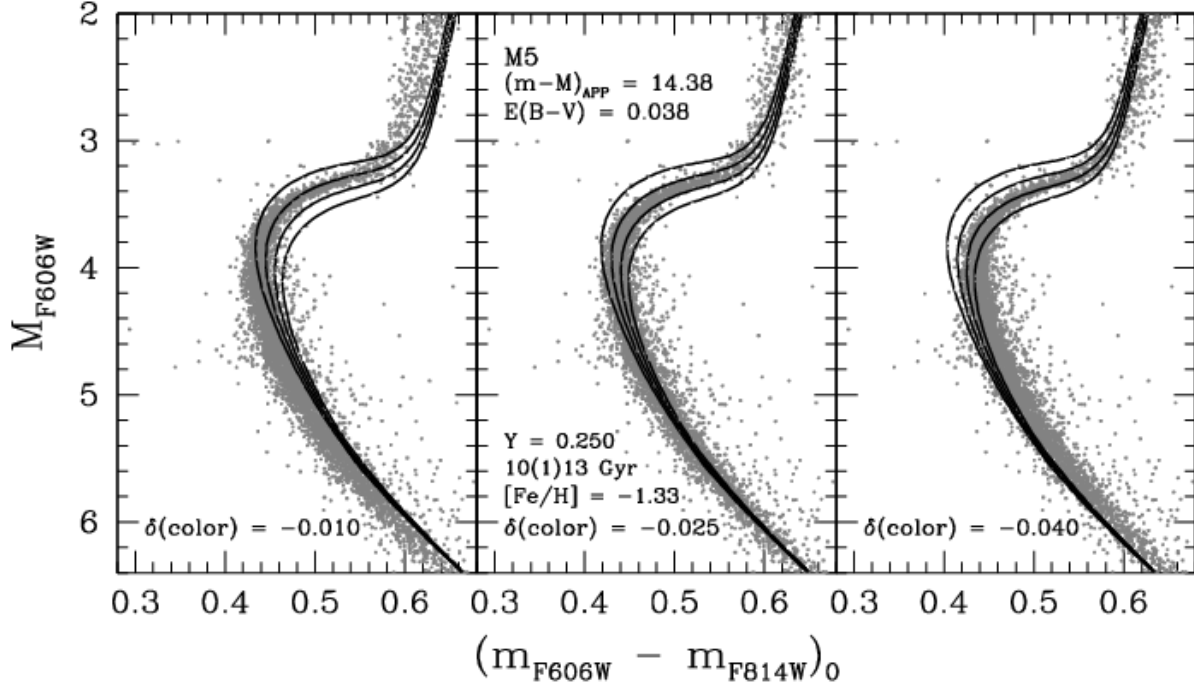


Fig. 9.— The *middle panel* presents a similar fit of isochrones to the CMD of M5 as that shown in Fig. 7, except that the various loci, which represent ages from 10 to 13 Gyr, in 1.0 Gyr increments, have not been shifted to a common turnoff color. This more traditional comparison of theory and observations indicates that an age of approximately 11.50 Gyr is required to match the observed subgiant stars, as found in the previous figure. In the *left-hand* and *right-hand panels*, different color offsets have been applied to the set of four isochrones, as specified just above the abscissa, to illustrate the difficulties of deriving an age when the best-fit isochrone does not reproduce the observed turnoff color.

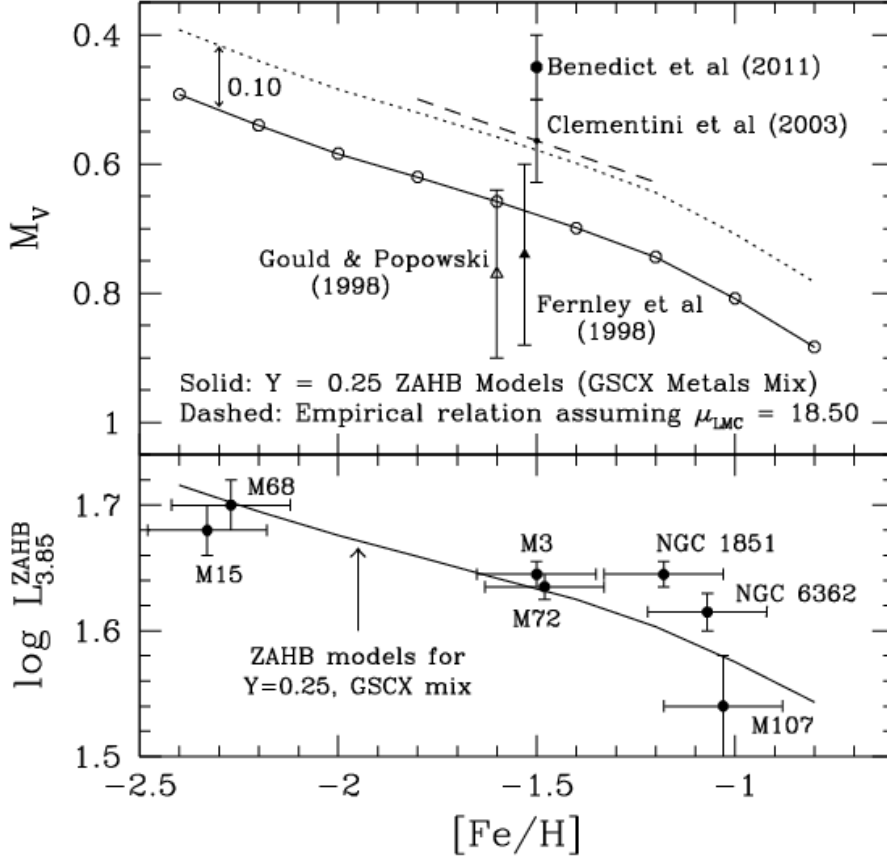


Fig. 10.— *Upper panel:* RR Lyrae M_V zero-points as determined from trigonometric parallaxes (Benedict et al. 2011), the apparent magnitudes of RR Lyraes in the LMC assuming $(m - M)_0 = 18.50$ (Clementini et al. 2003), statistical parallaxes (Gould & Popowski (1998), and the Baade-Wesselink method (Fernley et al. 1998). The slope of the *dashed line* is $\Delta M_V / \Delta [Fe/H] = 0.214$, as reported by Clementini et al. The *solid curve*, which connects individual ZAHB models for specific $[Fe/H]$ values (*open circles*), gives the predicted dependence of M_V on $[Fe/H]$. Since RR Lyraes in GCs that have $[Fe/H] \approx -1.5$ are observed to be ≈ 0.10 mag brighter than the faintest non-variable HB stars adjacent to the instability strip (Sandage 1993), the *dotted curve* (= *solid curve* minus 0.10 mag) represents the theoretical results that should be directly compared with the observations. *Lower panel:* The same ZAHB is compared with with the $\log L$ values that have been determined for ZAHB stars at $\log T_{\text{eff}} = 3.85$ (see the text) from the pulsational properties of variables in seven clusters, as indicated, by De Santis & Cassisi (1999).

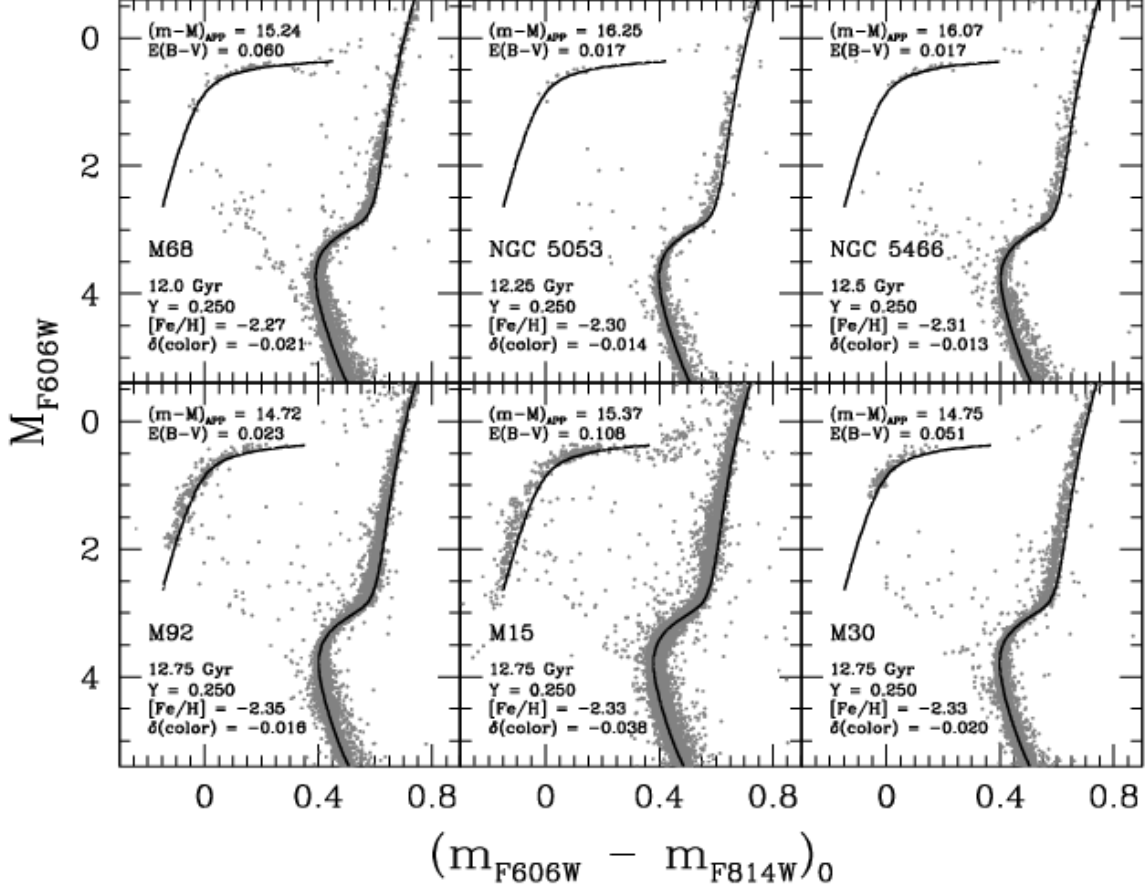


Fig. 11.— The CMDs of six globular clusters that have $[Fe/H] < -2.2$ (according to CBG09) are plotted on the assumption of the reddenings and the apparent distance moduli, as derived from the fit of a ZAHB to the lower bound of the distribution of cluster HB stars, that are given in the top left-hand corner of each panel. The derived ages, the assumed helium and $[Fe/H]$ abundances, and the adjustments in color that were needed in order for the selected isochrones to match the observed turnoff colors are specified below the cluster names. The main purpose of this and subsequent figures is to show that the ZAHB models provide good fits to the observed HB stars, especially to those with $0.0 \lesssim (m_{F606W} - m_{F814W})_0 \lesssim 0.3$ in this case, and that the best-fit isochrones do, indeed, reproduce the cluster photometry in the vicinity of the turnoff very well.

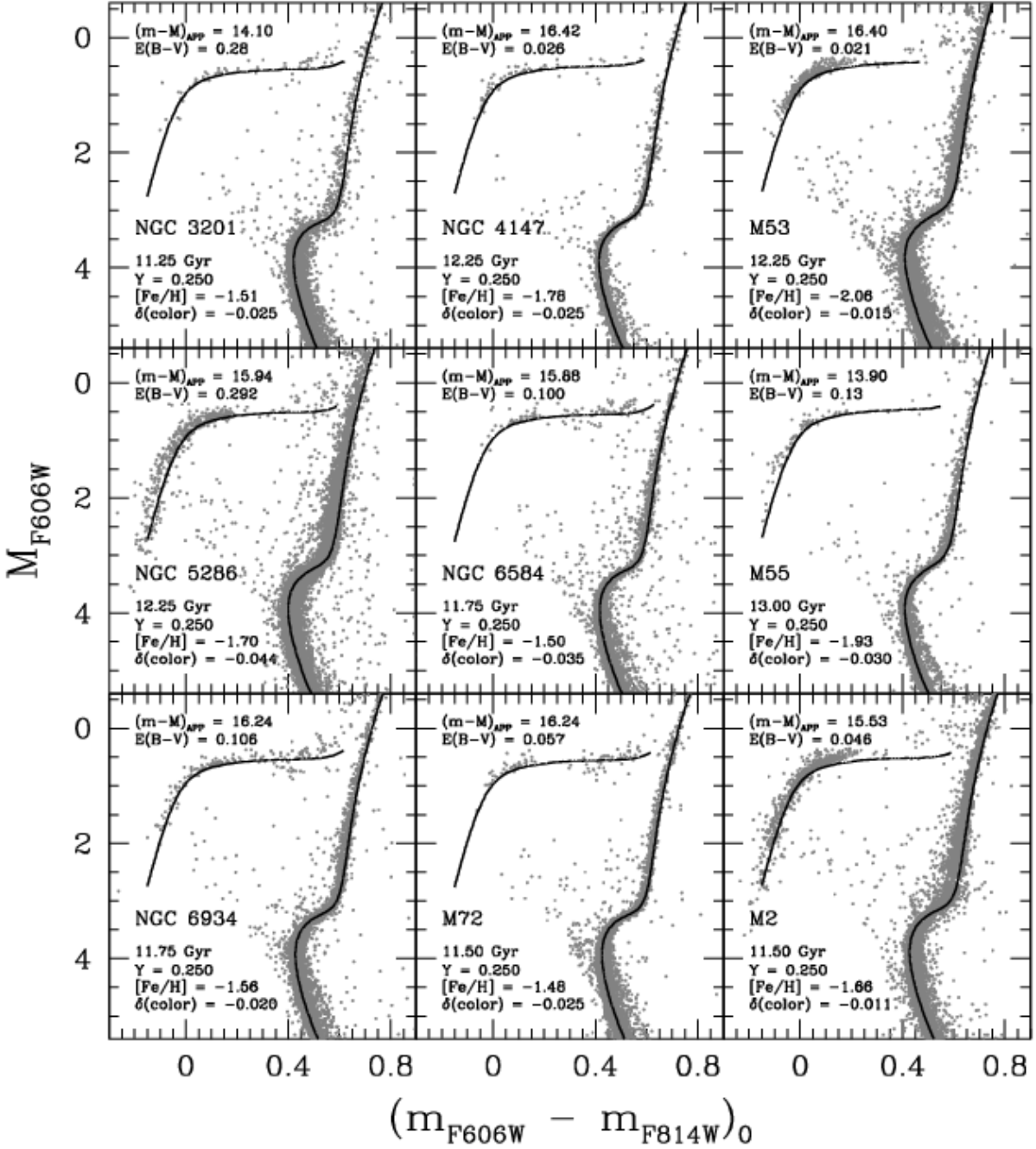


Fig. 12.— Similar to the previous figure; in this case, the CMDs of globular clusters that have $-1.50 > [Fe/H] \geq -2.2$ have been fitted by ZAHB loci and isochrones for the appropriate metallicities. The panels have been organized such that the cluster NGC numbers increase in the direction from left to right, beginning in the top row and ending in the bottom left-hand corner — though the Messier number is used if a given cluster has one.

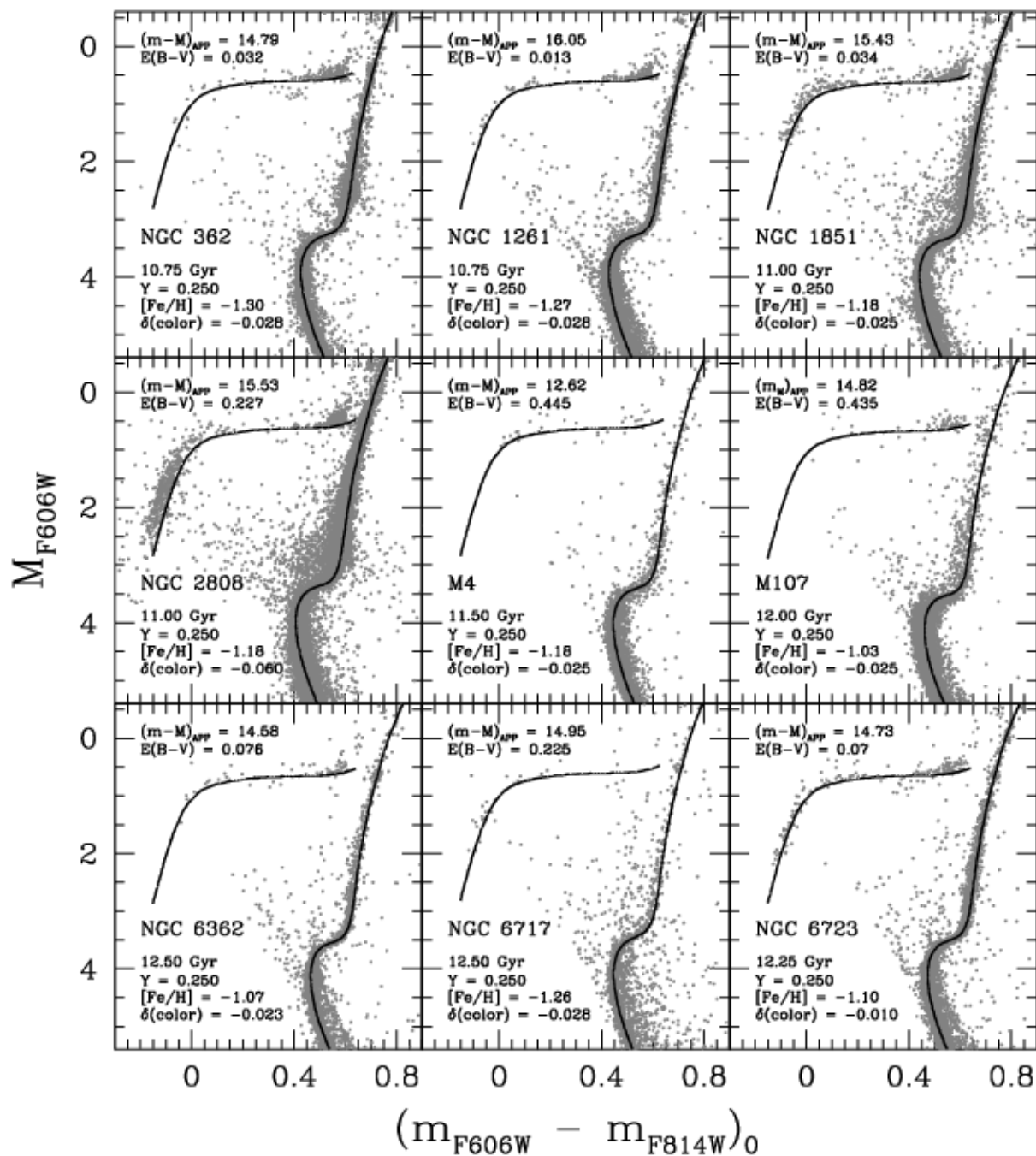


Fig. 13.— Similar to the previous figure; in this case, the CMDs of globular clusters that have $-1.00 > [Fe/H] \geq -1.50$ have been fitted by ZAHB loci and isochrones for the appropriate metallicities.

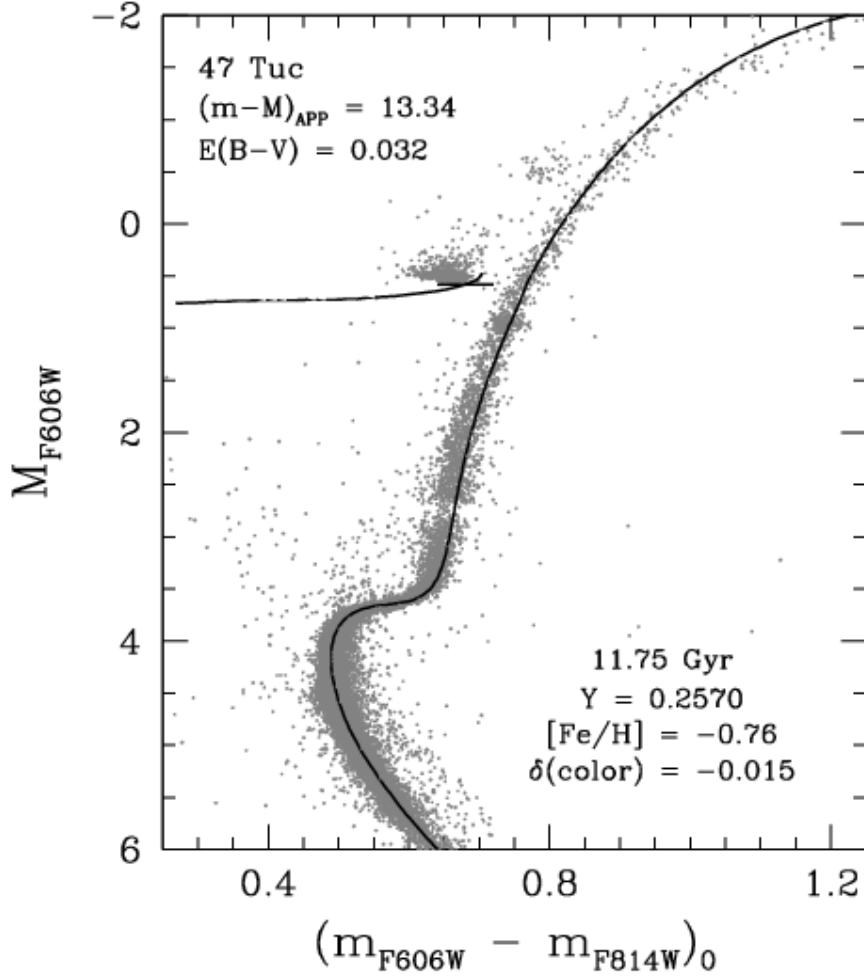


Fig. 14.— As in previous comparisons of isochrones and ZAHB loci with photometric data; in this case, for 47 Tucanae. Note that the red end of the ZAHB gives the location of star that has not undergone any mass loss prior to reaching the HB. Its mass is the same as that of the model at the RGB tip of the best-fit isochrone for the indicated age. The point at the intersection of the short horizontal line with the ZAHB indicates the location of a model that has a lower mass by $0.20M_{\odot}$. (The apparent gap at $M_{F606W} \approx 2.8$ is an artifact arising from the selection of stars that have photometric errors < 0.015 mag, given that short and long integrations were employed to obtain the photometry for the cluster giants and main-sequence stars, respectively.)

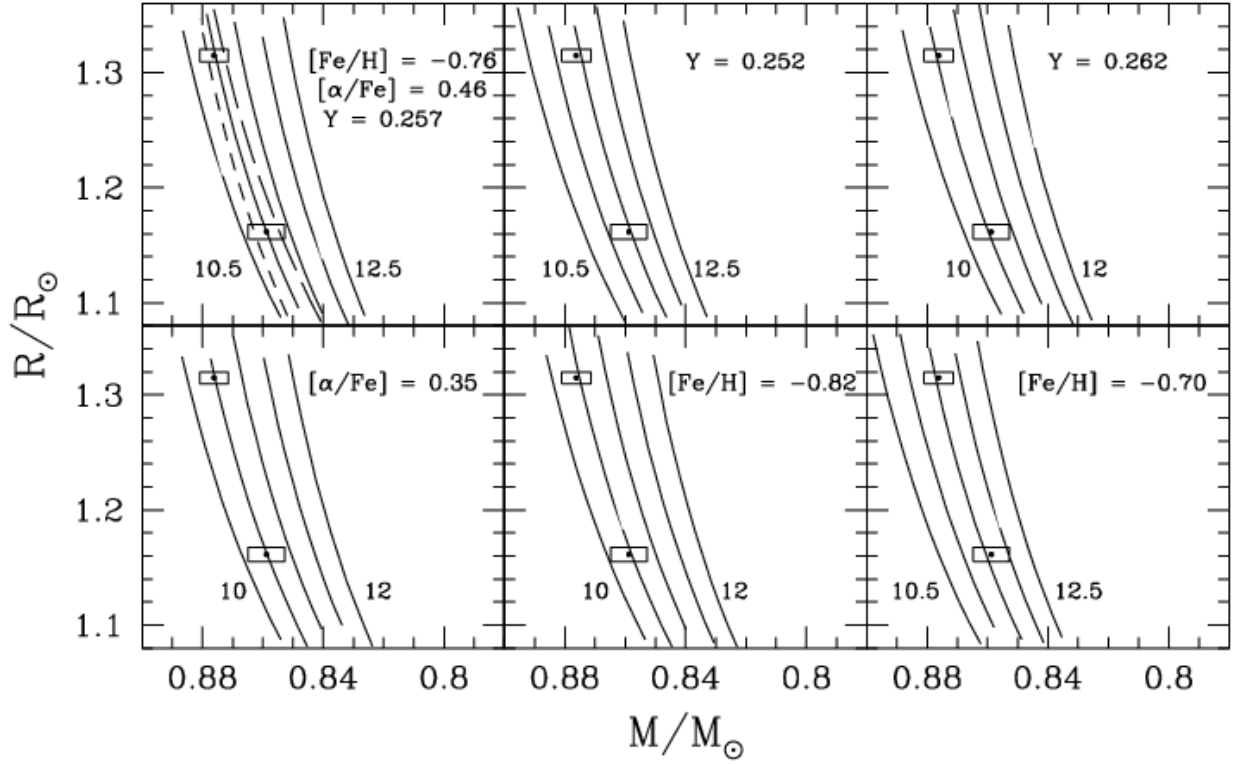


Fig. 15.— The filled circles and error boxes plot the masses and radii of the components of the binary, V69, as determined by Thompson et al. (2010), along with their uncertainties. The variations of radius with mass that are predicted by the same isochrones which have been used in the previous figure, but for ages of 10.5 to 12.5 Gyr in 0.5 Gyr intervals, have been plotted as solid curves in the upper *left-hand panel*. The adopted chemical properties for these models are listed in the top right-hand corner of this panel. If the temperatures along the 11.0 Gyr isochrone are increased by 75 K, the result is the short-dashed curve, while the long-dashed curve illustrates the effect of reducing the predicted temperatures by 75 K. The other panels show how the inferred age is affected if the values of the various abundance parameters are varied, in turn, by small amounts (as noted in each panel).

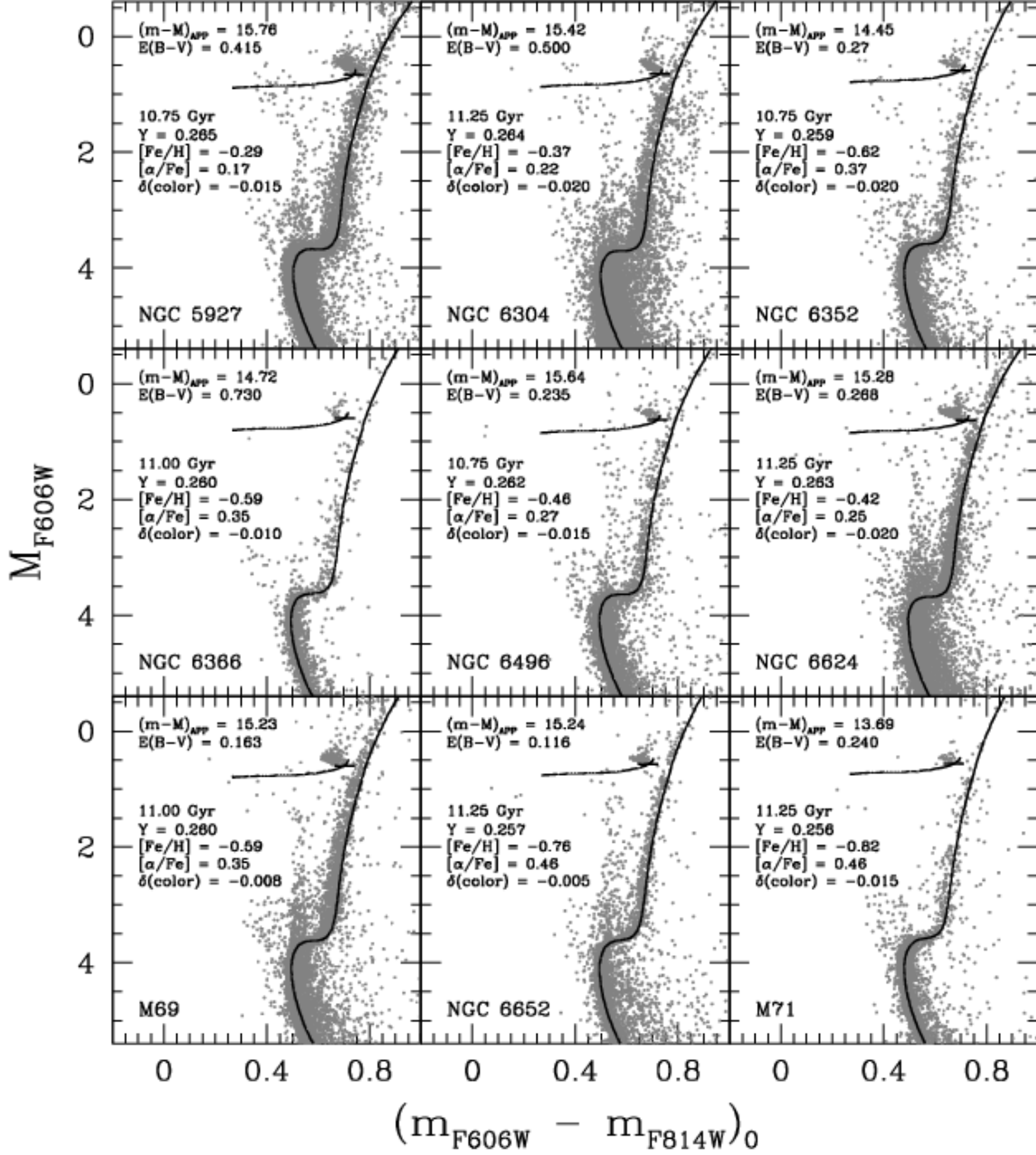


Fig. 16.— Similar to Fig. 14; in this case, the CMDs of globular clusters that have $[Fe/H] \geq -1.0$ have been fitted by ZAHB loci and isochrones for the appropriate metallicities.

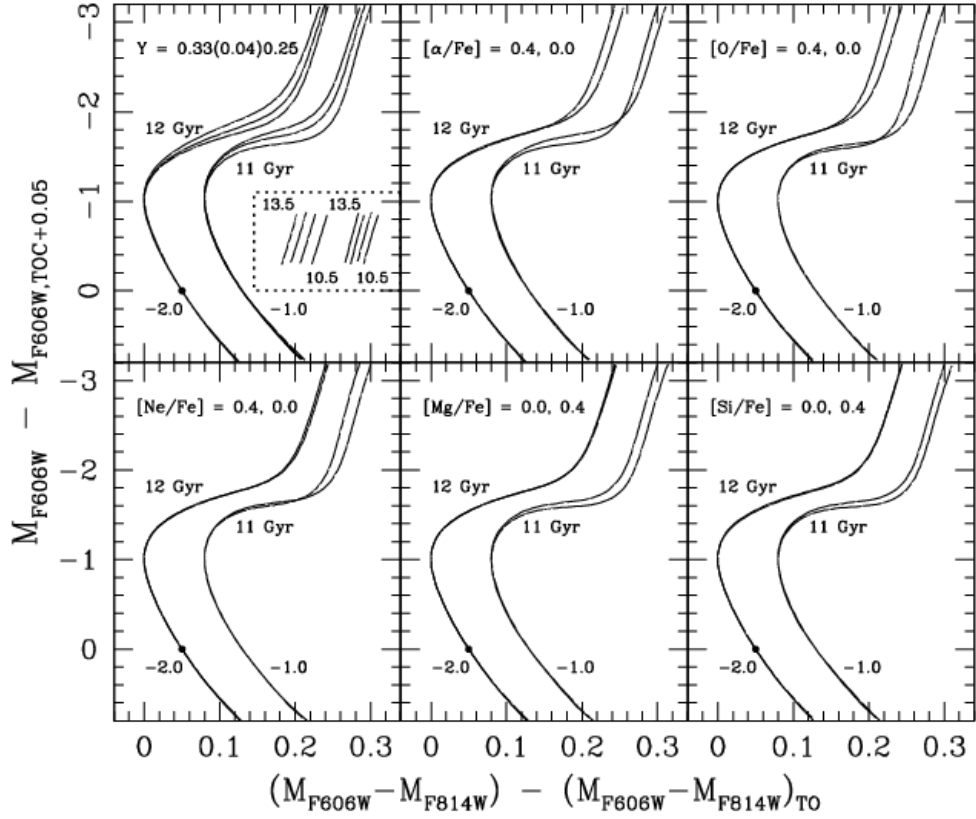


Fig. 17.— Isochrones for different choices of the chemical abundance parameters, as indicated in the top left-hand corner of each panel, have been superimposed such that they have the same turnoff colors and the same magnitudes at the point along the upper MS that is 0.05 mag redder than the TO. (These fiducial points define the abscissae and ordinate zero-points.) Isochrones for $[\text{Fe}/\text{H}] = -2.0$ and the different helium and heavy-element mixtures have been generated for an age of 12 Gyr, whereas those for $[\text{Fe}/\text{H}] = -1.0$ assume an age of 11 Gyr. Note that the grids of evolutionary tracks that are the basis of these isochrones were computed by VandenBerg et al. (2012) on the assumption of the Asplund, Grevesse, & Sauval (2005) solar metals mix, with enhanced abundances of a number of metals. (These are the only computations that are available to us at the present time in which the abundances of individual metals are enhanced, in turn, by 0.4 dex.) Note as well that, for the sake of clarity, the isochrones for $[\text{Fe}/\text{H}] = -1.0$ have been offset to the red by 0.1 mag. The loci contained within the dotted rectangle represent the RGB segments of 10.5 to 13.5 Gyr isochrones, in 1.0 Gyr intervals, for the reference mixture at ordinate values of ≈ -2.4 to -3.2 . By comparing these results with the predicted horizontal offsets of the RGB loci that are produced by the various abundance choices, an equivalent age difference can be estimated.

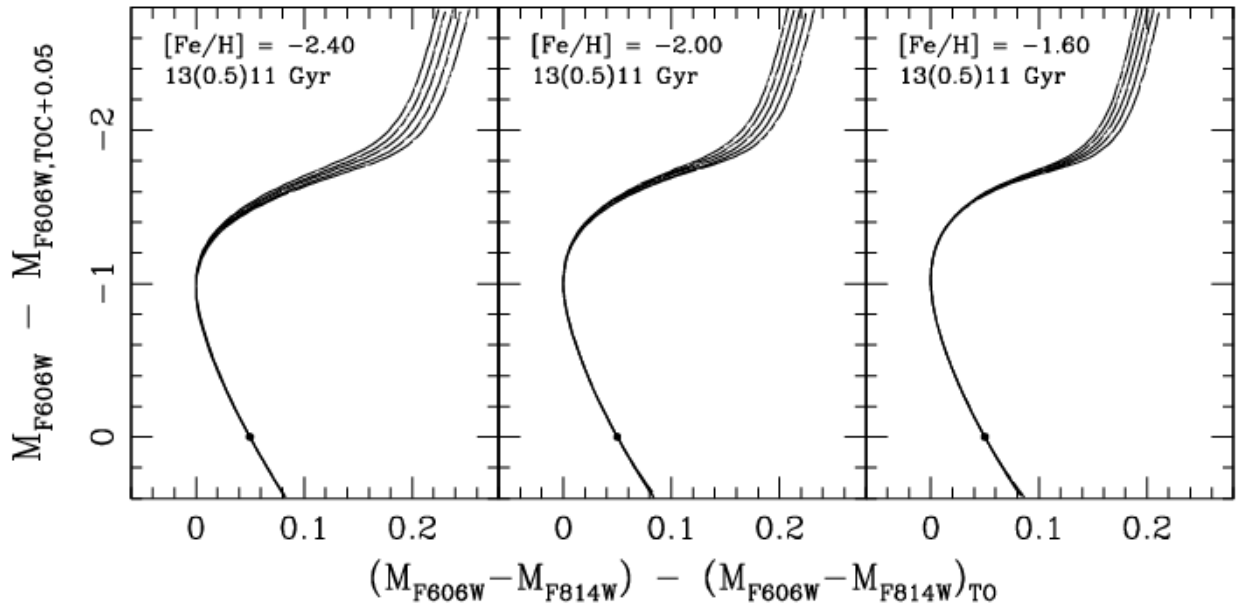


Fig. 18.— Similar to the previous figure, except that 11–13 isochrones for the GSCX mix and three values of $[Fe/H]$, as indicated, have been registered to one another.

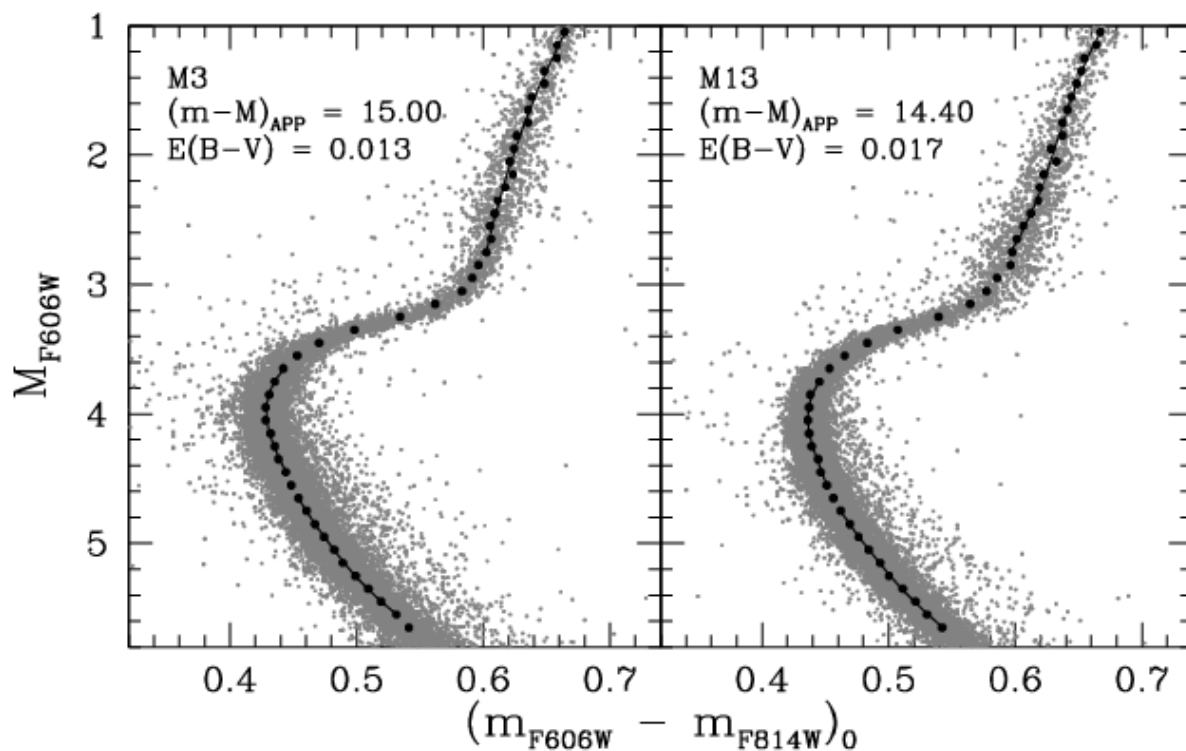


Fig. 19.— The CMDs of M3 (NGC 5272) and M13 (NGC 6205) showing the median points (*filled circles*) that have been derived in 0.1 mag bins along the photometric sequences. *Solid curves* illustrate the least-squares fits to the median points in three different parts of the CMD: the RGB, the vicinity of the turnoff, and the region enclosing that point on the upper MS which is 0.05 mag redder than the TO; see the text.

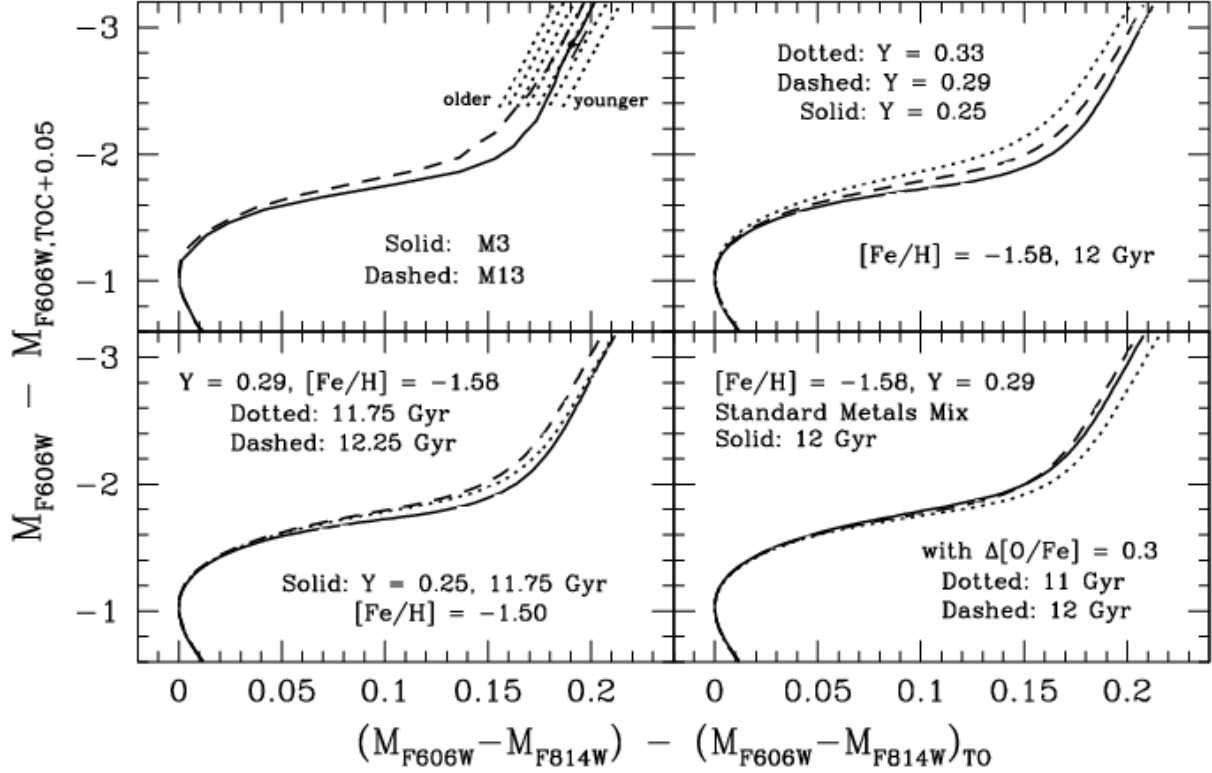


Fig. 20.— *Upper left:* The CMDs of M3 and M13 have been registered to the usual VBS90 abscissa and ordinate zero-points. The dotted lines represent the RGB segments of isochrones for $[Fe/H] = -1.50$ that differ in age, in turn, by 0.5 Gyr in the direction indicated. The offset of the short sloped line from the small filled circle at an ordinate value of -2.8 indicates the horizontal correction that should be applied to the M3 RGB to account for the difference in its $[Fe/H]$ value (-1.50) and that of M13 (-1.58). *Upper right:* 12 Gyr isochrones for $[Fe/H] = -1.58$ and $Y = 0.33$, 0.29 , and 0.25 (in the direction from left to right) have been similarly registered. *Bottom right:* 12 Gyr isochrones for $[Fe/H] = -1.58$ and $Y = 0.29$ with, or without, 0.3 dex enhancements in $[O/Fe]$ (in the direction from left to right) have been similarly registered. *Bottom left:* Registration of isochrones for those ages and chemical abundances that appear to be close to the values needed to explain the observations in the upper, left-hand panel.

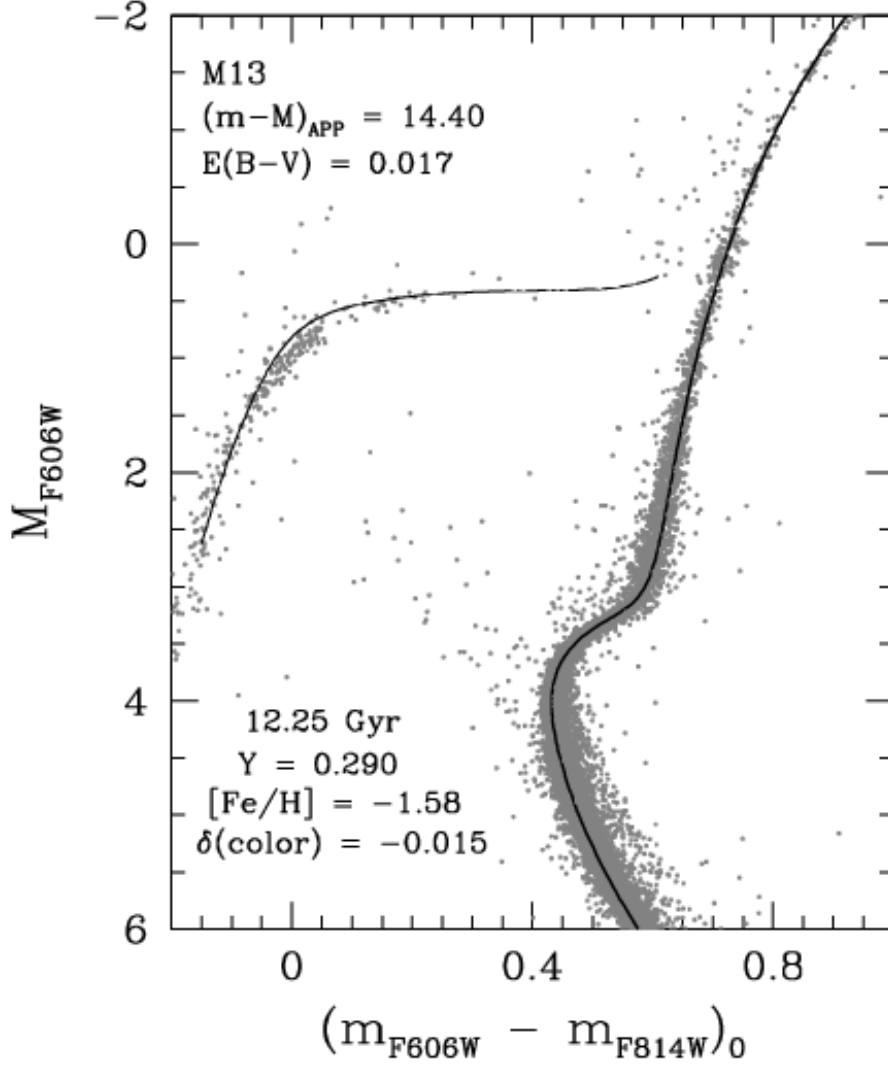


Fig. 21.— A 12.25 Gyr isochrone for $Y = 0.29$ and $[\text{Fe}/\text{H}] = -1.58$ has the same turnoff luminosity as M13 (as shown), if the cluster has $E(B-V) = 0.017$ (Schlegel et al. 1998) and an apparent distance modulus of 14.40 mag. Although the isochrones match the morphologies of the MS, SGB, and RGB quite well, a large fraction of the cluster HB stars are fainter than the corresponding ZAHB, which argues against this particular interpretation of the observed CMD.

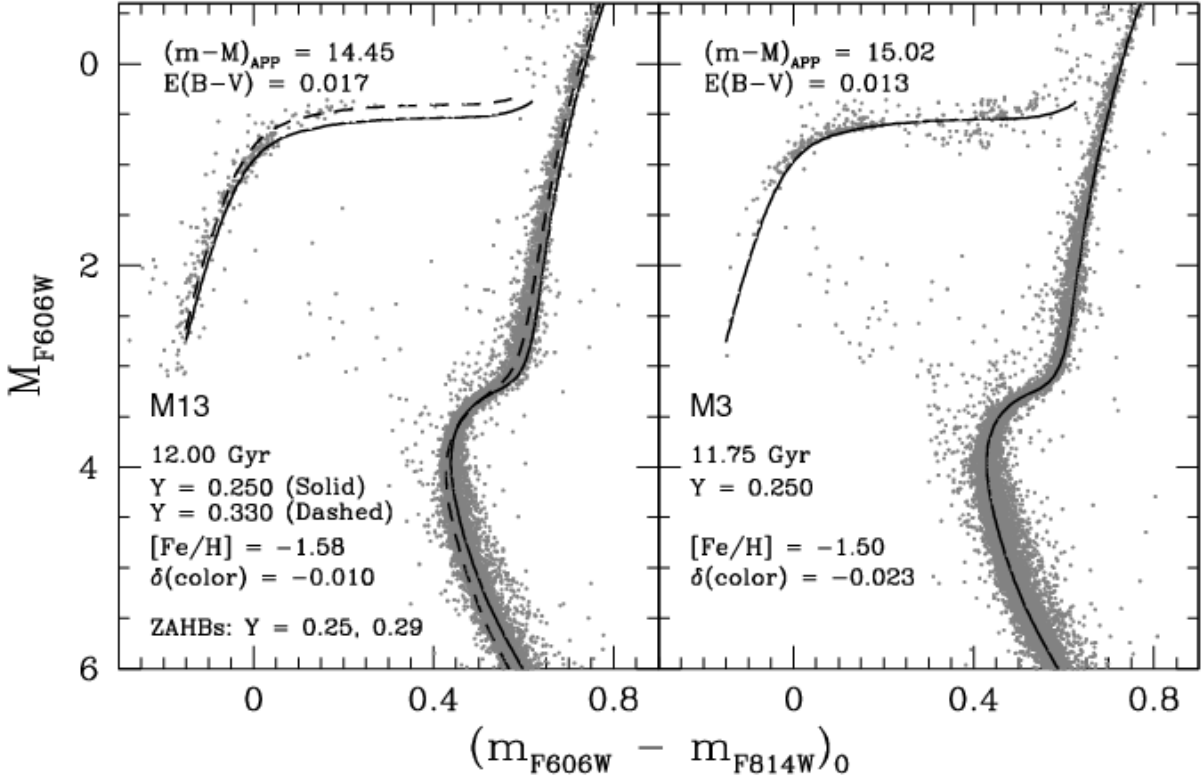


Fig. 22.— Fits of isochrones and ZAHB loci for the indicated parameters to the CMDs of M3 and M13 (*right-* and *left-hand panels*, respectively). In both cases, the adopted distance moduli are such that ZAHBs for $Y = 0.25$ provide satisfactory fits to the lower bounds of the observed HB populations. Isochrones for the same age, but different Y , are shown in the *left-hand panel*: morphological differences in the SGBs of M3 and M13 may be explained if the latter has a higher helium abundance, in the mean, than the former (see the text). If this inference is correct and the stars with the highest helium abundances in M13 evolve to ZAHB locations well to the blue of the instability strip, its observed HB may be satisfactorily reproduced by models that encompass a significant range in Y .

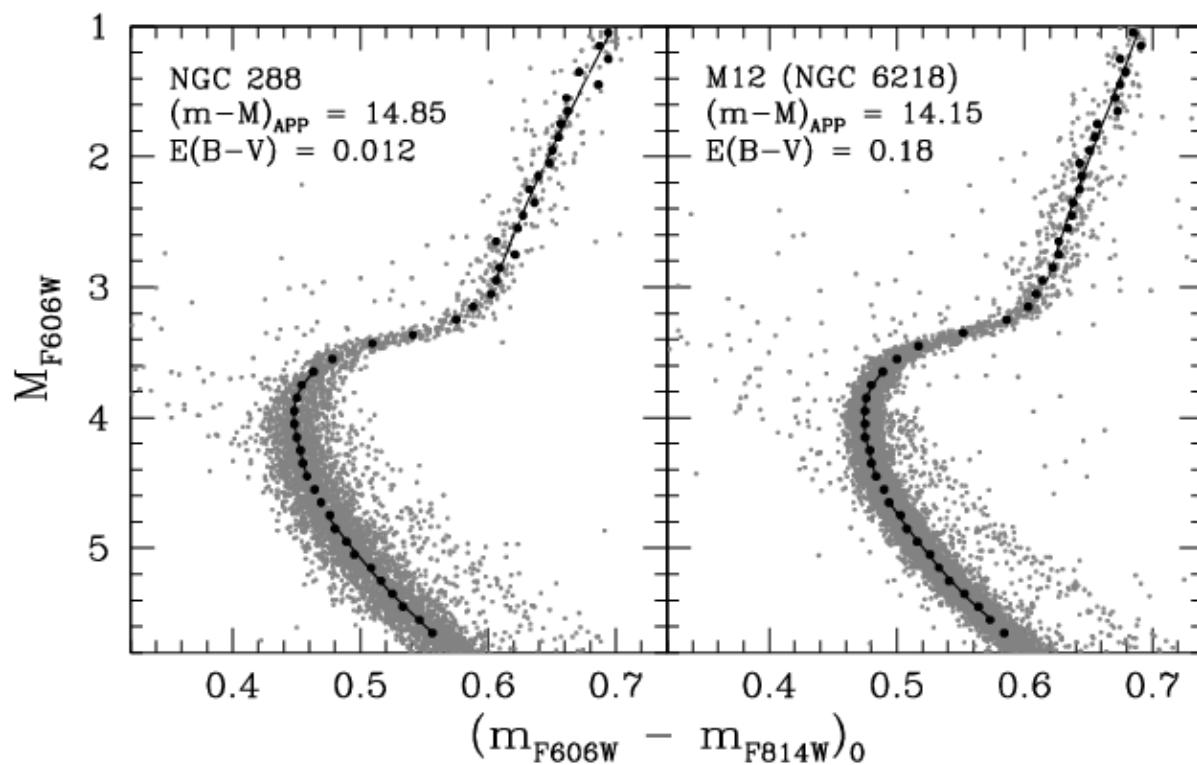


Fig. 23.— Similar to Fig. 19; in this case, the CMDs and the derived fiducial sequences are shown for NGC 288 and M 12 (NGC 6218). Interestingly, the different MS widths of the two clusters suggests that star-to-star chemical abundance variations are significantly larger in NGC 288 than in M 12.

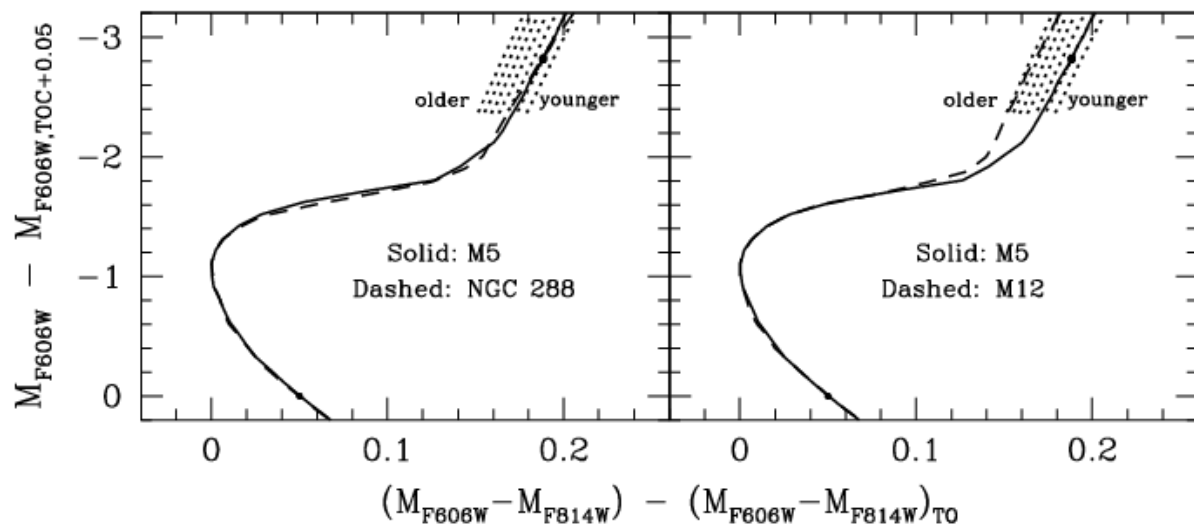


Fig. 24.— Similar to the upper left-hand panel in Fig. 20; in this case, the fiducial sequence of M5 (NGC 5904) has been registered to that of NGC 288 (*left-hand panel*) and to that of M12 (NGC 6218) (*right-hand panel*). This suggests that NGC 288 and M5 are nearly coeval, while M12 is significantly older than M5 (but see the discussion in the text).

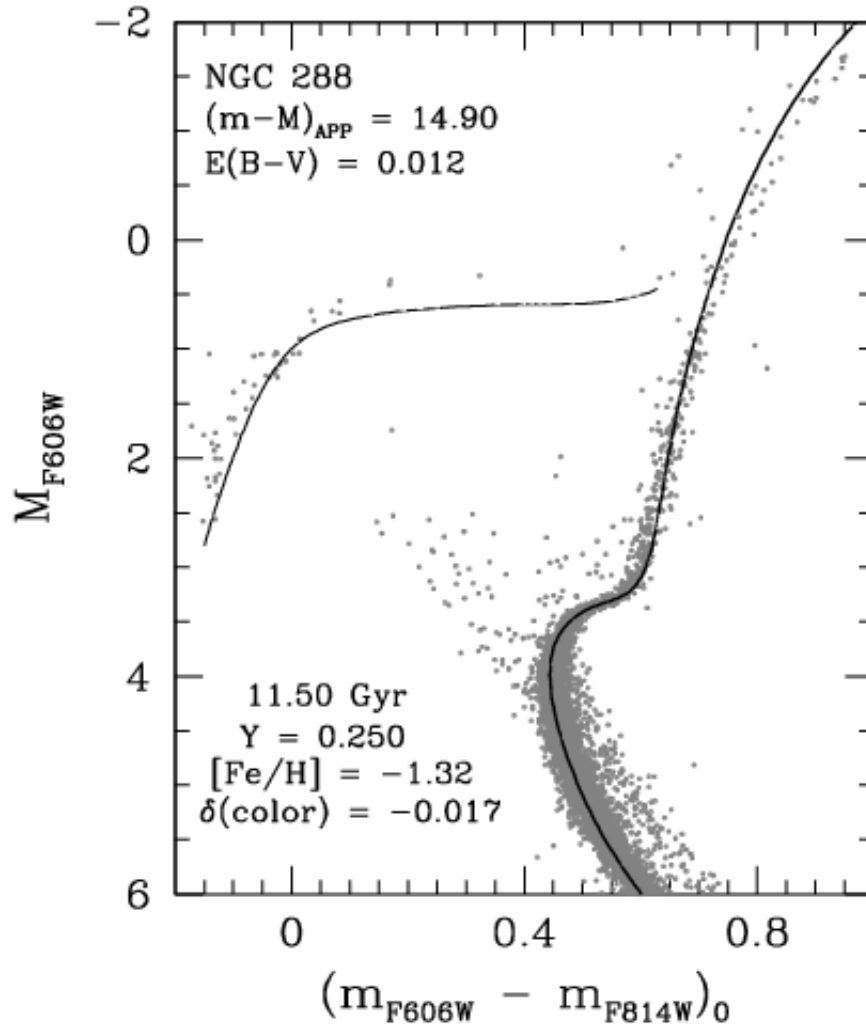


Fig. 25.— Fit of an isochrone for the indicated age and chemical abundances and a fully consistent ZAHB to the CMD of NGC 288 on the assumption of the apparent distance modulus and reddening that are specified in the upper left-hand corner.

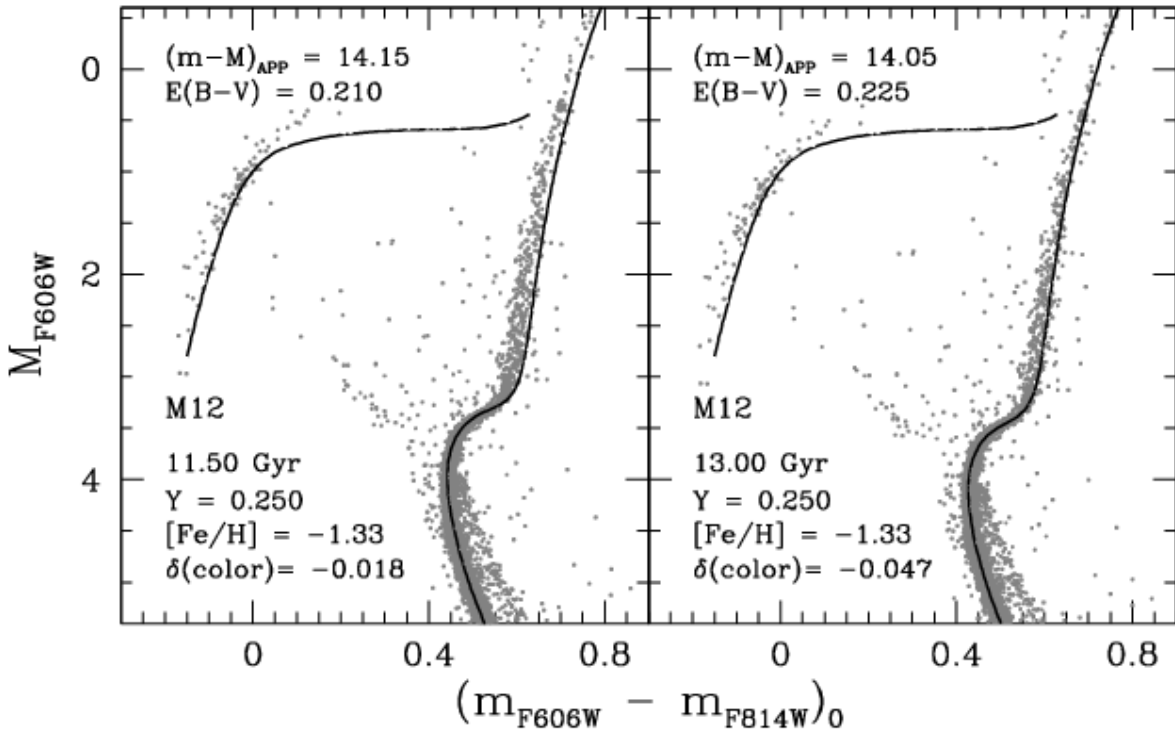


Fig. 26.— Similar to the previous figure; in this case, isochrones for the same chemical abundances (as indicated) and ages of 11.5 and 13.0 Gyr have been fitted to the photometry of M12 in the *left-* and *right-hand panels*, respectively. Note that there is no obvious difference in the quality of the fit to the cluster HB stars if the reddening is adjusted to accommodate a different distance modulus.

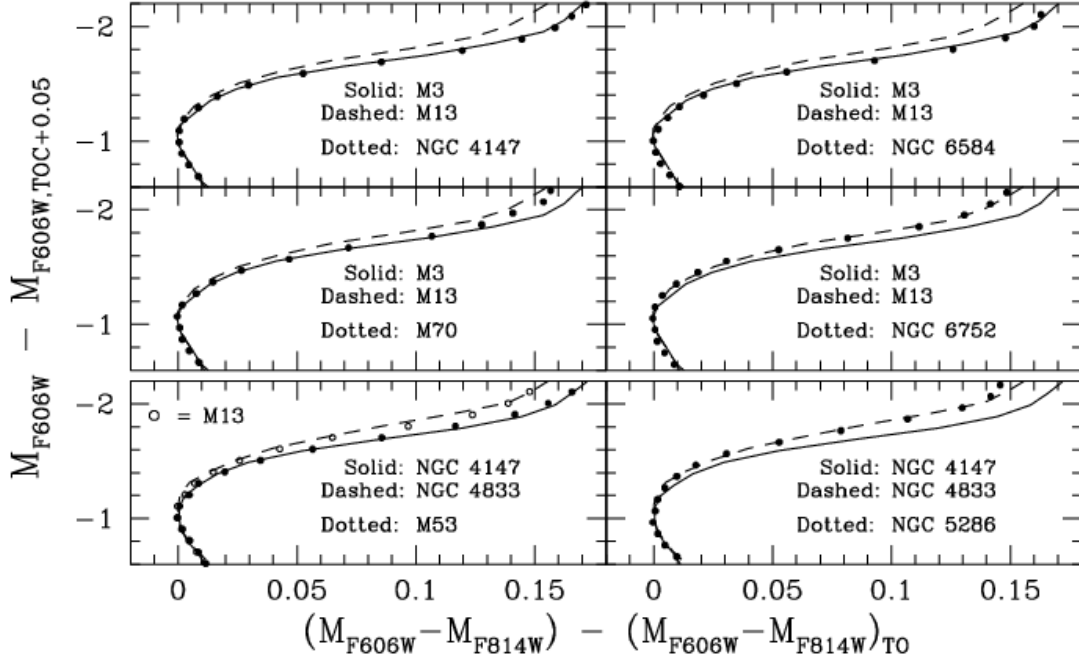


Fig. 27.— *Uppermost four panels:* the photometric sequences for the turnoff and subgiant stars of four target GCs (*dotted curves*) are compared with those of M 3 and M 13 (*solid and dashed loci*, respectively). With the exception of NGC 4147 (see the text), all of the clusters have the same $[\text{Fe}/\text{H}]$ values to within 0.10 dex. Note that NGC 6752 is the only target cluster which is “M 13-like” insofar as the slope of its SGB is concerned. *Bottom two panels:* the fiducial sequences for two lower-metallicity clusters, M 53 and NGC 5286, are compared with those of NGC 4147, which has a relatively flat SGB (like M 3) and NGC 4833, which has a steeper SGB (comparable to that of M 13). All of the cluster fiducials have been adjusted in the horizontal and vertical directions in order that they have the same turnoff color (the abscissa zero-point) and the same magnitude on the upper main sequence that is 0.05 mag redder than the TO (the ordinate zero-point).

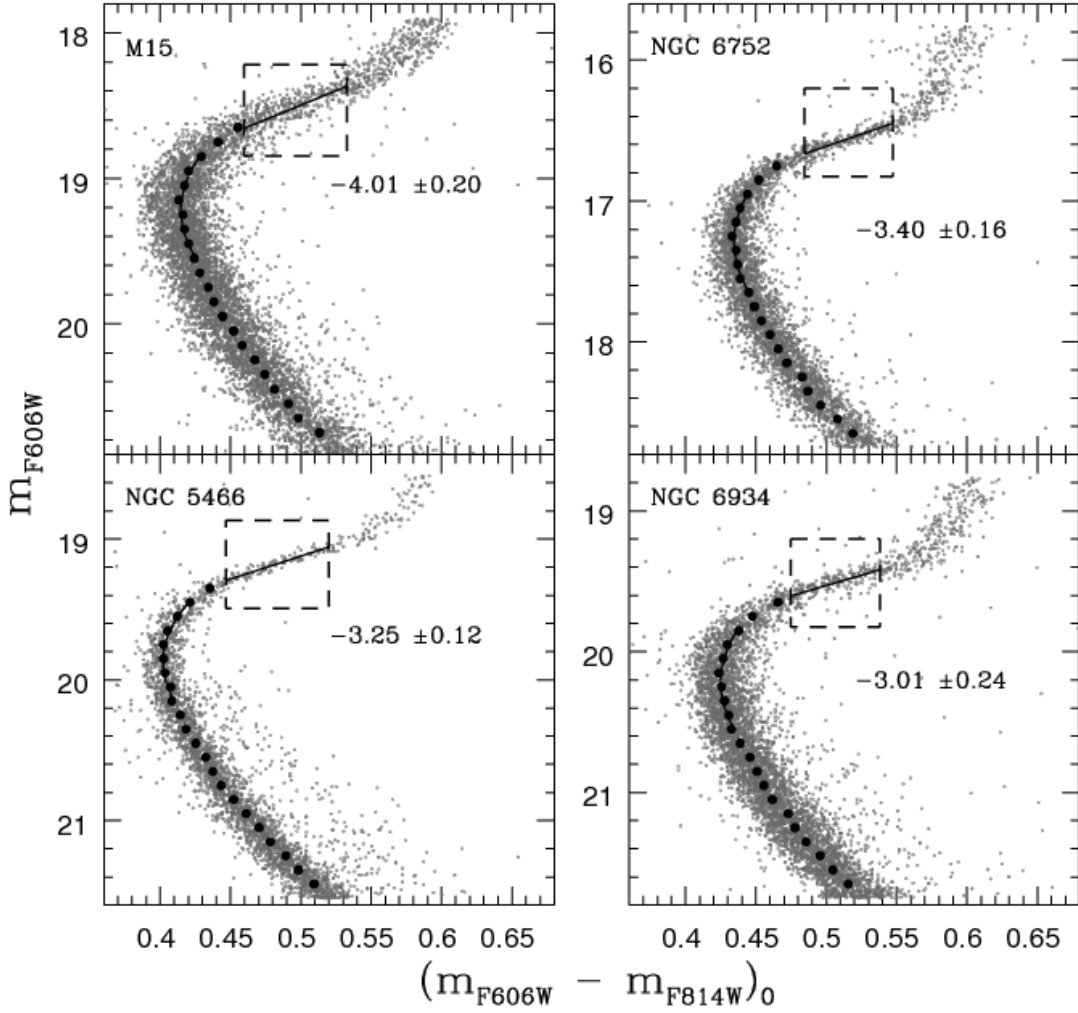


Fig. 28.— Representative examples of the linear least-squares fits that have been performed to the SGBs of all of the clusters that have $[\text{Fe}/\text{H}] \lesssim -1.5$ in order to determine the subgiant slopes and their uncertainties. Only those stars inside the *dashed rectangles* were fitted (see the text), resulting in the straight lines within them. Numerical values for the slopes of these lines, and their uncertainties, are given below and to the right of the rectangles. As in Fig. 26, the large filled circles define the fiducial cluster sequences for the upper MS and TO stars.

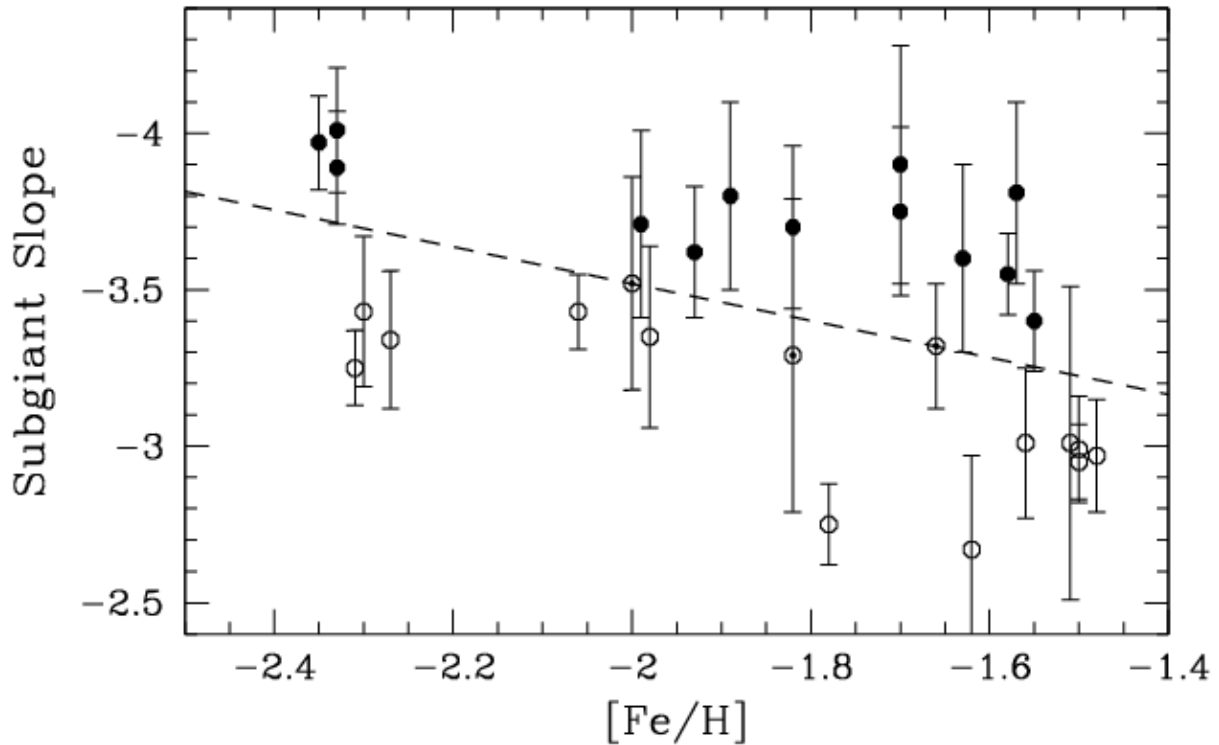


Fig. 29.— Plot of the subgiant slopes and their uncertainties as a function of $[\text{Fe}/\text{H}]$ for all of the clusters listed in Table 1. *Filled circles* identify clusters that have relatively steep SGB slopes (“M 13-like”), while those with shallower slopes (“M 3-like”) are represented by *open circles*. Composite symbols have been used for three clusters that have intermediate SGB slopes. A linear least-squares fit to all of the points resulted in the dashed line. Note that the interpretation of these results is complicated by the predictions that (i) at a fixed age, isochrones at lower metallicities have slightly steeper SGBs (see Fig. 3), and (ii), at a fixed $[\text{Fe}/\text{H}]$ value, there is some dependence of the SGB slope on age (especially at $[\text{Fe}/\text{H}] \lesssim -2$; see Fig. 18).

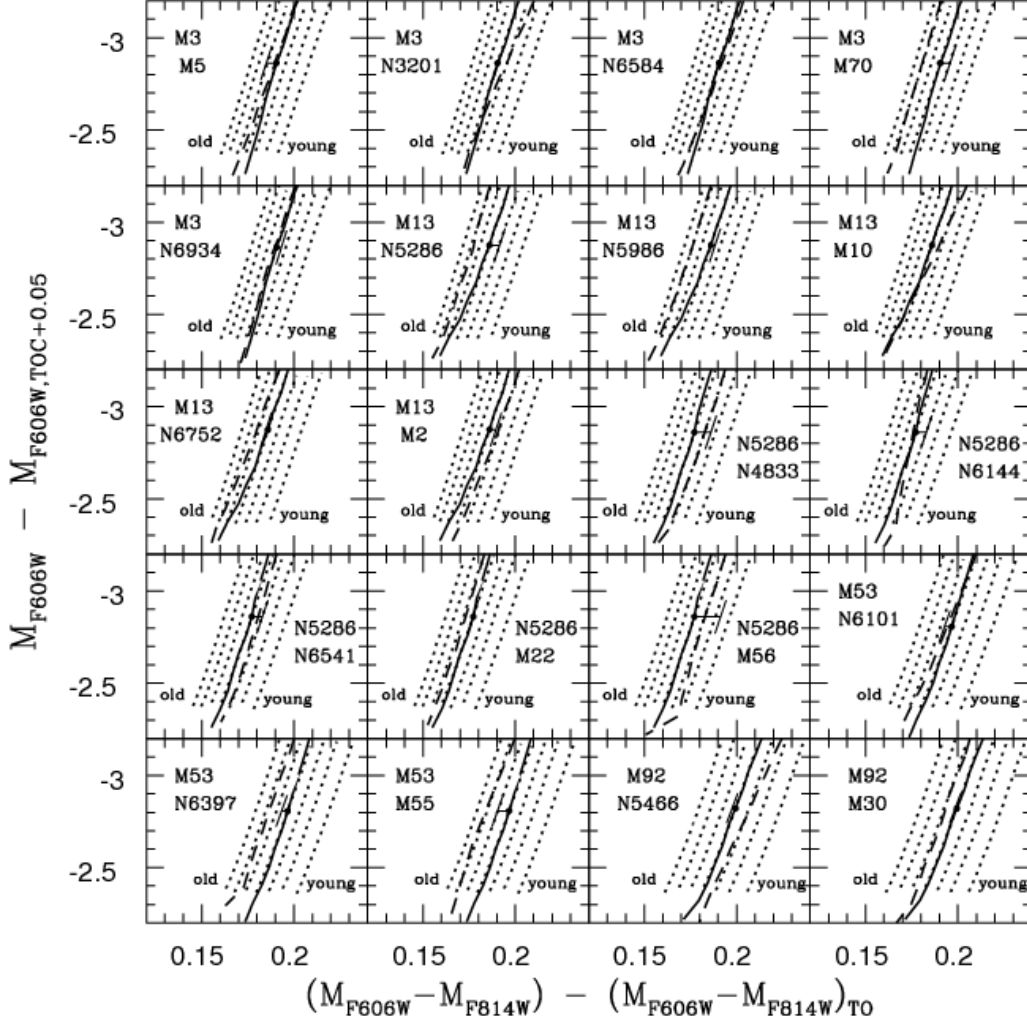


Fig. 30.— Differences in the ages of globular clusters as determined from the $\Delta H_{\text{TO,RGB}}$ technique. The clusters considered in each panel are identified in the upper left-hand corner (or to the right of center in the case of comparisons involving NGC 5286), where the upper and lower names correspond to the reference and target clusters, respectively: their lower-RGB fiducials are represented, in turn, by the solid and dashed curves. Giant-branch segments of isochrones, in 0.5 Gyr increments, for the $[\text{Fe}/\text{H}]$ value of the target cluster are shown as dotted lines. The correction, if any, that should be applied to the location of the fiducial sequence of the reference cluster to account for the difference in $[\text{Fe}/\text{H}]$ between it and the target cluster is given by the short horizontal line at an ordinate value of ≈ -2.8 .

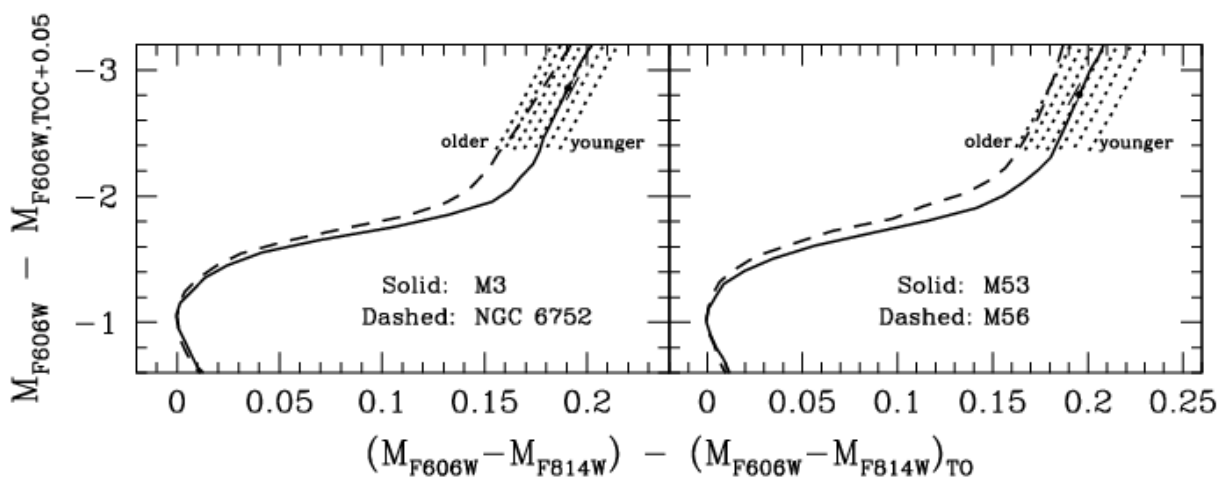


Fig. 31.— Similar to Fig. 24; in this case, the principal photometric sequences for the upper-MS to lower-RGB stars in M 3 and NGC 6752 (*left-hand panel*) and in M 53 and M 56 (*right-hand panel*) are compared after they have been registered to the usual abscissa and ordinate zero-points (see the text).

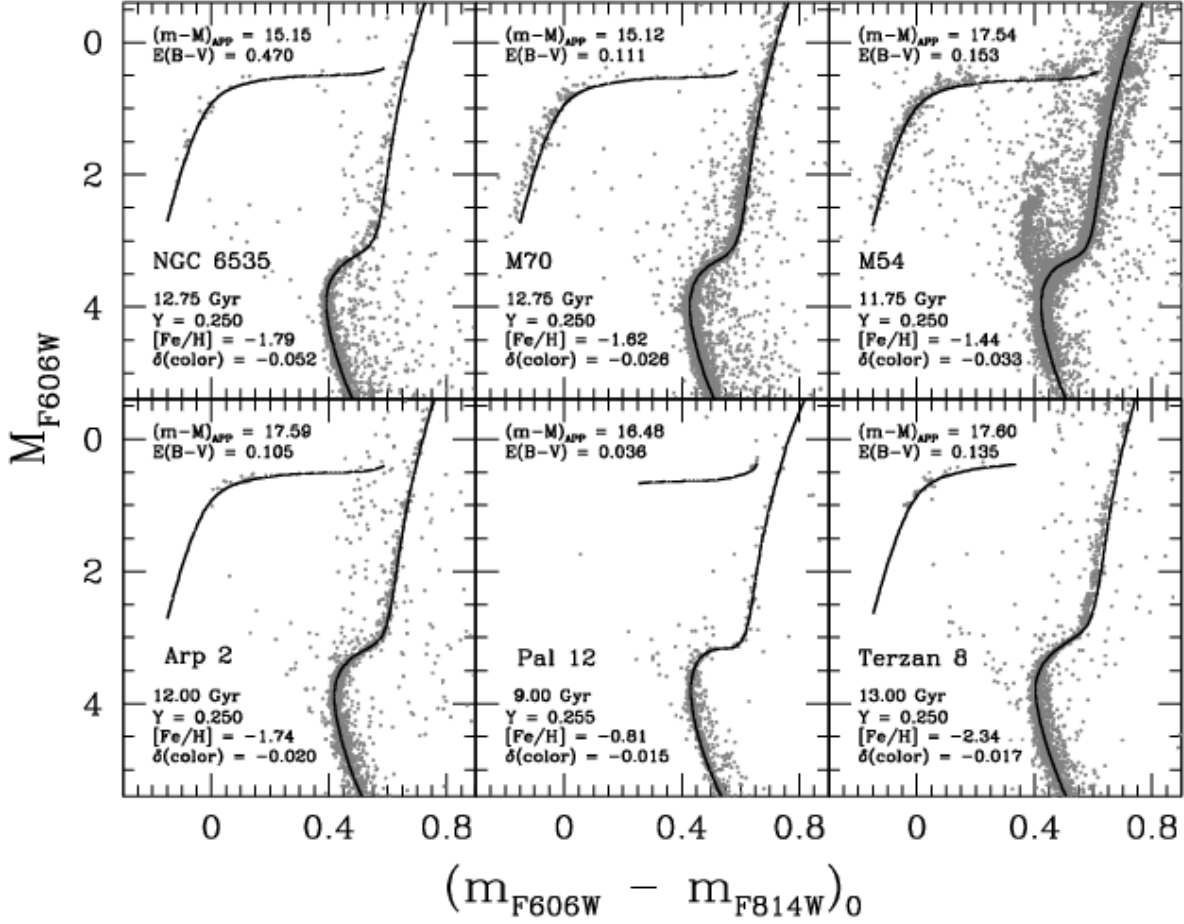


Fig. 32.— Similar to Fig. 11; in this case, isochrones and ZAHB loci have been fitted to the CMDs of NGC 6535 and M 70, as well as to those of four GCs that are associated with the Sagittarius dwarf galaxy. In the case of Pal 12, $[\alpha/Fe] = 0.0$ has been adopted: the other systems have been assumed to have normal α -element abundances for their metallicities.

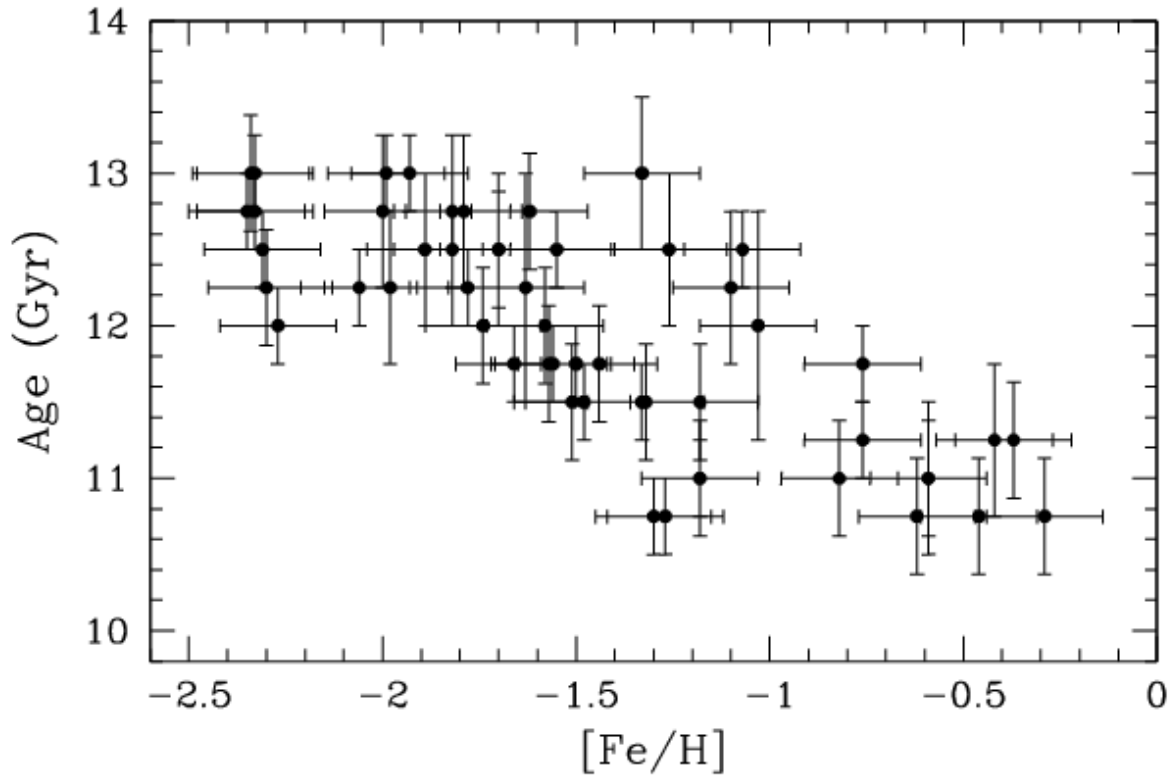


Fig. 33.— The age-[Fe/H] relationship that has been derived in this investigation; see Table 2 for numerical values of the data that have been plotted.

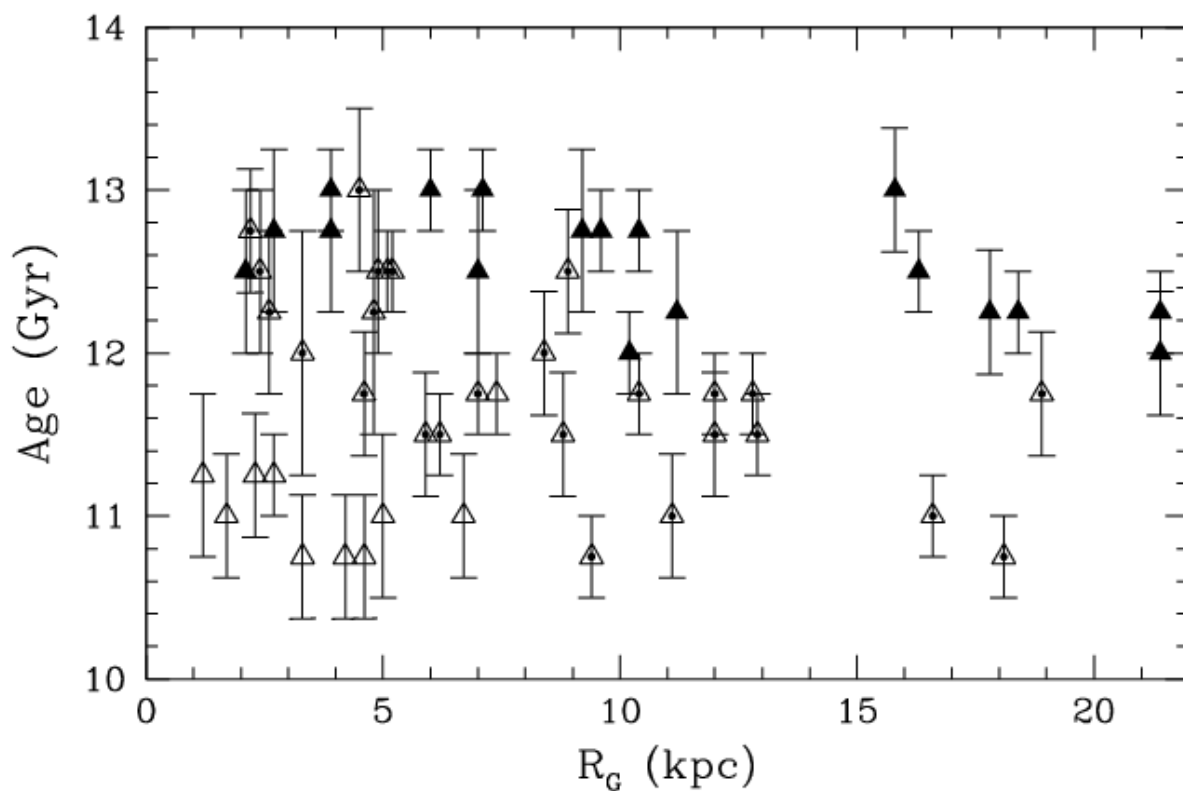


Fig. 34.— The age– R_G relationship that has been derived in this study. The data that have been plotted are given in Table 2. *Filled triangles*, *open triangles*, and *composite symbols* have been used to represent GCs that have $[\text{Fe}/\text{H}] < -1.7$, $[\text{Fe}/\text{H}] \geq -1.0$ and $-1.7 \leq [\text{Fe}/\text{H}] < -1.0$, respectively.

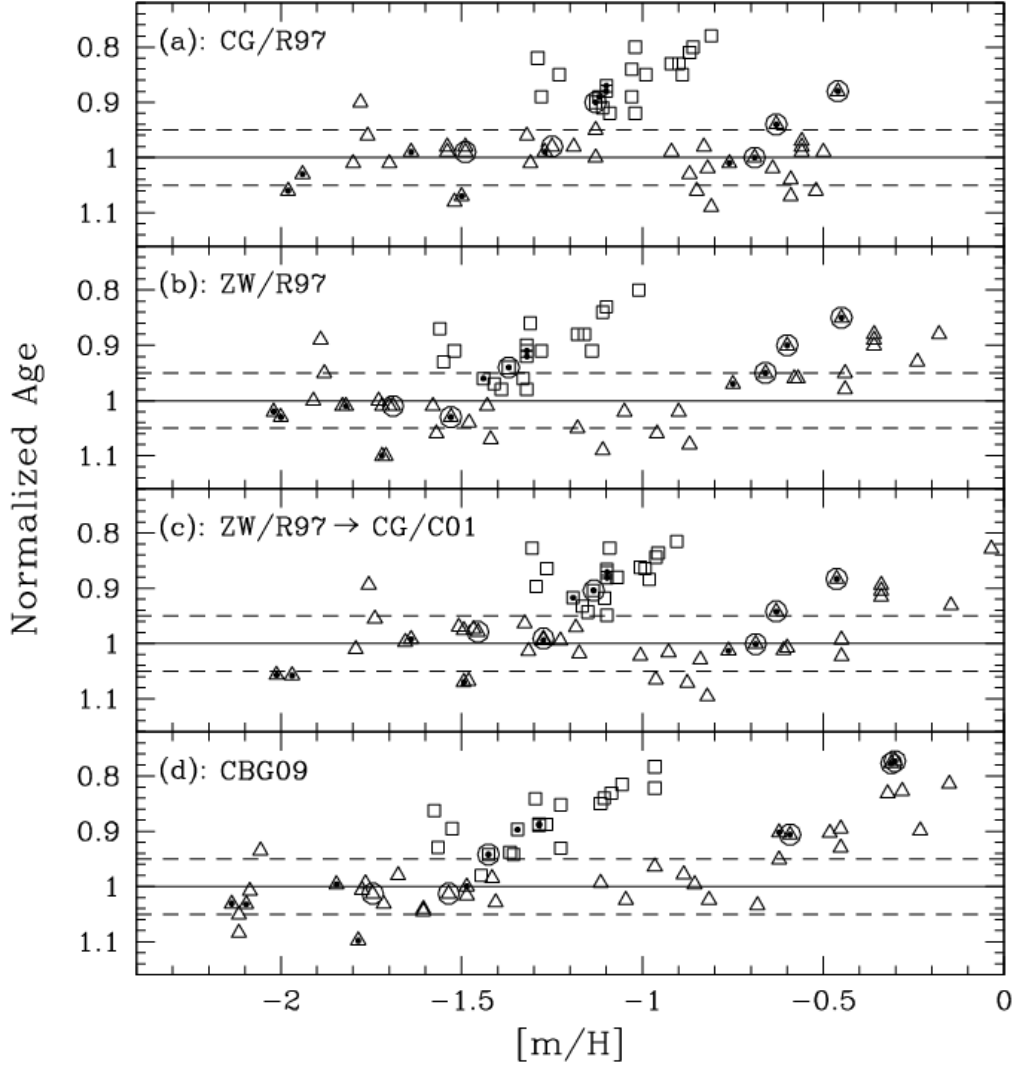


Fig. 35.— Normalized ages of globular clusters as determined using the rMSF method of MF09. Squares and triangles represent, in turn, GCs that belong to a young and an old group according to MF09. Large open circles denote clusters that are not included in our sample. Panels (a) and (b) reproduce the results reported by MF09 (their Figs. 10 and 11, respectively). Small filled circles denote those clusters which were not considered in the R97 study. Panels (c) and (d) portray, in turn, the results that MF09 would have obtained if they had transformed all of their ZW/R97 metal abundances to the CG scale using the equation provided by Carretta et al. (2001), or if they had been able to use the metallicities from CBG09, which were not published at that time.

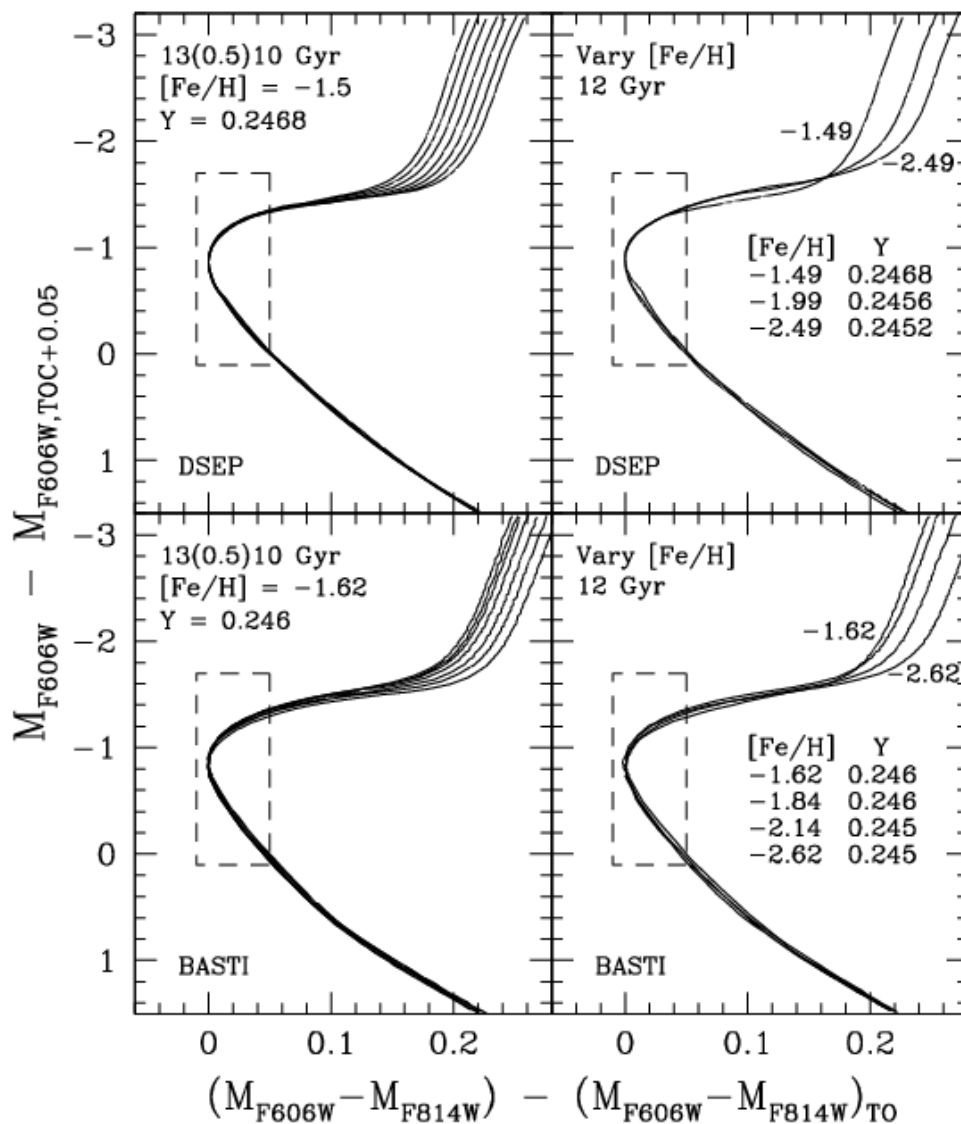


Fig. 36.— The registration of selected DESP and BASTI isochrones (from their respective web sites) to the usual zero-points to illustrate how their MSTO-to-RGB separations vary with age at a given metallicity (the *left-hand panels*) and with $[Fe/H]$ at a fixed age (the *right-hand panels*).

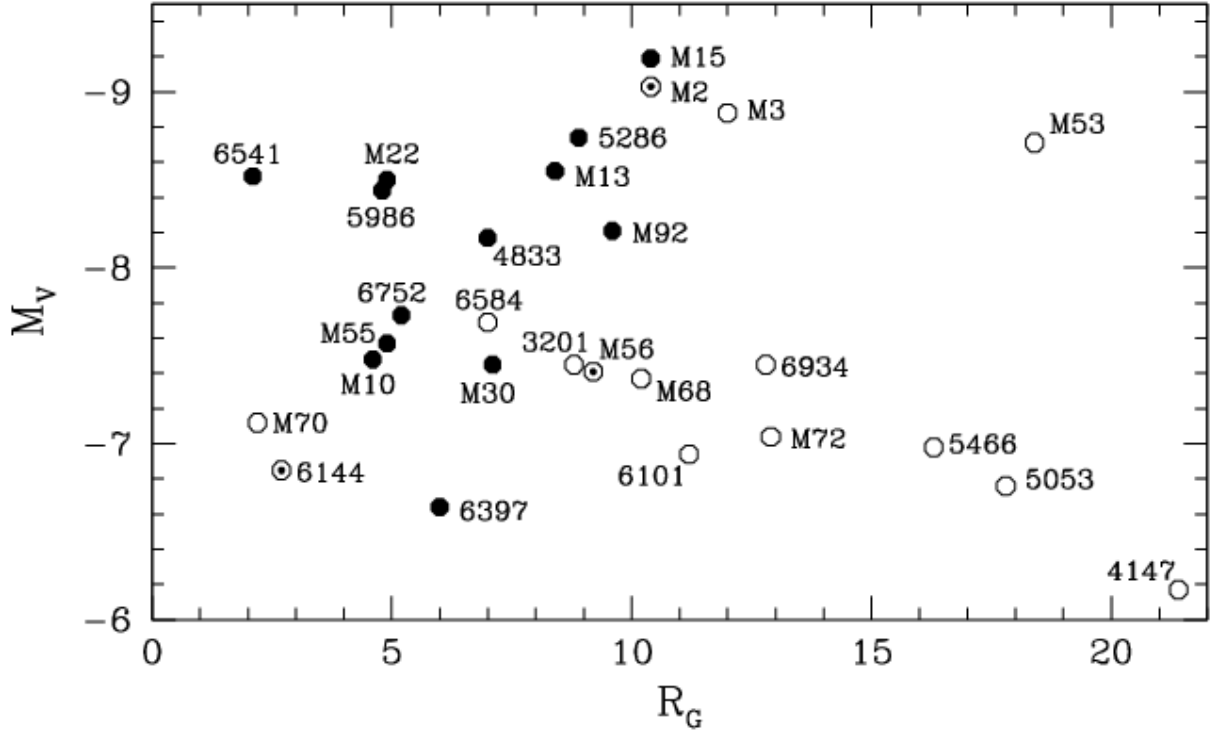


Fig. 37.— The variation of M_V (absolute integrated visual magnitude) with Galactocentric distance, R_G , for the clusters in our sample that have $[Fe/H] \lesssim -1.5$. The clusters, which are identified by their Messier or NGC numbers, have been classified as M3-like (*open circles*) or M13-like (*filled circles*) based on the slope of the subgiant branch in the observed CMDs. A black dot at the center of an open circle indicates that the classification is uncertain; i.e., the slope of the cluster SGB is intermediate to those in the aforementioned groups.

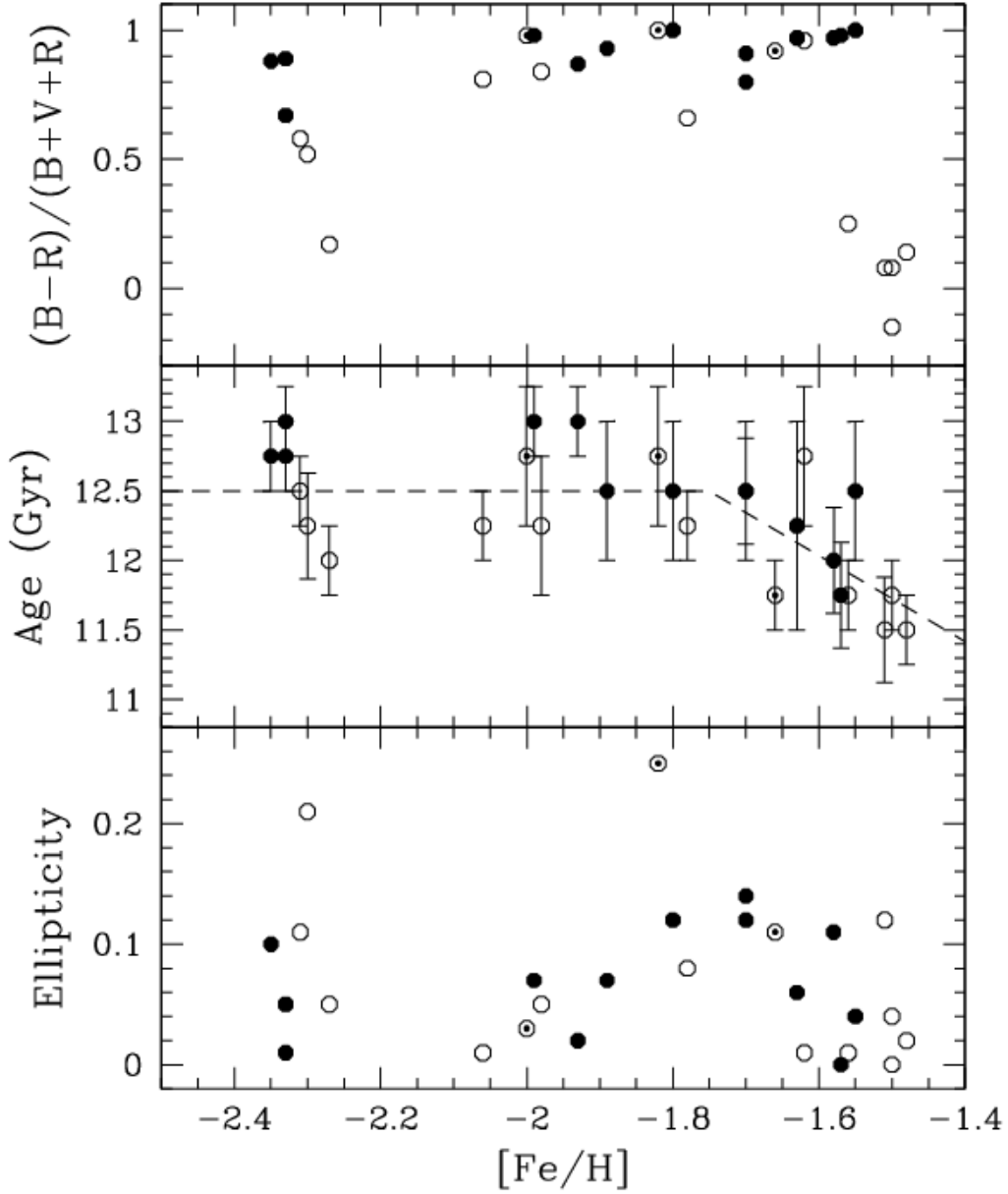


Fig. 38.— The HB types (*upper panel*), ages (*middle panel*), and cluster ellipticities (*lower panel*) of the same GCs that were considered in the previous figure are plotted as a function of their $[\text{Fe}/\text{H}]$ values. The same symbols have been used to represent the M3–like and M13–like clusters, as well as those with uncertain classifications. The sloped and dashed parts of the dashed line in the middle panel represent, respectively, the metal-poor branch of the bifurcated age-metallicity relation shown in Fig. 33 and its extension to the lowest $[\text{Fe}/\text{H}]$ values.

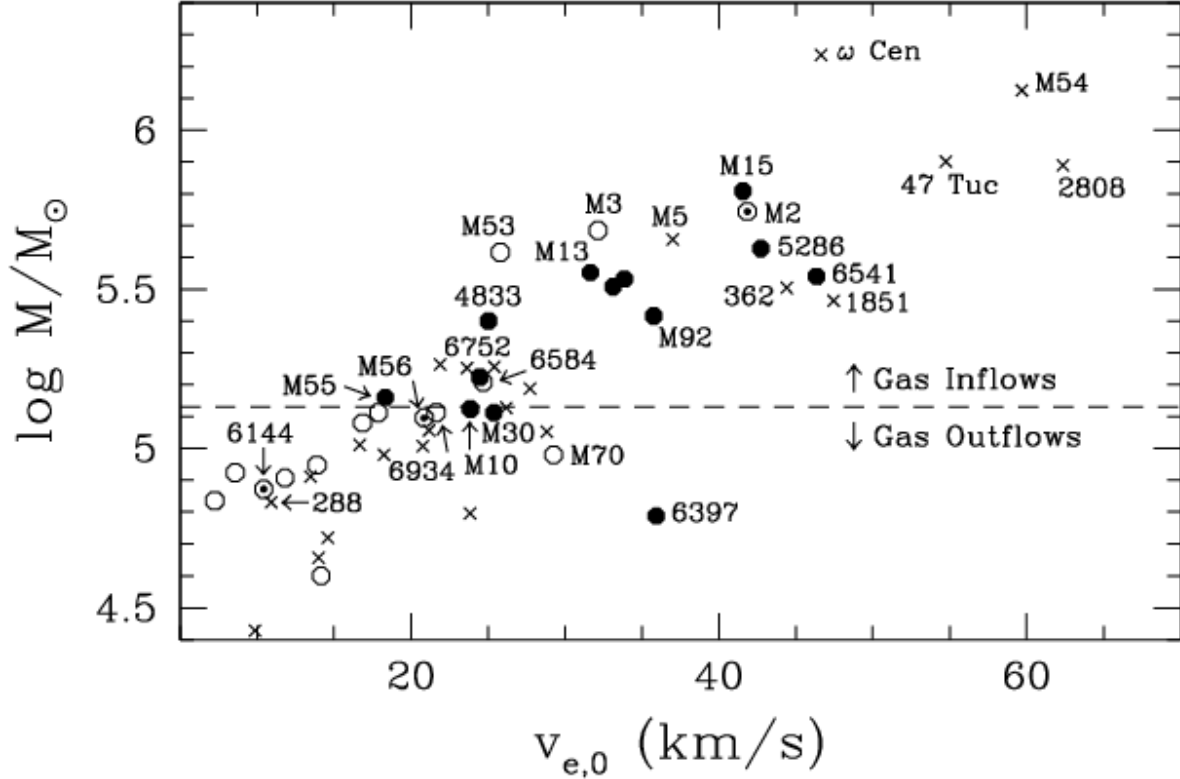


Fig. 39.— The masses of the GCs, in solar units, are plotted as a function of their central escape velocities, $v_{e,0}$. Open and filled circles have been used to represent the M3-like and M13-like clusters, respectively, while composite symbols indicate those clusters with uncertain classifications (as in the previous two figures). Crosses indicate GCs that have $[\text{Fe}/\text{H}] \gtrsim -1.5$ or those that show variations in $[\text{Fe}/\text{H}]$, like ω Cen. Clusters that are expected to develop GC winds, according to the models by Faulkner & Freeman (1977), lie below the horizontal dashed line, whereas those which may build up a central reservoir of the gas that is shed by mass-losing stars lie above that line. The location of this line is approximate as it depends on several factors (see the text). Of the clusters that have been explicitly identified, 47 Tuc, M15, M30, M53, NGC 6397, M70, and NGC 6752 all have central concentrations $c > 2.0$ (Harris 1996).

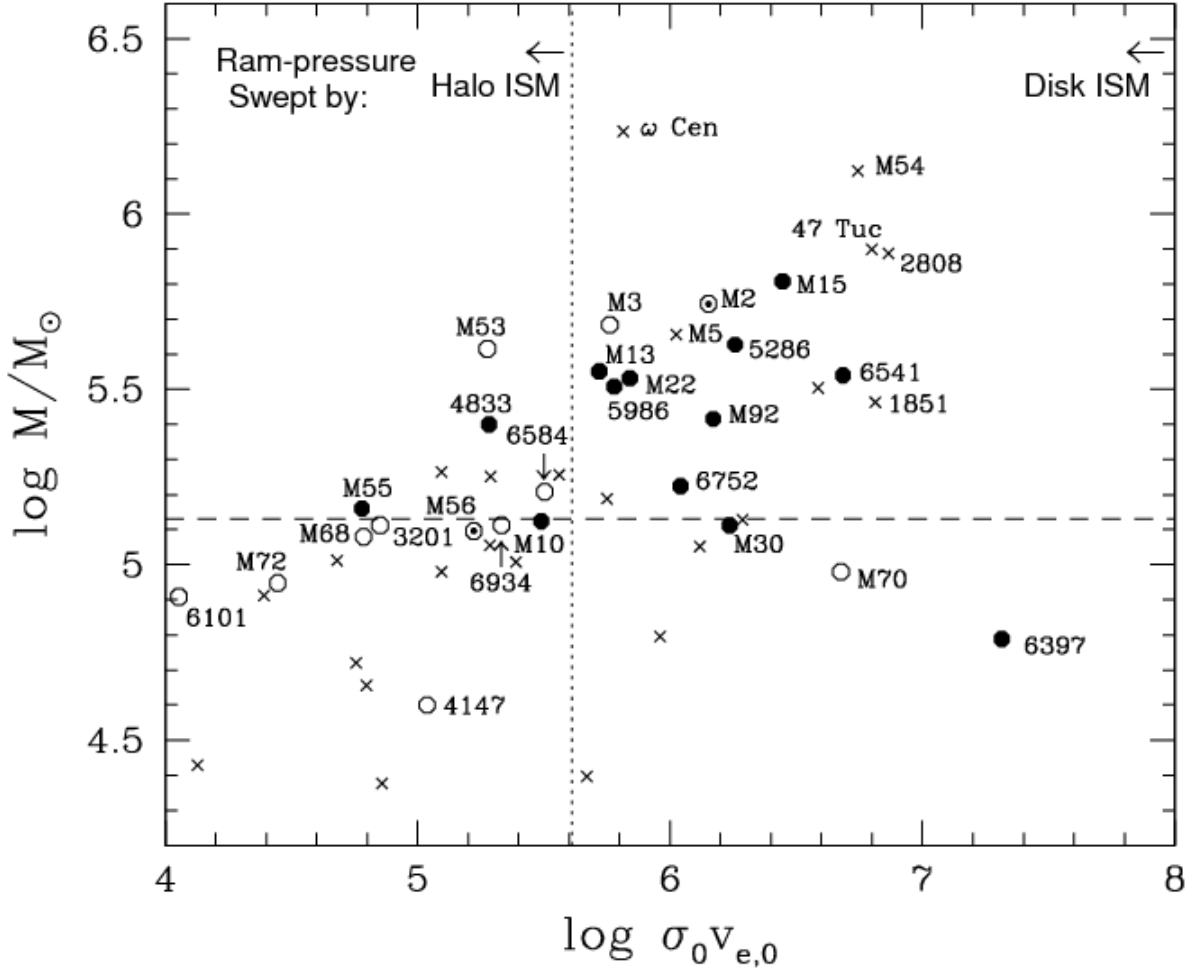


Fig. 40.— The masses of the GCs, in solar units, are plotted as a function of the logarithm of the product of the surface density of the stars at the cluster center, σ_0 , and the central escape velocity, $v_{e,0}$. The latter is correlated with the ability of a given GC to resist ram-pressure stripping of any gas that it contains as a result of its passage through the Galactic halo or disk. The vertical dotted line separates clusters in which ram-pressure sweeping would, or would not, be effective in removing gas from them by the halo interstellar medium. The location of this line is uncertain, but it is expected to be approximately where it has been drawn if the density of the halo medium is $1.5 \times 10^{-27} \text{ g/cm}^3$ and the proportional rate of mass loss from the cluster stars is $\alpha = 7 \times 10^{-20} \text{ s}^{-1}$ (see the text). Clusters that lie to the right of the dotted line would be ram-pressure swept of any gas that they are able to accumulate only when they pass through the Galactic disk. The symbols and the horizontal dashed line have the same definitions as in the previous figure.

Table 1. Subgiant Slopes of $[\text{Fe}/\text{H}] \lesssim -1.5$ Globular Clusters

NGC	Name	$[\text{Fe}/\text{H}]$	SGB slope
M3-like			
3201		-1.51	-3.01 ± 0.50
4147		-1.78	-2.75 ± 0.13
4590	M 68	-2.27	-3.34 ± 0.22
5024	M 53	-2.06	-3.43 ± 0.12
5053		-2.30	-3.43 ± 0.24
5272	M 3	-1.50	-2.95 ± 0.12
5466		-2.31	-3.25 ± 0.12
6101		-1.98	-3.35 ± 0.29
6584		-1.50	-2.99 ± 0.17
6681	M 70	-1.62	-2.67 ± 0.30
6934		-1.56	-3.01 ± 0.24
6981	M 72	-1.48	-2.97 ± 0.18
M13-like			
4833		-1.89	-3.80 ± 0.30
5286		-1.70	-3.75 ± 0.27
5986		-1.63	-3.60 ± 0.30
6205	M 13	-1.58	-3.55 ± 0.13
6254	M 10	-1.57	-3.81 ± 0.29
6341	M 92	-2.35	-3.97 ± 0.15
6397		-1.99	-3.71 ± 0.30
6541		-1.82	-3.70 ± 0.26
6656	M 22	-1.70	-3.90 ± 0.38
6752		-1.55	-3.40 ± 0.16
6809	M 55	-1.93	-3.62 ± 0.21
7078	M 15	-2.33	-4.01 ± 0.20
7099	M 30	-2.33	-3.89 ± 0.18
Intermediate/Uncertain			
6144		-1.82	-3.29 ± 0.50
6779	M 56	-2.00	-3.52 ± 0.34
7089	M 2	-1.66	-3.32 ± 0.20

Table 2. Ages and Other Properties of the Globular Cluster Sample

NGC	Name	[Fe/H]	Age	Method ^a	Fig(s).	Range ^b	HB type	R _G	M _V	v _{e,0}	log ₁₀ σ ₀
104	47 Tuc	-0.76	11.75 ± 0.25	V	14	11.50–11.75	-0.99	7.4	-9.42	54.8	5.061
288		-1.32	11.50 ± 0.38	H	24		+0.98	12.0	-6.75	10.9	2.953
362		-1.30	10.75 ± 0.25	V	13	10.75–11.00	-0.87	9.4	-8.43	44.4	4.938
1261		-1.27	10.75 ± 0.25	V	13	10.75–11.25	-0.71	18.1	-7.80	23.6	3.913
1851		-1.18	11.00 ± 0.25	V	13	10.75–11.25	-0.32	16.6	-8.33	47.6	5.136
2808		-1.18	11.00 ± 0.38	V	13	11.00–11.25	-0.49	11.1	-9.39	62.4	5.070
3201		-1.51	11.50 ± 0.38	A	12,30	11.25–11.75	+0.08	8.8	-7.45	17.9	3.599
4147		-1.78	12.25 ± 0.25	V	11	12.25–12.50	+0.66	21.4	-6.17	14.2	3.886
4590	M 68	-2.27	12.00 ± 0.25	V	11	12.00	+0.17	10.2	-7.37	16.9	3.559
4833		-1.89	12.50 ± 0.50	A	30		+0.93	7.0	-8.17	25.0	3.885
5024	M 53	-2.06	12.25 ± 0.25	V	12	12.25–12.50	+0.81	18.4	-8.71	25.8	3.866
5053		-2.30	12.25 ± 0.38	A	12	12.25–12.50	+0.52	17.8	-6.76	7.2	2.196
5272	M 3	-1.50	11.75 ± 0.25	V	22		+0.08	12.0	-8.88	32.1	4.254
5286		-1.70	12.50 ± 0.38	A	12,30	11.75–12.25	+0.80	8.9	-8.74	42.7	4.628
5466		-2.31	12.50 ± 0.25	V	11,30	12.25–12.50	+0.58	16.3	-6.98	8.6	2.453
5904	M 5	-1.33	11.50 ± 0.25	V	8	11.50–11.75	+0.31	6.2	-8.81	37.0	4.457
5927		-0.29	10.75 ± 0.38	V	16	10.50–10.75	-1.00	4.6	-7.81	25.4	4.156
5986		-1.63	12.25 ± 0.75	A	30		+0.97	4.8	-8.44	33.1	4.259
6101		-1.98	12.25 ± 0.50	H	30		+0.84	11.2	-6.94	11.8	2.980
6121	M 4	-1.18	11.50 ± 0.38	V	13	11.25–11.50	-0.06	5.9	-7.19	20.8	4.070
6144		-1.82	12.75 ± 0.50	H	30		+1.00	2.7	-6.85	10.4	2.975
6171	M 107	-1.03	12.00 ± 0.75	V	13		-0.73	3.3	-7.12	18.2	3.832
6205	M 13	-1.58	12.00 ± 0.38	A	20,22		+0.97	8.4	-8.56	31.7	4.219
6218	M 12	-1.33	13.00 ± 0.50	A	24,26		+0.98	4.5	-7.31	21.2	3.961
6254	M 10	-1.57	11.75 ± 0.38	H	30		+0.98	4.6	-7.48	23.9	4.112
6304		-0.37	11.25 ± 0.38	V	16	11.00–11.25	-1.00	2.3	-7.30	28.8	4.656
6341	M 92	-2.35	12.75 ± 0.25	V	11	12.75–13.25	+0.91	9.6	-8.21	35.8	4.618
6352		-0.62	10.75 ± 0.38	V	16	10.50–11.00	-1.00	3.3	-6.47	14.6	3.592
6362		-1.07	12.50 ± 0.25	V	13	12.25–12.75	-0.58	5.1	-6.95	13.5	3.261
6366		-0.59	11.00 ± 0.50	V	16	11.00	-0.97	5.0	-5.74	9.8	3.135
6397		-1.99	13.00 ± 0.25	A	30	13.00	+0.98	6.0	-6.64	35.9	5.759
6496		-0.46	10.75 ± 0.38	V	16	10.50–10.75	-1.00	4.2	-7.20	16.7	3.459
6535		-1.79	12.75 ± 0.50	V	32		+1.00	3.9	-4.75	8.2	3.327
6541		-1.82	12.50 ± 0.50	H	30		+1.00	2.1	-8.52	46.3	5.019
6584		-1.50	11.75 ± 0.25	A	12,30		-0.15	7.0	-7.69	24.7	4.112
6624		-0.42	11.25 ± 0.50	V	16	11.00–11.25	-1.00	1.2	-7.49	26.2	4.869
6637	M 69	-0.59	11.00 ± 0.38	V	16	11.00–11.25	-1.00	1.7	-7.64	27.7	4.308
6652		-0.76	11.25 ± 0.25	V	16	11.00–11.25	-1.00	2.7	-6.66	23.9	4.583
6656	M 22	-1.70	12.50 ± 0.50	H	30		+0.91	4.9	-8.50	33.9	4.311
6681	M 70	-1.62	12.75 ± 0.38	A	30,32		+0.96	2.2	-7.12	29.3	5.210
6715	M 54	-1.44	11.75 ± 0.50	V	32		+0.54	18.9	-9.98	59.7	4.968
6717		-1.26	12.50 ± 0.50	V	13		+0.98	2.4	-5.66	16.3	4.458
6723		-1.10	12.50 ± 0.25	V	13	12.25–12.75	-0.08	2.6	-7.83	21.9	3.755
6752		-1.55	12.50 ± 0.25	A	30		+1.00	5.2	-7.73	24.5	4.655
6779	M 56	-2.00	12.75 ± 0.50	H	30		+0.98	9.2	-7.41	20.8	3.905
6809	M 55	-1.93	13.00 ± 0.25	A	12,30	12.75–13.25	+0.87	3.9	-7.57	18.3	3.515

Table 2—Continued

NGC	Name	[Fe/H]	Age	Method ^a	Fig(s).	Range ^b	HB type	R _G	M _V	v _{e,0}	log ₁₀ σ ₀
6838	M 71	−0.82	11.00 ± 0.38	V	16	11.00	−1.00	6.7	−5.61	13.0	3.746
6934		−1.56	11.75 ± 0.25	V	12,30	11.50–12.00	+0.25	12.8	−7.45	21.6	3.998
6981	M 72	−1.48	11.50 ± 0.25	V	12,30	11.25–11.75	+0.14	12.9	−7.04	13.9	3.304
7078	M 15	−2.33	12.75 ± 0.25	V	11	12.50–12.75	+0.67	10.4	−9.19	41.6	4.827
7089	M 2	−1.66	11.75 ± 0.25	A	12,30	11.50–11.75	+0.92	10.4	−9.03	41.8	4.531
7099	M 30	−2.33	13.00 ± 0.25	A	11,30	12.75–13.00	+0.89	7.1	−7.45	25.4	4.831
	Arp 2	−1.74	12.00 ± 0.38	V	32		+0.53	21.4	−5.29	3.5	1.545
	Pal 12	−0.81	9.0 ± 0.38	V	32		−1.00	15.8	−4.47	4.3	3.297
	Ter 8	−2.34	13.00 ± 0.38	V	32		+1.00	19.4	−5.07	4.3	1.938

^aAges are based on the vertical (V) or horizontal (H) methods, or an average (A) of the former.

^bThis range encompasses the ages independently derived by DAV, KB, and RL.

Table 3. Orbital Parameters of $[\text{Fe}/\text{H}] \lesssim -1.5$ Globular Clusters

NGC	Name	e^a	$R_a^{a,b}$	$R_p^{a,b}$	$z_{\text{max}}^{a,b}$
M3-like SGB					
4147		0.72 ± 0.10	25.3 ± 2.6	4.1 ± 2.2	13.1 ± 1.7
4590	M 68	0.48 ± 0.03	24.4 ± 3.1	8.6 ± 0.3	9.1 ± 1.3
5024	M 53	0.40 ± 0.12	36.0 ± 16.8	15.5 ± 1.9	24.2 ± 8.1
5272	M 3	0.42 ± 0.07	13.4 ± 0.8	5.5 ± 0.8	8.7 ± 0.5
5466		0.79 ± 0.03	57.1 ± 24.6	6.6 ± 1.5	34.1 ± 14.4
6584		0.87 ± 0.05	12.6 ± 2.4	0.9 ± 0.7	3.1 ± 2.3
6934		0.72 ± 0.07	37.5 ± 15.2	6.0 ± 1.6	21.2 ± 9.5
M13-like SGB					
6205	M 13	0.62 ± 0.06	21.5 ± 4.7	5.0 ± 0.5	13.2 ± 2.1
6254	M 10	0.19 ± 0.05	4.9 ± 0.2	3.4 ± 0.4	2.4 ± 0.2
6341	M 92	0.76 ± 0.03	9.9 ± 0.4	1.4 ± 0.2	3.8 ± 0.5
6397		0.34 ± 0.02	6.3 ± 0.1	3.1 ± 0.2	1.5 ± 0.1
6656	M 22	0.53 ± 0.01	9.3 ± 0.7	2.9 ± 0.2	1.9 ± 0.1
6752		0.08 ± 0.02	5.6 ± 0.2	4.8 ± 0.3	1.6 ± 0.1
7078	M 15	0.32 ± 0.05	10.3 ± 0.7	5.4 ± 1.1	4.9 ± 0.8
7099	M 30	0.39 ± 0.06	6.9 ± 0.3	3.0 ± 0.4	4.4 ± 0.3
Intermediate SGB Slope					
6144		0.25 ± 0.15	3.0 ± 0.7	1.8 ± 0.2	2.4 ± 0.2
6779	M 56	0.86 ± 0.03	12.4 ± 1.5	0.9 ± 0.3	1.1 ± 0.7
7089	M 2	0.68 ± 0.06	33.6 ± 12.5	6.4 ± 1.1	20.0 ± 6.5

^aFrom Dinescu et al. (1999).

^bIn kpc.